Dissertation

submitted to the
Combined Faculties for the Natural Sciences and for Mathematics
of the Ruperto-Carola University of Heidelberg, Germany
for the degree of
Doctor of Natural Sciences

presented by
Jana Friedrich
born in Berlin, Germany
Oral examination: 01.12.2017

A novel Role for the *Hox* Gene *Deformed* in the Control of a Motor System required for Feeding in *Drosophila*

Referees:

Prof. Dr. Jochen Wittbrodt

Prof. Dr. Ingrid Lohmann

The work presented in this thesis was performed in the laboratory of Prof. Dr. Ingrid Lohmann at the University of Heidelberg, Germany.

Table of Contents

Summary I
Zusammenfassung III
Acknowledgements V
Frequently used Abbreviations VII
Publications and Contributions IX
1_Introduction 1
1.1 Development of the Fly's Central Nervous System 1
1.2 Neuromuscular Connectivity 5
1.3 Synapse Formation in developing Motor Systems 7
1.5 Development of Motor Behaviours in *Drosophila* 10
1.6 Feeding Behaviour in *Drosophila* 12
1.7 *Hox* Genes in *Drosophila* Neural Development 13
1.8 Aims of this Thesis 17
2_Results 19
2.1 Deformed is expressed in Neural Cells of the Subesophageal Zone 19
2.2 The Dfd^{NAE667} Enhancer recapitulates Deformed Expression in Neural Cells of the Subesophageal Zone 22
2.3 Deformed-positive Motoneurons innervate the Mouth Hook Elevator 24
2.4 Mouth Hook Motility and Head Muscles are affected in *Deformed* Mutants 26
2.5 Deformed-positive Motoneurons control Mouth Hook Elevation 29
2.6 Deformed-mutant Cells are defective in their Developmental Program 32
2.7 Regulation of Target Genes by Deformed 38
2.8 Neural Specification and Axon Guidance are affected in *Dfd* Mutants 39
2.9 Deformed controls the Synaptic Targeting Molecule Connectin 43
2.10 Inactivation of Deformed during late Embryogenesis affects Mouth Hook-associated behaviour 45
2.11 Partial deletion of *Dfd* causes Lethality during postembryonic Development 47
2.12 Loss of Deformed results in Defects in NMJ Morphology 49
2.13 Ankyrin2-XL, a synaptic Protein, is regulated by Deformed 51
2.14 Knockdown of *ankyrin-2* expression resembles the Defects in NMJ Morphology observed upon Loss of functional Deformed 56
2.15 The *Drosophila* autoregulatory Enhancer of *Deformed* drives Expression in Hindbrain Neurons of the Teleost Fish Medaka (*Oryzias latipes*) 57

3_Discussion **59**
3.1 Deformed is expressed in Neural Cells of a Feeding Motor Unit in the Head of *Drosophila* 60
3.2 Deformed is critically required for feeding-related Behaviours 63
3.3 Deformed determines the developmental Program of Neural Cells 65
3.4 Deformed connects Neurons and Muscles 69
3.5 Deformed Function is required throughout Embryogenesis and beyond 72
3.6 Deformed is active in Neurons to prevent neuronal Decline 73
3.7 The Activity of Deformed is conserved 77
4_Conclusions **79**
5_Materials **81**
5.1 Equipment and Consumables 81
5.2 Antibodies 84
5.3 Oligonucleotides 85
5.4 Plasmids 86
5.5 Bacterial Strains 87
5.6 Fly Stocks 87
5.7 Media and Standard Solutions 88
5.8 Software 92
6_Methods **93**
6.1 Fly Maintenance 93
6.2 Embryo Collection 93
6.3 Drosophila Genetics 94
6.3.1 The Gal4-UAS binary system *94*
6.3.2 The FINGR method *94*
6.3.3 RNA interference *94*
6.4 Methods in Molecular Biology 95
6.4.1 Extraction of genomic DNA from Drosophila flies *95*
7.4.2 Transformation of competent bacteria *95*
6.4.3 Plasmid DNA preparation *95*
6.4.4 Cloning of Dfd^{NAE667}-Gal4 and Dfd^{NAE661}-GFP *95*
6.4.5 Preparation of Digoxigenin (DIG)- and Biotin (BIO)-labelled antisense RNA probes *96*
6.5 Immunohistochemistry 97
6.5.1 In-situ hybridisation on Drosophila embryos *97*
6.5.2 In-situ hybridisation on Drosophila larval dissections *98*
6.5.3 Whole-mount antibody stainings on Drosophila embryos *98*

6.5.4 Antibody stainings on Drosophila larval dissections *99*
6.5.5 Tunel labelling *99*
6.6 *Drosophila* Cuticle Preparation 99
6.7 Behavioural Assays 100
6.7.1 Time-lapse movies *100*
6.7.2 Temperature-shift experiments *100*
6.7.3 Tetanus toxin assay in Drosophila embryos *100*
6.7.4 Tetanus toxin assay in Drosophila larvae *101*
Adult feeding assay *101*
6.8 Injection of *O. latipes* Embryos 101
6.9 Image Analysis and Statistics 101
7_References **103**
8_Appendix **119**

Summary

Animals interact with their environment based on stereotypical movement patterns, such as those performed during running, breathing or feeding. *Hox* regulatory genes had been known to be essential for establishing coordinated movements, but the molecular underpinnings of feeding behaviour were not well understood.

Using *Drosophila melanogaster* as a model system, the present work demonstrates that a specific *Hox* gene, *Deformed*, controls the establishment of a motor unit in the fly's head during embryonic development. This unit comprises a muscle and a set of stimulating neurons and enables feeding-related movements. The loss of functional Deformed caused severe defects in the formation of the feeding motor unit and subsequently led to death. Furthermore, inactivation of *Deformed* at the end of embryogenesis, once the motor unit was successfully assembled, uncovered a novel role for Deformed in maintaining the functionality and integrity of the motor unit later in life. Finally, perturbations in motor behaviour were pinned to the role of Deformed in the control of molecules essential for synapse stability at the junctions between neurons and muscles. One of the identified direct targets of Deformed is Ankyrin, a molecule previously shown to be involved in neurodegenerative diseases such as Alzheimer's. Hence, the results presented here suggest that *Hox* genes might have a neuroprotective function and once this function is gone, the neurons degenerate, a hypothesis that will be of interest to study in the future.

Interestingly, Deformed is co-expressed in muscles and neurons forming the functional feeding motor unit, pointing at its role as a master regulator of feeding behaviour. In support of this hypothesis, Deformed was shown to act as one of the negative upstream regulators of Connectin, a molecule essentially required for the correct matching between the two partners.

Is the function of Hox transcription factors in the establishment of feeding motor units conserved across the animal phylogeny? This work uncovered a fly neural regulatory element of *Deformed*, which contains highly conserved Hox-binding sites, to be active in neurons located within the hindbrain of the vertebrate fish model *Oryzias latipes*, suggesting that the transcriptional network controlling the assembly and function of the feeding unit in fish and flies is conserved.

Zusammenfassung

Stereotype Bewegungen ermöglichen Individuen sich in ihrer Umwelt fortzubewegen, zu atmen oder Nahrung aufzunehmen. *Hox*-Gene sind eine Familie von regulatorischen Genen, die für die Etablierung koordinierter Bewegungsabläufe von essentieller Bedeutung sind. Jedoch ist bis heute wenig darüber bekannt wie Hox-Proteine auf molekularer Ebene die Ausbildung von Verhaltensweisen wie die der Nahrungsaufnahme steuern.

In dieser Arbeit konnte mit Hilfe von Untersuchungen am Modellorganismus *Drosophila melanogaster* gezeigt werden, dass ein spezielles *Hox*-Gen, *Deformed*, die Entwicklung einer motorischen Einheit im Kopf der Fliege kontrolliert, die aus einem Muskel und den ihn anregenden Neuronen besteht. Diese Einheit wird bereits während der Embryogenese etabliert und ermöglicht der Fliegenlarve Nahrung aufzunehmen. *Deformed* ist jedoch nicht nur für die Etablierung, sondern auch für die Funktion und Aufrechterhaltung dieser motorischen Einheit in späteren Lebensphasen wichtig. Dies wurde deutlich nachdem das Deformed-Protein zu einem Zeitpunkt inaktiviert wurde, als die Ausbildung der motorischen Einheit bereits als abgeschlossen galt und trotzdem die typischen Bewegungsmuster der Nahrungsaufnahme verloren gingen. Auch der Grund für den Kontrollverlust konnte im Rahmen dieser Arbeit ermittelt werden. Es wurde gezeigt, dass Deformed das Realisieren der Information, auch Expression genannt, von Genen steuert, die für Stabilität und somit Funktionalität an den Verknüpfungsstellen zwischen Neuronen und Muskeln sorgen. Eines dieser Gene kodiert für das Protein Ankyrin2. In Abwesenheit von Deformed wurde auch *Ankyrin2* nicht mehr exprimiert, was letzten Endes zur Degeneration der betroffenen Neurone führte. Aus Untersuchungen am Menschen geht hervor, dass Ankyrine im Zusammenhang mit der neurodegenerativen Krankheit Alzheimer stehen. Somit könnte *Hox*-Genen eine entscheidende Schutzfunktion in Neuronen zugesprochen werden, die erlischt wenn *Hox*-Gene in ihrer Expression oder Wirkungsweise beeinträchtigt werden. Diese neue und bislang unbekannte Funktion muss jedoch zukünftig noch weiterführend untersucht werden.

Des weiteren zeigt die vorliegende Arbeit, dass Deformed sowohl in Neuronen, als auch in den dazugehörigen Muskeln aktiv ist und dort die Expression von Molekülen steuert, die für die korrekte Verknüpfung zwischen den beiden Geweben entscheidend sind.

Eines dieser Moleküle ist Connectin, welches nicht nur auf der Oberfläche von Muskeln, sondern auch auf den Fortsätzen der entsprechenden Neurone, die diesen Muskel stimulieren, zu finden ist. Hier konnte gezeigt werden, dass das *Connectin*-Gen negativ von Deformed reguliert wird.

Hox-Gene sind innerhalb des Tierreiches hoch konserviert, jedoch wurde ihre Funktion aus evolutionärer Sicht und in Hinblick auf die Etablierung von motorischen Einheiten, die der Nahrungsaufnahme dienen, noch nicht weitergehend studiert. In dieser Arbeit wurden grundlegende Erkenntnisse darüber gewonnen. Es konnte gezeigt werden, dass eine regulatorische Einheit, die in *Drosophila melanogaster* die Expression von *Deformed* in Neuronen widerspiegelt, auch im Japanischen Reisfisch (*Oryzias latipes*) aktiv ist, vermutlich in denjenigen Neuronen, die auch im Fisch für die Aufnahme von Nahrung von Bedeutung sind. Dies deutet darauf hin, dass auch in höheren Wirbeltieren Hox-Proteine an der Etablierung und Aufrechterhaltung motorischer Einheiten im Kopf beteiligt sind.

Acknowledgements

Foremost I deeply wish to thank Prof. Ingrid Lohmann for giving me the opportunity to do my thesis in her group. I am very grateful for her support, her trust in me, the fruitful discussions and especially her patience.

I want to thank Prof. Jochen Wittbrodt for being my doctor father and for all the helpful feedback throughout my thesis.

I am very grateful to Steffen Lemke, whose never-ending interest, suggestions and encouragement supported me during the time of my thesis.

Furthermore, I would like to thank Dr. Michael Eichenlaub for collaborating with me on the fish work and Fatmire Bujupi, who took over this challenging project during my maternal leave time.

Moreover, I deeply wish to thank Natalie Grace Schulz and her sticky notes. Thank you so much, my dear.

Special thanks I want to express to the members and former members of the Lohmann lab.

They will not be able to understand at the time this thesis was written, but I deeply wish to thank my daughters Lara and Julie for being part of my life and for tolerating those times I have not been able to take care of them, but instead worked on this project. The purple colour within this thesis is dedicated to Lara as it is her favourite one.

I wish to thank the INF685 Kinderkrippe and INF159 for taking care of Lara, and our nanny Anna-Lena Dumbeck for taking care of Julie during the times I have been working in the lab.

Particularly, I would like to thank my sister and her family and my friends, Jeanette, Christopher, Hermann, the Klaimans, the Schallers, Eva and Ricardo and Christine, who encouraged me all the time.

I am deeply indebted to my companion in life, Sebastian Sorge. He did not only support me all the time at home and in the lab, but also accepted the challenge and found a family with me during the time of my graduate studies.

Zum Schluß möchte ich meinen Eltern danken, die immer an mich glauben und ohne deren Hilfe und Unterstützung ich nicht bis hierher gekommen wäre.

Frequently used Abbreviations

AEL	After egg laying
AN	Antennal nerve
Antp-C	Antennapedia Complex
AZ	Active zone
BL	Brain lobe
BX-C	Bithorax complex
CAM	Cell adhesion molecule
CAZ	Cytomatrix of the active zone
ChIPseq	Chromatin immunoprecipitation coupled to massively parallel sequencing
CDM	Cibarial dilator musculature
CNS	Central nervous system
CPS	Cephalopharyngeal skeleton
EGFP	Enhanced green fluorescent protein
GFP	Green fluorescent protein
GluR	Glutamate receptor
GMC	Ganglion mother cell
GO	Gene ontology
Gr	Gustatory receptor
GRN	Gustatory receptor neurons
h	hours
HRE	Hox-response element
HRP	Horseradish peroxidase
ISN	Intersegmental nerve
LR	Labial retractor
MH	Mouth hook
MHD	Mouth hook depressor
MHE	Mouth hook elevator
MN	Maxillary nerve
NB	Neuroblast
NMJ	Neuromuscular junction
PaN	Prothoracic accessory nerve
PCD	Programmed cell death
PER	Proboscis extension reflex

PG	Peripheral glia
$Pro_{do}A$	Dorsal protractor muscles A
$Pro_{do}B$	Dorsal protractor muscles B
SEZ	Subesophageal zone
SN	Segmental nerve
SPZ	Supraesophageal zone
SSR	Subsynaptic reticulum
TF	Transcription factor
TNT	Tetanus toxin
TUNEL	terminal deoxynucleotide transferase-mediated dUTP end labelling
ts	temperature sensitive
VNC	Ventral nerve cord

Publications and Contributions

The following articles are related to this thesis and have been published:

Jana Friedrich, Sebastian Sorge, Fatmire Bujupi, Michael P. Eichenlaub, Natalie G. Schulz, Jochen Wittbrodt and Ingrid Lohmann. **Hox Function is required for the Development and Maintenance of the *Drosophila* Feeding Motor Unit.** *Cell Reports*, 14(4), 2 February 2016, pp.1-11.

Sebastian Sorge*, Nati Ha*, Maria Polychronidou*, Jana Friedrich*, Daniela Bezdan*, Petra Kaspar, Martin H Schaefer, Stephan Ossowski, Stefan R Henz, Juliane Mundorf, Jenny Rätzer, Fani Papagiannouli and Ingrid Lohmann. **The *cis*-regulatory code of Hox function in Drosophila.** *The EMBO Journal*, 31(15), Published online 10 July 2012, pp.3323–3333.

* equal contribution

In the following people are listed who contributed experimental data to this thesis.

Sebastian Sorge designed and constructed the Dfd^{NAE667}-Flp-construct and *Dfd-siRNA*, established some of the fly lines and performed a statistical analysis on nerve outgrowth that is described in chapter 2.6.

Fatmire Bujupi conceived and conducted the angle measurements and imaging of the $tubGAL80^{ts}$,Dfd^{NAE667}:: *IMPTNT*(*V1*) and $tubGAL80^{ts}$,Dfd^{NAE667}:: *TNT-R* animals. The results of the experiment are shown in figure 2.6.

Dr. Michael P. Eichenlaub conducted the imaging of transiently injected medaka embryos shown in Figure 2.19.

Natalie Grace Schulz conducted the fluorescent *in-situ* hybridisation on *Deformed* and *Connectin* shown in Figure 2.11.

1__ Introduction

1.1 Development of the Fly's Central Nervous System

In *Drosophila,* the fertilised egg is able to develop a functional nervous system in only 21 hours, a remarkably short time. The fly's central nervous system (CNS) can be subdivided into the brain and the segmental units of the ventral nerve cord (VNC), called neuromeres. The brain can be divided further into the supraesophageal zone (SPZ) and the subesophageal zone (SEZ) (Ito et al. 2014). While the SPZ comprises of the protocerebral, deutocerebral and tritocerebral neuromeres, the SEZ is formed by the mandibular, maxillary and labial neuromeres. The VNC is formed by the thoracic and abdominal neuromeres.

The CNS arises from the neuroectoderm located in the ventral-lateral region of the *Drosophila* embryo (**Figure 1.1, B**). The neuroectoderm is patterned during early stages of embryogenesis into neural equivalence groups. Cells within each equivalent group interact in order to select one cell to acquire the fate of a CNS stem cell. Neural stem cells, called neuroblasts (NBs) in *Drosophila*, are the basic building blocks of the fly CNS. Once selected, the NB enlarges and delaminates from the neuroectoderm in a precise spatiotemporal pattern to the interior of the embryo (Skeath & Thor 2003) (**Figure 1.1, A and B**). NBs delaminate in five waves, beginning at stage 9 of embryogenesis and concluding at stage 11. From anterior to posterior the embryonic CNS in *Drosophila* is symmetric. Hence, each neuromere can be split into halves (referred to as hemineuromeres), which are separated by the CNS midline. Within each hemineuromere, a stereotypic pattern of approximately 30 NBs is created (**Figure 1.1, C**). Dependent on the time point and position of its delamination, the combinatorial code of genes its

expresses, and the lineage it gives rise to, each NB acquires a unique identity. Detailed maps of NB patterns have been created for all the segments in *Drosophila* (Doe 1992; Broadus et al. 1995; Urbach 2003; Urbach & Technau 2003; Urbach et al. 2003; Birkholz, Rickert, et al. 2013; Urbach et al. 2016). Strikingly, the number of NBs has been shown to be neuromere specific and varies, especially in the brain and in the tail (Birkholz, et al. 2013; Urbach et al. 2016). Moreover, NBs developing in the same location in every segments are characterised by their similar identity and, hence, represent serial homologs (Skeath & Thor 2003; Technau et al. 2006)

The newly delaminated NB begins to divide in a series of self-renewing, asymmetric divisions, giving rise to chains of smaller secondary precursor cells, called ganglion mother cells (GMCs) (**Figure 1.1, B**). Asymmetric cell division in NBs is controlled by basal and apical protein complexes, which function in concert to allow the partitioning of the cell-fate determinant Prospero (Pros) exclusively into GMCs. Pros is tethered to the basal cortex of NBs by Miranda, which hinders Pros to enter the nucleus during mitosis (Spana & Doe 1995; Shen et al. 1997). Once inherited to the GMC, Pros transiently localises to the cell cortex before it enters the nucleus and facilitates cell-cycle exit and differentiation. The apical complex controls the orientation of the mitotic spindle and is sequestered during interphase. It comprises of Inscuteable (Insc), Bazooka (Baz), Partner of inscuteable (Pins), atypical protein kinase C (aPKC), Mushroom body defect (Mud), the heterotrimeric G-protein α- subunit Gαi, and members of the partitioning-defective (Par) complex (reviewed by Betschinger & Jürgen A Knoblich 2004; Juergen A Knoblich 2008; Buchman & Tsai 2007). Additional proteins are recruited during metaphase (Albertson & Doe 2003; Barros et al. 2003; Erben et al. 2008). A cascade of protein interactions within the complex leads to the attraction of one of the spindle poles towards the apical side late in mitosis thereby triggering the correct formation of the spindle. GMCs are usually placed opposite to the epithelia-NB contact site. This apical-basal polarity is achieved by extrinsic signalling towards the NBs from the overlaying epithelium (Siegrist & Doe 2006).

GMCs divide once to produce postmitotic neurons and/or glial cells, thus generating a final pool of around 400 postmitotic cells per hemineuromere (Skeath & Thor 2003) (**Figure 1.1, B**). Individual postmitotic cells within the pool are unique in their fate and molecular identity. They express specific cell lineage markers, decisive for their morphologies and synaptic partners, expression of neurotransmitters, neuropeptides or ion channels (Schmid et al. 1999).

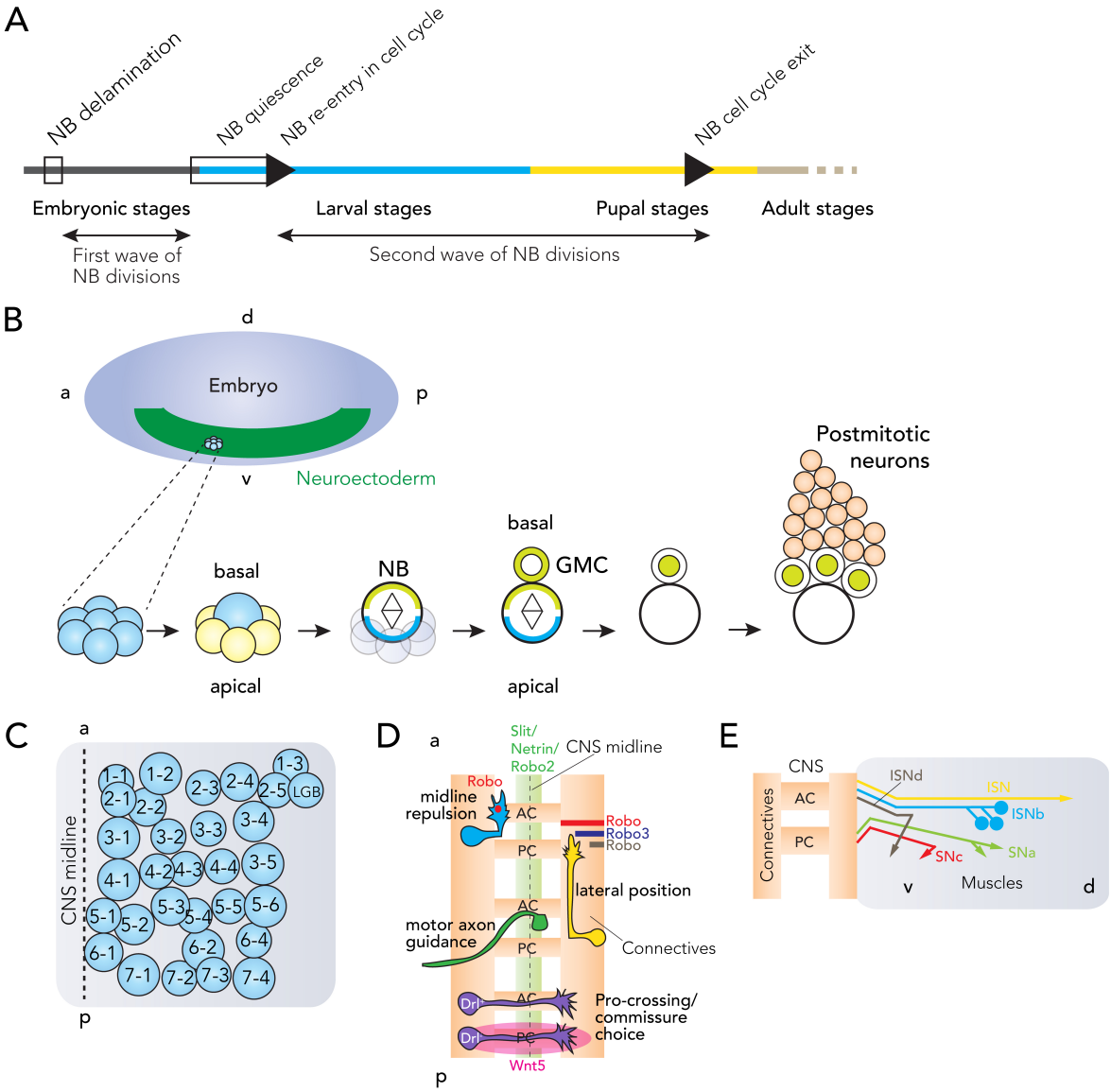

Figure 1.1: Overview of CNS development in *Drosophila*. (**A**) Time line depicting the two waves of NB divisions during *Drosophila* development. NBs delaminate and undergo several rounds of cell divisions before they arrest their cell cycle and become quiescent at the end of embryogenesis. They re-enter mitosis and start to proliferate again during larval stages. NBs leave the cell cycle at different phases during pupal stages and disappear. (**B**) Scheme of a stage 9 embryo. NBs delaminate from the neuroectoderm (green). In each equivalent group (blue), one cell is selected to become a stem cell (blue). This NB enlarges and moves from the external surface to the interior of the embryo. Soon after the NB is delaminated, it starts to divide in an asymmetric manner. Divisions are controlled by basal (light green) and apical (blue) protein complexes. Pros (light green) is sequestered to the basal cortex of the NB and segregates into the GMC, where it transiently remains at the cortex, but rapidly translocates to the nucleus. GMCs give rise to postmitotic lineages (orange). a, anterior; p, posterior; d, dorsal; v, ventral. (**C**) Scheme of a representative abdominal hemineuromere. The pattern of 30 NBs (and the additional longitudinal glioblast) are depicted. (**D**) Summary of axon guidance decisions within the CNS. Midline guidance (repulsion or pro-crossing), commissure choice, lateral positioning and motor-axon guidance are shown. See details in the text. (**E**) Motoneuron axon pathways in *Drosophila*. Motoneurons exit the CNS into one of five nerve branches to innervate specific muscles in the body wall. Figures adapted from Homem and Knoblich (Homem & Knoblich 2012), Skeath and Thor (Skeath & Thor 2003), Technau et al. (Technau et al. 2006), Araúja et al. (Araújo & Tear 2003), and Evans (Evans 2016).

In the embryonic VNC, postmitotic cells cluster into motoneurons (36 per abdominal hemineuromere), interneurons (270 per abdominal hemineuromere) (Rickert et al. 2011) and glia (32 per abdominal hemineuromere) (Ito et al. 1995; Stork et al. 2011; Beckervordersandforth et al. 2008). Remarkably, the whole larval CNS is formed by primary neurons, which are produced in the embryo during the first wave of NB divisions (**Figure 1.1, A**). The majority of NBs in the abdominal segments undergo programmed cell death (PCD) after they have produced their whole neuronal lineages. In contrast, NBs in the brain- and thoracic-region arrest their cell cycle and remain quiescent until the late phase of the first larval stage (**Figure 1.1, A**) (reviewed by Egger et al. 2008; Homem & Juergen A Knoblich 2012). Only then, NBs re-enter mitosis and generate secondary neurons in a second wave of neurogenesis. Secondary neurons form the bulk of the adult-specific neurons in the CNS, but remain immature during larval stages. They begin to mature during pupal stages and alongside with the remaining, yet reconfigured, primary neurons form the adult CNS (reviewed by Egger et al. 2008; Homem & Juergen A Knoblich 2012) (**Figure 1.1, A**).

Embryonically born neurons start to differentiate around embryonic stage 12, after the majority of NBs have delaminated. They extend axons, which are guided within the embryo by stereotypic axon guidance decisions (**Figure 1.1, D**). These are determined by the molecular identity of the neuron and the presence of molecules secreted by, or displayed on the cell membrane of other neurons and/or glial cells. Despite the relative simplicity of the embryonic CNS, guidance decisions are complex (**Figure 1.1, D**). In *Drosophila*, the axon tracts of the CNS are organised in a latter-like structure, with longitudinal tracts positioned either side of the midline cells and two commissures within each segment, which extend across the midline and connect both sides (Nassif et al. 1998). Most axons cross the midline once to project on the contralateral side of the CNS, yet never cross again.

Midline guidance of axons is controlled by two major signalling pathways, the Frazzled (Fra)-Netrin (Net) pathway that mediates attraction (Kolodziej et al. 1996; R. Harris et al. 1996; Mitchell et al. 1996), and the Slit-Roundabout (Robo) pathway, which mediates repulsion (Kidd, Brose, et al. 1998; Kidd et al. 1999; K. Brose et al. 1999) (**Figure 1.1, D**). Net is secreted by midline glial cells and attracts axons expressing the Fra-receptor. In addition, midline cells secrete Slit, which prevents abnormal midline crossing by repelling Robo-expressing axons. However, before crossing the midline, Robo repulsion is inhibited by Commissureless (Comm) or Robo2, which is expressed on

midline cells (Kidd, Russell, et al. 1998; Keleman et al. 2002; Keleman et al. 2005; Evans et al. 2015).

The choice in crossing the proper commissure is regulated by secreted Wnt5 and its receptor Derailed (Drl) (Bonkowsky et al. 1999; Yoshikawa et al. 2003) (**Figure 1.1, D**). Wnt5 is expressed in a region around the posterior commissure and acts to repel axons expressing the Drl receptor, which in turn project across the anterior commissure. Axons that do not express Drl cross in the posterior commissure.

The lateral position within longitudinal axon tracts is specified by the set of Robo receptors the axon expresses (Rajagopalan, et al. 2000; Simpson et al. 2000). Axons closest to the midline express Robo, axons within an intermediate zone are characterised by the expression of Robo and Robo3, and axons in the outer-most zone express Robo, Robo2 and Robo3 (**Figure 1.1, D**).

1.2 Neuromuscular Connectivity

Thirty-six motor neurons per hemineuromere of the VNC send their axons through one of the five branches of peripheral nerves, the intersegmental nerves (ISN, ISNb and ISNd) and segmental nerves (SNa and SNc) (Landgraf et al. 1997) (**Figure 1.1, E**). Each side of the abdominal body wall comprises 30 muscles per segment, which are innervated by the thirty-six motoneurons in a highly stereotypic manner. The muscles can be clustered into specific domains, dependent on the specific branch a given domain is innervated by ISN motoneurons target internal muscles in the dorsal, dorsal-lateral, ventral and ventral-lateral domain, whereas those of the SN innervate external muscles in the lateral and ventral domains. Notably, transcription factors are known to regulate the choice of branch (reviewed by Landgraf & Thor 2006). Projection to the dorsal branch ISN is regulated by the homeobox-transcription factor Even-skipped (Eve) (Landgraf et al. 1999), while projections to the ventral branches ISNb and ISNd are controlled by the homeobox proteins HGTX/Nkx6 (Broihier et al. 2004), Exex/Hb9 (Broihier & Skeath 2002), Islet/tailup, Lim3 (Certel & Thor 2004; Thor et al. 1999) and Drifter/Ventral veins lacking (Vvl).

Motor axons leave the CNS in bundles that split into the five distinct nerve branches described above, in a process called axon defasciculation. To date, several genes that regulate the processes of motor axon defasciculation and motor axon guidance in invertebrates have been described (reviewed by Araújo & Tear 2003). Mutations of these genes cause the failure of axons to leave their common motor pathway at choice points

and therefore fail to enter their appropriate muscle fields. Instead, axons remain closely fasciculated, a phenomenon described as bypass phenotype (Krueger et al. 1996; Fambrough & Goodman 1996; H. H. Yu et al. 1998). Another prominent phenotype that is caused by disruptions in motor axon guidance, is revealed by the stalling of axon, which in turn fail to innervate target muscles (Hu et al. 2001).

Once a motoneuron, which is guided through peripheral nerves, reaches the area with the prospective target muscle, target recognition molecules expressed by the muscle and/or motoneuron facilitate the matching between the two partners (reviewed by (Nose 2012). The process of target finding is highly specific as the motoneuron selects its unique target muscle with remarkable reproducibility. Correct matching in turn leads to the formation of synapses. Interestingly, pre- and post-synaptic partners have been shown to actively seek and find each other (Kohsaka & Nose 2009).

Target recognition molecules can be either attractive, including Capricious (Caps) (Shishido et al. 1998; Kurusu et al. 2008), Connectin (Con) (Nose et al. 1992; Nose et al. 1997), FasII (G. W. Davis et al. 1997; Kohsaka et al. 2007), FasciclinIII (FasIII) (Chiba et al. 1995; Kose et al. 1997) or NetrinB (NetB), or repulsive, such as Wnt4 and Sema2a. Whereas Wnt4, Sema2a and NetB are secreted factors, Caps, Con, FasIII are homophilic membrane spanning cell-adhesion molecules (CAMs), which are expressed on both synaptic partners, in subsets of muscles and the motoneurons that innervate these muscles. For example, Caps, a transmembrane protein with leucine-rich repeats, is expressed in the RP5 motoneurons and its target muscle, M12. Ectopic expression of *caps* in the neighbouring not-target muscle M13 leads to an inappropriate innervation of this muscle in addition to M12 (Shishido et al. 1998). However, *caps* loss-of-function mutants do not reveal dramatic targeting phenotypes as the closely related Tartan molecule was shown to act redundantly (Kurusu et al. 2008). Moreover, Caps has been shown to cluster at the tips of myopodia, dynamic protrusions on the *Drosophila* muscle. Simultaneous live imaging of presynaptic motoneurons and postsynaptic myopodia revealed that initial neuromuscular contacts are made between the tips of myopodia, where Caps accumulates (Kohsaka & Nose 2009), and motoneuron protusions (called filopodia).

It has been generally shown that loss-of-function of target recognition molecules, like Caps, only partly disrupts synaptic matching (Nose et al. 1994; Chiba et al. 1995; Nose et al. 1997; Shishido et al. 1998; Abrell & Jäckle 2001). This supports the idea that information of multiple attractive and/or repulsive cues will finally be integrated by the

motoneuron in a dynamic and flexible manner in order choose the proper target muscle (relative balance model, (Winberg et al. 1998).

1.3 Synapse Formation in developing Motor Systems

Synapses build fundamental units in developing motor systems and enable complex behaviours. They are asymmetric in their structure, comprising a presynaptic membrane that contains neurotransmitter-filled vesicles, and a postsynaptic membrane harbouring receptors that bind to the neurotransmitter(s) released by the presynaptic cell. The neuromuscular junction (NMJ) is a type of synapse that forms between motoneurons and muscles and uses different, species-specific neurotransmitters. As one example acetylcholine is used in vertebrates and glutamate in *Drosophila* to evoke muscle excitation and contraction. In *Drosophila*, a single muscle bundle can receive innervation from up to four motoneurons (Hoang & Chiba 2001). However, in vertebrates multiple motoneurons initially innervate one muscle and later in development are eliminated with the exception of one residing motoneuron (Sanes & Lichtman 1999).

Drosophila NMJ development is characterised by the differentiation of growth cones at the tip of the axon of motoneurons into presynaptic terminals during late stages of embryogenesis (reviewed by K. P. Harris & Littleton 2015). Prior to this, the axonal growth cone has to get in contact with its target muscle, where postsynaptic glutamate receptors (GluRs) begin to cluster at the contact site (**Figure 1.2, A and B**). Mature NMJs comprise oval-shaped synaptic boutons with multiple active zones (AZs), highly specialized neurotransmitter release sites that are located opposite to a distinct GluR cluster on the postsynaptic muscle (**Figure 1.2, B**). In addition to GluRs, the complex postsynaptic membrane, which is called subsynaptic reticulum (SSR), often forms numerous folds and invaginations and harbours ion channels, scaffolding and adhesion molecules, and postsynaptic signalling complexes (**Figure 1.2, B**).

During postembryonic development, NMJs expand significantly due to dramatic growth during the larval period. As the postsynaptic surface area of each muscle increases by up to 100-fold, the number of total boutons and number of AZs per bouton increases by up to 10-fold (Schuster et al. 1996).

Synaptic assembly at the presynaptic AZ of the NMJ requires a dense network of scaffolding proteins, termed the cytomatrix of the active zone (CAZ) (reviewed by K. P. Harris & Littleton 2015) (**Figure 1.2, C**). The CAZ functions as a protein-binding hub for other presynaptic components and facilitates synaptic vesicle docking and fusion. The

networks of proteins can be identified as electron-dense specializations, so called T-bars. Besides the major AZ scaffolding protein Bruchpilot (Brp) (Kittel et al. 2006), which shapes the structure of the T-bar, *Drosophila* RIM-binding protein (DRBP) (Liu et al. 2011), Rho GTPase activating protein at 100F (Syd-1) (Owald et al. 2010), Liprin-α or the voltage-gated N-type Calcium channel Cacophony (Cac) (Kawasaki et al. 2004; Owald et al. 2010) localise within the AZ protein network. Mutants of these genes show defects in synaptic assembly and organisation, T-bar formation or calcium channel clustering, leading to failures in neurotransmitter release (Kawasaki et al. 2004; Owald et al. 2010). Cac was also shown to have a dual role promoting not only bouton formation, but also synaptic vesicle fusion important for neurotransmission (Rieckhof et al. 2003; Xing et al. 2005).

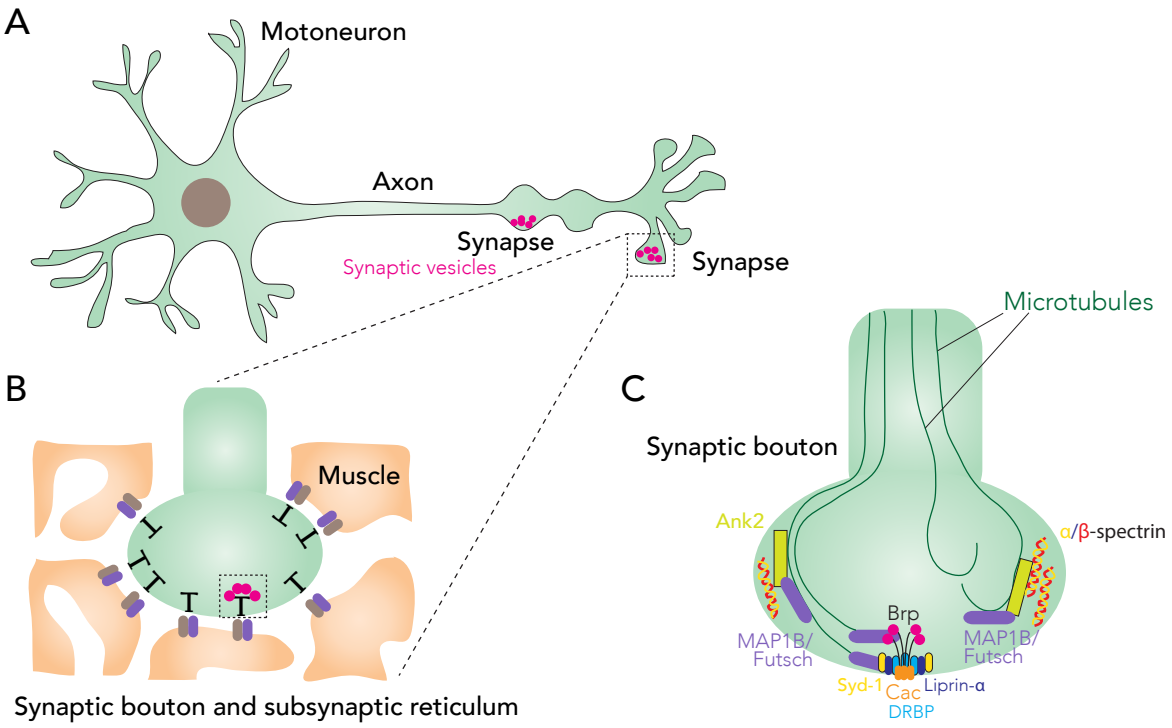

Figure 1.2: Structure of motoneurons and synaptic boutons at the NMJ in *Drosophila*. (**A**) Simplified scheme of a motoneuron. Synaptic boutons are filled with synaptic vesicles (pink). (**B**) Magnification of a single bouton at the NMJ. The presynaptic terminal is embedded in the subsynaptic reticulum (SSR) of the muscle, which is deeply folded. An exemplary active zone (AZ) is indicated by the dashed square. AZ are characterised by T-bars, which consist of synaptic vesicles bound to Brp, and are located opposite to ionotropic glutatame receptors (GluRs) on the postsynaptic site. (**C**) Scheme depicting the organisation of a synaptic bouton. The cytomatrix of the active zone (CAZ) comprises a network of scaffolding proteins. The microtubule cytoskeleton is connected to the AZ via MAP1B/Futsch, which binds to Brp and Cac. Ank2 links α/β-spectrin subunits and microtubules, or membrane spanning cell-adhesion molecules (not shown), respectively. Figures adapted from Harris and Littleton (K. P. Harris & Littleton 2015), Bodaleo and Gonzalez Billault (Bodaleo & Gonzalez-Billault 2016), and Chia et al. (Chia et al. 2013).

Fusion of synaptic vesicles and release of neurotransmitters at AZs in *Drosophila*, which in turn activates postsynaptic glutamate receptors, is triggered by stimulus-induced calcium influx into the axon terminal (Neher & Sakaba 2008). Synaptic vesicle fusion and neurotransmitter release are mediated by the SNARE complex (Weber et al. 1998) and Synaptotagmin (Syt) (DeBello et al. 1993). Vesicle-anchored v-SNAREs (Synaptobrevin) and target-membrane t-SNARE (Syntaxin and SNAP-25) form a complex and, hence, facilitate the close contact between the plasma membrane and the synaptic vesicles. Rapid calcium-dependent fusion of vesicles is accomplished by proteins, which directly bind to the SNARE complex, including Syt. Syt is an integral membrane protein of synaptic vesicles and functions to sense Calcium influx (DeBello et al. 1993).

Synaptic vesicle- and AZ-proteins are synthesised in the cell body and transported to synapses by microtubule-based molecular motor proteins, such as kinesins and dyneins. The proper polarity of microtubule filaments allows the anterograde and retrograde trafficking of cargos along the axon (reviewed by Chia et al. 2013). In addition to this, microtubules are present at NMJ presynaptic terminals where they play crucial roles in the establishment and maintenance of synapses (Sanes & Lichtman 1999; Roos et al. 2000). The *Drosophila* homolog MAP1B/Futsch directly interacts with presynaptic microtubules and connects components of the AZ, like Brp and Cac, and microtubules (Hummel et al. 2000; Roos et al. 2000; Lepicard et al. 2014) (**Figure 1.2, C**). These interactions are crucial for the stability of microtubules at presynaptic endings and for the integrity of AZs.

Moreover, studies on *Drosophila* NMJs have uncovered the importance of the presynaptic spectrin-actin cytoskeleton for synapse stability. Spectrin forms hetero-tetramers, which consist of α- and β-spectrin subunits, and can interact with actin filaments to form a spectrin-actin network. This spectrin-based skeleton is linked to various membrane proteins, including neural cell adhesion molecules (CAMs), via adaptor proteins of the Ankyrin family and has been shown to be essential for the organisation and maintenance of two specific CAMs, Neuroglian (Nrg) and FasciclinII (FasII), at the synapse. Loss of presynaptic spectrins results in the loss of Nrg and FasII prior to synapse retraction, which finally lead to the disassembly and elimination of the NMJ (Pielage et al. 2005). In *Drosophila,* two *ankyrin* genes exist, the ubiquitously expressed *ankyrin1* gene, which is enriched in postsynaptic muscle membranes of the NMJ (Dubreuil & J. Yu 1994) (Pielage et al. 2006), and the neural gene *ankyrin2* (*ank2*) (Bouley et al. 2000; Hortsch et al. 2002).

Ank2 does also provide a link between the spectrin-based cytoskeleton and the core presynaptic microtubule cytoskeleton (Koch et al. 2008; Pielage et al. 2008) (**Figure 1.2, C**). Disruptions in the spectrin cytoskeleton consequently affect microtubule organisation and in turn lead to the disassembly of the synapse (Pielage et al. 2005; Massaro et al. 2009). Ank2 giant isoforms (Ank2-L and Ank2-XL) are known to form a membrane-associated microtubule organising complex with MAP1B/Futsch, which is essential for microtubule organisation, synapse stability and function (Stephan et al. 2015).

Notably, disruptions in the microtubule-dependent transport and microtubule cytoskeleton at synapses are believed to contribute to the pathogenesis of neurodegenerative diseases.

1.5 Development of Motor Behaviours in *Drosophila*

Drosophila embryos perform peristaltic movements similar to those observed in mature larvae (Pereanu et al. 2007; Crisp et al. 2008; Crisp et al. 2011). However, before movements become coordinated and complex, they are locally restricted to single segments and consist of body wall twitches, which reflect weak muscle contractions (**Figure 1.3**). These first and brief muscle twitches appear about 14 hours after egg laying (h AEL) and become stronger and more frequent as development proceeds. At the end of embryogenesis, movements are matured and rhythmic and can be clustered into active and inactive phases. Local muscle twitches are replaced by coordinated peristaltic forward and backward waves of high frequency and along the entire body length. Shortly before the late embryo/first instar larva hatches out of the eggshell, these peristaltic waves of contraction are accompanied by frequent strong head flexion and extension. Crucially required for hatching is the alternating elevation and depression of mandible derived structures, so-called mouth hooks (MHs), which are part of a sclerotised head skeleton (referred to as cephalopharygeal skeleton, CPS).

Coordinated movements in the late embryo represent the original state of all behavioural patterns in the *Drosophila* larva, like forward and backward locomotion, which is temporary halted by bending and turning, rearing and burrowing behaviour (Pereanu et al. 2007). Bending of the head often occurs in between phases of larval feeding in order to search for food. Feeding is a relatively simple, yet crucial behaviour characterised by coordinated and rhythmic movements of distinct muscles in the larval head. Notably, feeding cycles include some of the stereotypic movement patterns that

have been used already earlier in development for larval hatching, head flexion and extension and the coordinated movements of the MHs.

Peristaltic waves move the larva forward and backward. Peristaltic crawling has been analysed extensively and was shown to be regulated by *Hox* genes (Dixit et al. 2008). Dixit and colleagues examined the crawling behaviour of larvae deficient for the entire bithorax-complex (BX-C) and revealed their complete inability to perform peristaltic movements, indicating that the motor systems required for crawling are under the control of the BX-C. In contrast, peristaltic movements expanded from the abdomen towards more anterior segments when a certain gene of the complex, Ultrabithorax (Ubx), was ectopically expressed in all segments (Dixit et al. 2008).

The onset of movements in the *Drosophila* embryo matches the time point of neuromuscular maturation. The first action potentials that trigger the contraction of muscles are generated in motoneurons 17 hours AEL, around stage 17b of embryonic development.

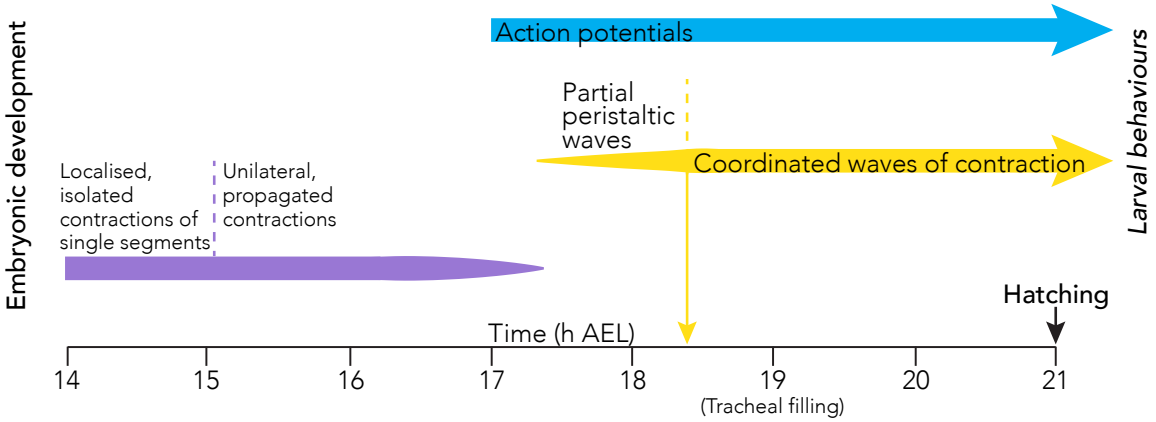

Figure 1.3: Timeline of motor behavioural development in *Drosophila*. Summary diagram showing the behavioural and electrical (Action potentials) development of motor behaviour during embryogenesis. 16-18.5 hours AEL (h AEL) correspond to stages 17b-d of Pereanu et al. (Pereanu et al. 2007). At 19 h AEL the trachea fill with air. Figure adapted from Crisp et al. (Crisp et al. 2008; Crisp et al. 2011).

1.6 Feeding Behaviour in *Drosophila*

In adult flies, feeding is accomplished by the extension and retraction of the proboscis followed by the opening and closing of the labellar lobes at the tip of the proboscis (Flood et al. 2014). The labellum depicts the insect equivalent of the vertebrate tongue and is covered with taste sensilla. Stimulation of gustatory receptor neurons (GRN) housed within these sensilla triggers the extension of the proboscis. The rhythmic activity of the pharyngeal pump is further used for food ingestion (Flood et al. 2014).

Taste information is relayed to the primary taste centre of the fly brain, the subesophageal zone (SEZ), where taste neuron activity has been shown to directly affect the activity of motoneurons, which innervate the musculature of the proboscis (Gordon & Scott 2009). As one example, activation of the gustatory receptor 5a has been shown to evoke attractive taste behaviours, including the proboscis extension reflex (PER) (Zhang et al. 2007; Gordon & Scott 2009).

Feeding behaviour in *Drosophila* larvae is characterised by the motor output of well-described neuromuscular units in the larval head (**Figure 1.4**, Schoofs et al. 2010). The motor units mediating the uptake of food consist of muscle bundles that are coupled to the MHs. One pair of muscle bundles is attached to the dorsal protuberance of the MH and is referred to as the mouth hook elevator (MHE). Elevation of the MHs is accomplished by the activity of the MHEs. Two pairs of muscle bundles are attached to the ventral extension of the MH to form the mouth hook depressor (MHD), which enables the depression of the MHs. Innervation of these muscles is realised by motoneurons that converge within the maxillary nerve. The maxillary nerve emerges from the maxillary neuromere, exits the connectives at the level of the anterior maxillary commissure and is homologous with the SN of the abdominal and thoracic VNC (Nassif et al. 1998). Food ingestion is achieved by pharyngeal pumping and the contraction of the cibarial dilator musculature (CDM), which receives input from the antennal nerve (Schoofs et al. 2010). In order to take up and ingest food, the larval head is tilted by the action of the dorsal protractor muscles A and B ($Pro_{do}A$ and $Pro_{do}B$), which attach the head skeleton to the body wall of the larva. Both protractor muscles are innervated by the prothoracic accessory nerve (PaN). Feeding-related motoneurons have been traced and assigned to distinct clusters within the SEZ according to their anatomy (Hückesfeld et al. 2015). A tight cluster of up to 11 motoneurons has been shown to project via the AN, whereas axons of only two neurons were labelled within the PaN. In total, 9 motoneurons were identified at the ventral-lateral border of the SEZ to project via the maxillary nerve.

Manipulation of these feeding-related motoneurons by blocking synaptic transmission completely eliminated food ingestion and all feeding-related MH and head movements (Hückesfeld et al. 2015).

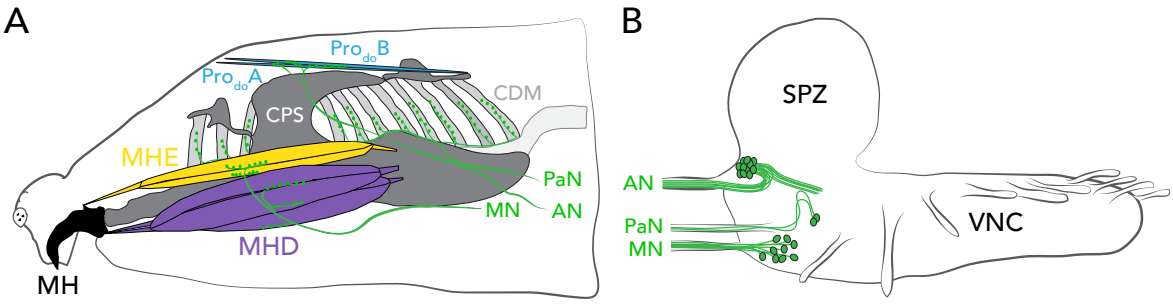

Figure 1.4: The feeding motor system of *Drosophila* larvae. (**A** and **B**) Schematic drawings of the muscles, nerves and neurons involved in feeding in the *Drosophila* larva. (**A**) Lateral view of the larval head. Several muscles are attached to the head skeleton (cephalopharyngeal skeleton, CPS) and innervated by distinct nerves. MH, mouth hooks; MHE, mouth hook elevator; MHD, mouth hook depressor; Pro$_{do}$A/B, dorsal protractor muscle A/B; CDM, cibarial dilator muscle; MN, maxillary nerve; AN, antennal nerve; PaN, prothoracic accessory nerve. (**B**) Lateral view of the larval CNS. Motoneurons within the SEZ and their respective nerve routes are highlighted in green. SPZ, Supraesophageal zone; VNC, ventral nerve cord. Figures adapted from Schoofs et al. and Hückesfeld et al. (Schoofs et al. 2010; Hückesfeld et al. 2016; Hückesfeld et al. 2015).

1.7 *Hox* Genes in *Drosophila* Neural Development

Precise connections between motoneurons and their postsynaptic targets are pivotal for basic behaviours, like feeding. Motor units that shape basic behaviours are established during embryogenesis. In the embryo, patterning systems define the molecular profiles of neural progenitors and their postmitotic progenies, ensuring a tremendous diversity in neural subtypes. Work over the past decade revealed that subtype identity is conferred to neurons dependent on their position along the anterior-posterior axis of animals (Dasen & Jessell 2009).

Hox genes encode an important class of transcriptional regulators that endow neural cell types with positional identity. They are strikingly conserved among the animal kingdom and are generally found in clusters or complexes in a collinear arrangement. The position of *Hox* genes within the complex reflects the relative position of the cells and structures they specify along the anterior-posterior axis. In *Drosophila*, *Hox* genes cluster into two main complexes, the antennapedia-complex (Antp-C) and the BX-C.

The Antp-C encodes five *Hox* genes, *labial* (*lab*), *proboscipedia* (*pb*), *Deformed* (*Dfd*), *Sex combs reduced* (*Scr*) and *Antennapedia* (*Antp*). Another three *Hox* genes, *Ubx*, *abdominal-A* (*abd-A*) and *Abdominal-B* (*Abd-B*) constitute the BX-C. *Hox* gene expression and function has been shown in the embryonic and larval CNS, in neural stem cells as well as postmitotic cells (Rogulja-Ortmann & Technau 2014; Birkholz et al. 2013; Rogulja-Ortmann et al. 2008; Becker et al. 2016; Urbach et al. 2016; Birkholz, Rickert, et al. 2013; Kuert et al. 2012; Kuert et al. 2014; Hirth et al. 1998; Cobeta et al. 2017; Gummalla et al. 2014).

In order to promote segmental diversity in the CNS, *Hox* genes control various aspects of embryonic and postembryonic CNS development, such as cell-specification and cell number. At the level of cell-type specification, *Hox* genes control the segment-specific identity of NBs. Abdominal NBs, for example, are often specified differently to their serial homologs in the thoracic neuromeres. Analysis on the fate of NB-1-1 revealed that *Ubx* and *abd-A* are required and sufficient to induce the abdominal fate of NB1-1 (Udolph et al. 1993; Prokop & Technau 1994). NB1-1 in abdominal neuromeres generates mixed lineages of motoneurons and glial cells. However, in thoracic neuromeres it gives rise exclusively to neurons. NB7-3 is controlled via similar regulatory mechanisms (Rogulja-Ortmann et al. 2008). The abdominal fate of NB6-4 is specified by *abd-A* and *Abd-B* (Berger et al. 2004), whereas the thoracic NB6-4 does not require Hox-input for proper specification. Another recent study revealed that mutations in *Dfd* lead to homeotic transformations of the maxillary NB6-4 (Becker et al. 2016). The maxillary NB6-4 usually give rise to only glial cells, however, mixed lineages comprising neurons and glial cells were formed in Dfd^{16}-mutant embryos, equal to those of NB6-4 located in the labial neuromere (Becker et al. 2016).

Cell numbers are regulated by cell proliferation or elimination and contribute to segmental diversity. The controlled elimination of cells can be achieved by a common mechanism, programmed cell death (PCD). Compared to an invariant number of NBs in abdominal and thoracic neuromeres, the amount of NBs in the SEZ and in the tail region of the embryo is remarkably diminished (Birkholz et al. 2013; Urbach et al. 2016). This can be attributed to the activity of Dfd and Abd-B, which suppress the formation of NBs in the mandibular and anterior part of the maxillary neuromeres, or in the abdominal neuromere A10, respectively. Therefore, normal expression of both *Hox* genes is pivotal for the reduced number of NBs in these segments. Previous fate mapping analysis on NBs within the SEZ have uncovered a slightly increased number of NBs within the maxillary segment in *Dfd* null-mutant embryos compared to wildtype, comprising an

ectopic NB at the position of NB6-4 (Urbach et al. 2016). NB6-4 has also been found in cell-death deficient *Df(3L)H99* embryos showing that PCD normally suppresses the formation of this NB (Urbach et al. 2016). This is in line with studies in the larval SEZ, where clonal loss-of-function of *Dfd* in postembryonic SEZ cells lead to ectopic NB lineage formation (Kuert et al. 2014). Ectopic lineages similar to those found in *Dfd* mutant clones were recovered when apoptosis-blocked NBs were induced, indicating again that Dfd prevents the formation of ectopic NB lineages in the wild-type larval SEZ by inducing apoptosis in the corresponding NBs (Kuert et al. 2014). The same findings have been described earlier for the *Hox* gene *labial* (Kuert et al. 2012).

As mentioned earlier, the majority of embryonic NBs in the abdominal neuromeres undergo PCD at the end of embryogenesis. Dividing postembryonic NBs are limited in their proliferative capacity by cell death, rather than cell cycle. A pulse of Abd-A protein in third-instar larvae triggers apoptosis and, hence, limits the production of neural progenies in abdominal neuromeres (Bello et al. 2003). In addition to NBs, PCD is abundant in the majority of postmitotic neurons within NB lineages. Segment-specific elimination of the GW motoneuron, which is part of the NB7-3 lineage, depends on the expression of *Antp* (Rogulja-Ortmann et al. 2008). Antp is required for the survival of this particular neuron in the labial neuromere, however, in abdominal segments this neuron undergoes cell death.

Moreover, Hox regulation in *Drosophila* has been linked to neuronal differentiation. As one example, Lab is crucial for the development of the tritocerebrum and loss of functional *lab* has been associated with regionalised patterning defects in the embryonic brain (Hirth et al. 1995). Postmitotic cells are generated in these mutants, yet do not acquire the proper identity and fail to extend axons.

A role of *Hox* genes in the control of motor patterns underlying crawling behaviour has been addressed in one of the previous chapters. In general, crawling movements rely on the proper connection between motoneurons and their respective target muscles. A recent study from Hessinger et al. uncovered that Ubx function is required for the establishment of target specificity between motoneurons and muscles (Hessinger et al. 2017). Ubx exerts its dual function by regulating the expression of *Wnt4* in the muscle, whereas it interacts with the Wnt4-signalling pathway in the matching motoneuron.

1.8 Aims of this Thesis

More recent progress in understanding the role of *Hox* genes in the development of the CNS comes from studies in *Drosophila* and vertebrates (Philippidou et al. 2012; Baek et al. 2013; Catela et al. 2016). All these studies provide evidence for a general function of Hox transcription factors in the direct transcriptional control of genes required at subsequent steps during development of motoneurons and beyond.

Therefore, the main motivation of this study was to

evaluate the role of the Hox gene Deformed in the establishment and maintenance of motor systems in Drosophila.

The first aim of this project was to characterise the expression of *Dfd* in the fly nervous system and within a particular motor unit in the head of *Drosophila*. To approach this, embryos as well as larvae were analysed in order to visualise *Dfd*-expressing motoneurons and their corresponding target muscles.

Second, this study aimed to unravel the critical steps in the establishment of the motor unit under Dfd control. To this end, different approaches were used to interfere with the function of Dfd at different stages during development. Subsequently, morphological phenotypes and behavioural outputs were analysed in embryos and larvae.

Finally, this work aimed to break down the molecular basis of motor unit formation, function and maintenance. To that end, the expression of recently identified, putative transcriptional targets of Dfd was examined in animals of different genetic background.

2 Results

2.1 Deformed is expressed in Neural Cells of the Subesophageal Zone

In *Drosophila* the Hox protein Deformed (Dfd) has been shown to be regionally expressed in differentiated neurons of the mandibular and anterior half of the maxillary neuromeres of the SEZ (Hirth et al. 1998).

First, the expression pattern of Dfd during neural development was analysed in more detail, beginning in NBs. Comprehensive NB maps summarize the expression of homeotic and other genes in the SEZ and show that Dfd is expressed in all NBs of the mandibular and anterior half of the maxillary neuromere (Urbach et al. 2016).

Immunolabelling experiments were carried out with a Dfd specific antibody and antibodies against Prospero (Pros) and Engrailed (En). The transcription factor Pros is expressed in NBs and segregates into NB progenies during asymmetric cell divisions. En is a segment polarity gene, which is expressed in posterior NBs, thereby indicating segmental boundaries. Strong expression of Dfd in all Pros-labelled NBs located within the mandibular and anterior half of the maxillary neuromere was observed at late stage 11 of embryogenesis (**Figure 2.1, A**). At this developmental stage the final pattern of NBs is established, with a total of around 26 NBs per maxillary hemisegment and around 22 NBs per mandibular hemisegment aside the two unpaired median NBs (MNBs) (Urbach et al. 2016). Later on, around stage 16 of embryonic development, Dfd expression was found in a variety of neurons within its expression domain, stained by the postmitotic marker Embryonic lethal abnormal vision (Elav) (**Figure 2.1, B and C**). However, some of

the neurons stained by Elav did not express Dfd, suggesting that further differentiation of these neurons is regulated by other factors (**Figure 2.1, C**).

The main focus of this thesis is on motor systems that rely on motoneuron outputs. Thus, the expression of Dfd in motoneurons was analysed in more detail using the *OK371-Gal4* enhancer trap line, which is driven by the enhancer of the *Drosophila vesicular glutamate transporter* (*DVGlut*) gene (Mahr & Aberle 2006). *DVGlut* is expressed throughout development in all glutamatergic motoneurons and in some glutamatergic interneurons. Transcripts are detectable earliest at stage 12 of embryonic development (Mahr & Aberle 2006). Whereas the total number of glutamatergic motoneurons in the VNC was estimated to be approximately 36 per abdominal half-segment (Landgraf et al. 1997; Landgraf et al. 2003), the number of these neurons within the SEZ is extremely reduced (Hückesfeld et al. 2015). A total of 9 glutamatergic neurons were identified to project through the maxillary nerve (Hückesfeld et al. 2015).

The expression of a membrane targeted GFP-marker (mCD8-GFP) (Lee & Luo 1999) driven by *OK371-Gal4* was found in a number of Dfd-positive cells within the embryonic maxillary segment visualized by the co-expression of GFP and Dfd (**2.1, D and E**). Nevertheless, the precise number of motoneurons expressing mCD8-GFP and Dfd at the same time was not determined due to limitations in the preparation procedure. In addition to the reporter staining in Dfd-positive motoneuronal cell bodies, mCD8-GFP was detected in efferent motor axons of those cells within the peripheral maxillary nerve (**Figure 2.1, E**). However, at late stages of embryogenesis mCD8-GFP was missing in neuromuscular junctions (NMJs), a phenomenon already observed and explained by the slow transport of mCD8-GFP into axons (Mahr & Aberle 2006).

In summary, these results show that Dfd is expressed in neural stem cells and later on in differentiated motoneurons in both mandibular and maxillary neuromeres. Axon projections of labelled Dfd-positive motoneurons enter the maxillary nerve.

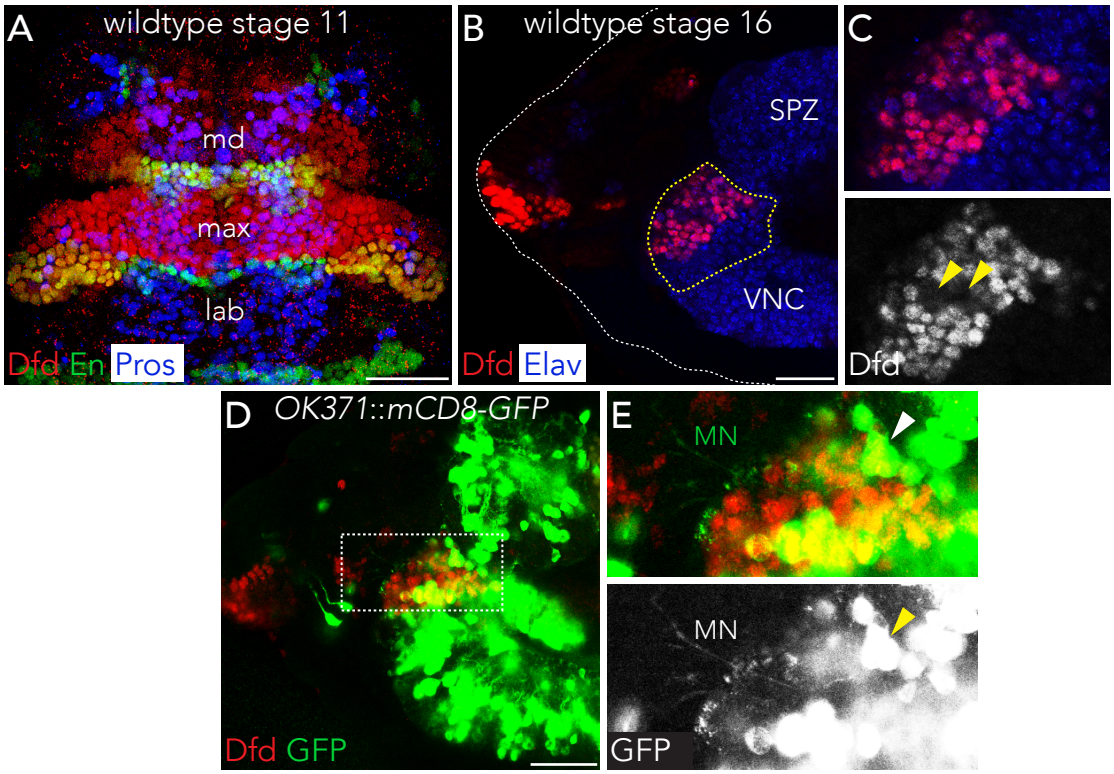

Figure 2.1: Dfd is expressed in neuroblasts and motoneuronal cell bodies. (**A**) Flat preparation of the embryonic CNS of a stage 11 embryo. Dfd protein (red) is expressed in NBs located within the mandibular (md) and maxillary (max) neuromeres. NBs are marked by the expression of Pros (blue). Posterior segmental boundaries are indicated by En expression (green). lab, labial neuromere. (**B**) Dfd expression (red) in postmitotic neurons stained by Embryonic lethal abnormal vision (Elav, blue) within the subesophageal zone (SEZ, area marked by the dashed yellow line). (**C**) Enlarged view of B. Note that Dfd-negative cells (yellow arrowhead) reside within the Dfd-expression domain. SPZ, supraesophageal zone; VNC, ventral nerve cord. Lateral view of a stage 16 embryo. (**D**) Membrane targeted GFP is driven by the motoneuronal driver line *OK371-Gal4*. Dfd protein (red) localises to motoneurons (green) that project axons through the maxillary nerve (MN). (**E**) Enlarged view of D. Dfd-expressing motoneurons are indicated by arrowheads. Lateral view. Scale bars, 20µm.

2.2 The Dfd^{NAE667} Enhancer recapitulates Deformed Expression in Neural Cells of the Subesophageal Zone

To confer segmental identity *Dfd* transcripts are restricted to the mandibular and maxillary segments of the *Drosophila* embryo. Nevertheless, Hox proteins are required in various tissues and confining their expression to specific cell types is often hard to accomplish. Even more intriguing was the identification of a neural enhancer fragment limiting the expression of *Dfd* to neurons (Lou et al. 1995). As this enhancer was shown to be autoregulatory it was named neural autoregulatory enhancer of *Dfd* (*Dfd*-NAE) (Lou et al. 1995). In the present work 667 basepairs of the *Dfd*-NAE, including the smallest identified sub-element of 608 basepairs length (Lou et al. 1995), were cloned to obtain Dfd^{NAE667} and used for further experiments.

Reporter gene expression directed by a *Dfd^{NAE667}-Gal4* construct started during mid-embryogenesis in CNS neurons of the developing SEZ and continued to late stages of embryogenesis (**Figure 2.2**). Expression of Tau-β-galactosidase, a reporter that labels neural cell bodies and axons (Callahan & Thomas 1994), was further detected in proneural clusters, specialized parts of the ectoderm that later in development form the sensory complexes of the peripheral nervous system (PNS) (Ghysen & Dambly-Chaudiere 1989) (**Figure 2.2, A**). At stage 11 of embryogenesis reporter gene expression driven by *Dfd^{NAE667}-Gal4* was confined to neural cells within the SEZ (**Figure 2.2, A and B**), while at late stages (stage 16-17) Tau-β-galactosidase expression in PNS neurons extended towards more anterior and posterior segments (**Figure 2.2, C**). Nevertheless, staining of the CNS remained strong in the SEZ, although week staining in neurons was observed in the SPZ and VNC, concluding that *Dfd^{NAE667}-Gal4* directed expression is principally strong and robust in CNS neurons within the SEZ, whereas expression in sensory complexes was unspecific beyond the expression domain of Dfd.

To determine the overlap of *Dfd^{NAE667}-Gal4* driven reporter gene expression and endogenous Dfd protein, mCD8-GFP and antibodies against GFP and Dfd were utilized. The majority of cells expressing Dfd protein appeared to be positive for GFP, although the domain of GFP expression was slightly larger than that of Dfd, spanning the entire SEZ in stage 17 embryos (**Figure 2.2, D**). This might be explained by the binding of the Hox protein Sex comb reduced (Scr), which was shown recently to be expressed in the posterior half of the maxillary neuromere and the anterior half of the labial neuromere (Hirth et al. 1998), to sequences within the Dfd^{NAE667}-Enhancer.

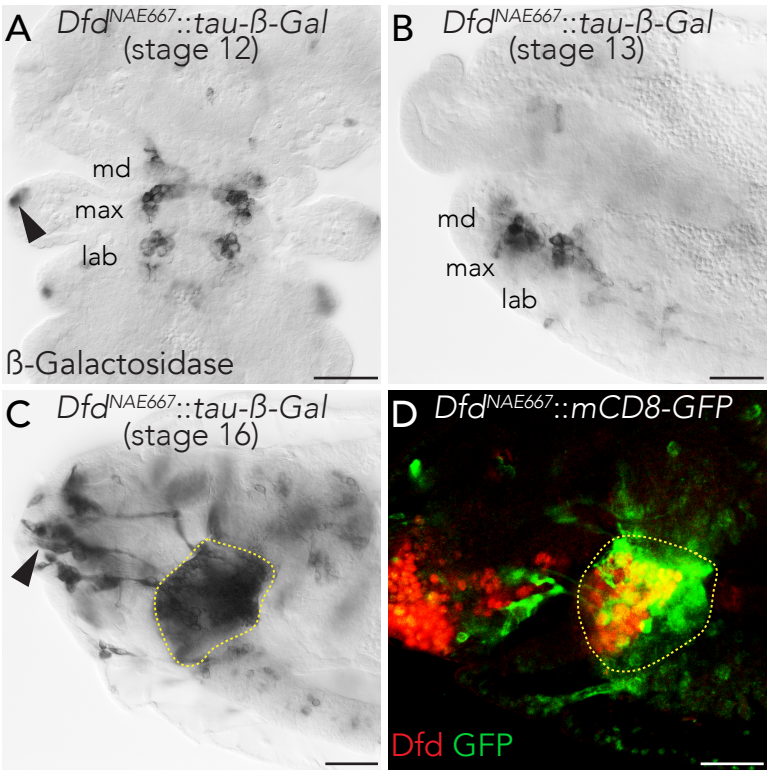

Figure 2.2: The *Dfd* neural enhancer drives reporter gene expression in neurons of the SEZ. (**A-C**) *Dfd*^{NAE667}*-Gal4* mediated expression of a *tau-β-galactosidase* transgene in cells of the SEZ during different stages of embryogenesis (stage 12, A; 13, B; and 16, C). Transgene expression can be detected in neural cells located within the md, max and lab neuromeres. Note the expression in the peripheral nervous system (PNS) (arrowheads). (**D**) Membrane associated GFP (green) driven by *Dfd*^{NAE667}*-Gal4* co-localises with Dfd expressing neural cells (red) within the embryonic SEZ (area marked by the dashed yellow line). Note that reporter gene expression extends the expression domain of Dfd. (A) Flat preparation. Ventral view. (B-D) Lateral view. Scale bars, 20µm.

As described earlier for reporter gene expression driven by the motoneuronal driver line *OK371-Gal4*, mCD8-GFP was detected in peripheral nerves, but not in NMJs at late embryonic stages (stage 16-17). Besides staining of the maxillary nerve, GFP signal was visible in the antennal and labial nerves (**Figure 2.2, C and D**). Moreover, peripheral nerves normally harbour efferent motor axons and afferent sensory axons, and thus reporter staining was either the result of both types of axons or the single output.

These results show that the neural autoregulatory enhancer of *Dfd* (Dfd^{NAE667}) used in this study precisely recapitulates the expression of Dfd in neural cells during embryogenesis, although the activity of the enhancer extends at late embryonic stages, spanning the entire SEZ and comprising PNS cells of the remaining segments and outside the Dfd region. Thus, subsequent experiments were undertaken on the basis of the Dfd^{NAE667}.

2.3 Deformed-positive Motoneurons innervate the Mouth Hook Elevator

As previously shown in this thesis, Dfd-positive motoneurons project axons through the maxillary nerve, but their muscle targets so far could not be identified due to the absence of mCD8-GFP signal in embryonic NMJs. Third-instar larvae represent a great model to elucidate motoneuronal connections within the maxillary nerve in more detail, because axons and NMJs on target muscles are relatively large and accessible at that developmental time point. This time an intersectional approach, the Flippase (Flp)-induced intersectional GAL80/Gal4 repression (FINGR) method, was applied and mCD8-GFP expression was restricted to Dfd-positive motoneurons (Bohm et al. 2010). Dfd^{NAE667}, which was shown to faithfully recapitulate expression of Dfd in CNS-neurons of the SEZ (**Figure 2.2**), was used to construct Dfd^{NAE667}-Flp and crossed further to obtain *Dfd^{NAE667}-Flp, tubP>GAL80>, OK371::mCD8-GFP* larvae.

In contrast to the VNC, motoneurons in the SEZ are not generated postembryonically via reactivation of embryonically born neuroblasts (Kuert et al. 2014). Instead, all motoneurons in the SEZ derive from the approximately 80 neuroblast lineages in the embryonic SEZ. Adult-specific secondary neurons in the larval SEZ are interneurons and derive from a total of 14 recently identified postembryonic neuroblast lineages (Kuert et al. 2014). Therefore, all Dfd-positive motoneurons were labelled in *Dfd^{NAE667}-Flp, tubP>GAL80>, OK371::mCD8-GFP* larvae. Expression of the mCD8-GFP reporter was first detectable at late stages of embryogenesis (stage 16-17) (**Figure 2.3, A**) and became strong during larval stages (**Figure 2.3, B-F**).

In third-instar larvae robust GFP-expression was found in around a dozen of clearly distinguishable cells per hemisegment on the ventral side of the SEZ and co-stainings with a Dfd specific antibody verified the presence of Dfd protein in all of the cells (**Figure 2.3, B and C**). Moreover, two to three of these cells per hemisegment projected axons within the maxillary nerve and, therefore, were classified as motoneurons (**Figure 2.3, C magnification**). Besides these motoneurons a couple of other cells, most likely glutamatergic interneurons, were labelled and marked by the co-expression of GFP and Dfd. Further analysis on the muscle targets of the identified motoneurons revealed that synapses on the MHE were labelled by GFP, a MH-associated muscle required for the elevation of the MHs during feeding (Schoofs et al. 2010) (**Figure 2.3, D-F**). Muscles were visualized by Myosin- and synapses by staining for the Drosophila Vesicular glutamate transporter (DVGlut), as this protein was shown to accumulate at NMJs (Mahr & Aberle

2006). GFP was found to co-localise with DVGlut on the MHE, but not on the antagonistic muscle enabling depression of the MHs, the MHD (Schoofs et al. 2010), indicating that the MHD was innervated by motoneurons devoid of Dfd.

Consequently, Dfd is active in two to three motoneurons targeting the MHE, but not the opposing MHD.

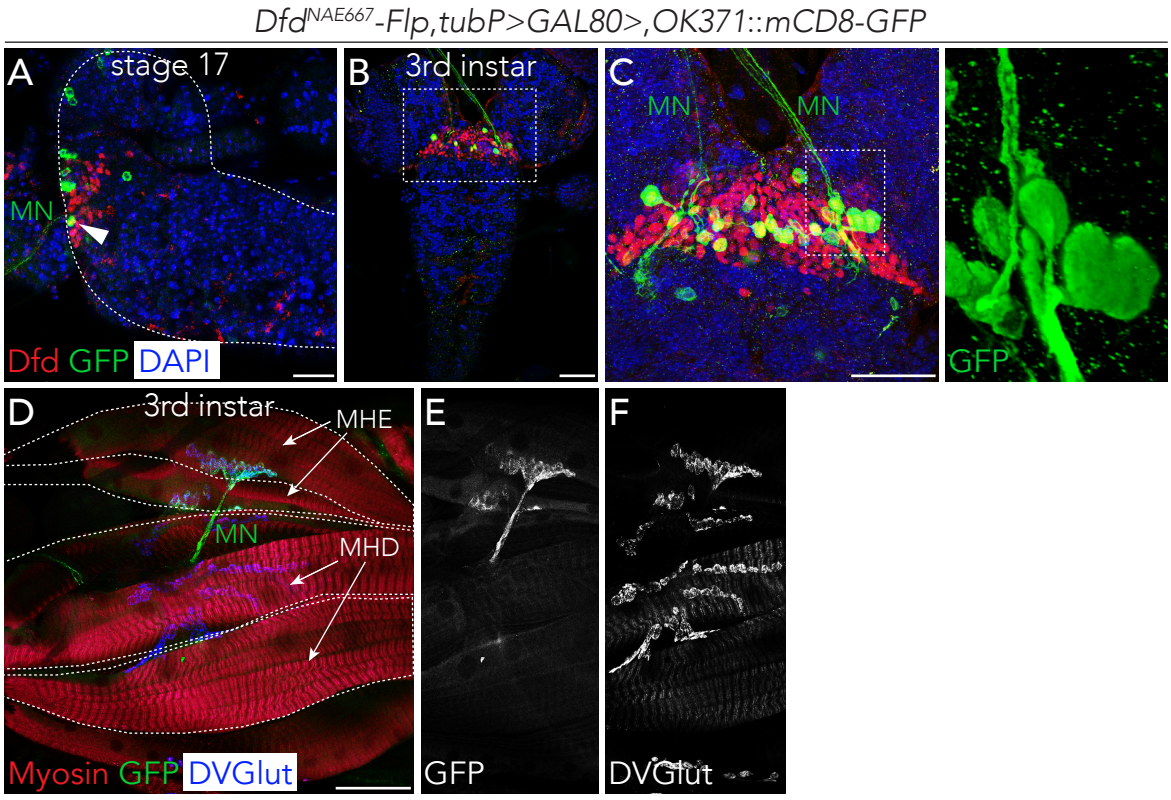

Figure 2.3: Dfd is expressed in motoneurons located within the SEZ that innervate the mouth hook elevator (MHE) muscle. (**A-C**) CNS of a early first instar (stage 17 of embryogenesis) (A) and third-instar larva (B and C) of the genotype *Dfd*^{NAE667}*-flp,tubP>GAL80>,OK371::mCD8-GFP*. Glutamatergic neurons are labelled in green, DNA in blue and Dfd protein in red. (C) Enlarged view of B. Note that only 2-3 Dfd-positive motoneurons project into the maxillary nerve (MN). The magnification shows a 3D reconstruction of these neurons. (A) lateral view, (B and C) ventral views. (**D**) Mouth hook elevator (MHE) and mouth hook depressor (MHD) muscles in third-instar larva of the genotype *Dfd*^{NAE667}*-flp,tubP>GAL80>,OK371::mCD8-GFP* stained with Myosin (red) to label muscles, DVGlut to mark synapses (blue) and GFP (green). Interestingly, only the MHE is innervated by Dfd-positive motoneurons, but not the MHD (D-F). Scale bars, 50µm.

2.4 Mouth Hook Motility and Head Muscles are affected in *Deformed* Mutants

As shown before in third-instar larvae, Dfd-positive motoneurons innervate the MHE, a muscle that enables rhythmic MH elevation during feeding (Schoofs et al. 2010). Preceding feeding, strong involvement of MH elevation is required for hatching behaviour earlier in development (Siekhaus & Fuller 1999; Pereanu et al. 2007). Hatching behaviour is characterised by vigorous elevation and depression of the MHs in order to tear open the chorion. It has been shown that *Dfd* loss-of-function mutants (Dfd^{16}) are unable to hatch from the eggshell and already die at the end of embryogenesis as fully developed first-instar larvae (Merrill et al. 1987; Regulski et al. 1987).

To correlate the inability of *Dfd* mutants to hatch with possible motor defects and impaired hatching movements, Dfd^{16} mutants were analysed further. Due to the absence of MHs in these animals (Merrill et al. 1987; Regulski et al. 1987) (**Figure 2.4, C**) general head movements of first-instar larvae were monitored prior to intrinsic hatching, 21-22 hours after egg laying (AEL), at the end of embryogenesis (stage 17) (Pereanu et al. 2007). The ratio of hatched to unhatched larvae was calculated 47 hours AEL, the time point of the first larval moult and the beginning of the second larval instar in wildtype. MH movements in wild-type larvae were fast and coordinated and accompanied by frequent strong head flexion and extension, whereas Dfd^{16}-mutant larvae only slightly moved their head in an uncoordinated way. Interestingly, peristaltic movements of more posterior body parts were completely normal in the mutant background. Nevertheless, Dfd^{16} mutants were found dead within their eggshells in 100 % of cases (**Figure 2.4, A**).

In order to prove that a loss of motor activity rather than the absence of MHs alone accounts for the inability of *Dfd* mutants to hatch from the eggshell, mutants carrying weaker (hypomorphic) alleles of *Dfd* and showing less severe phenotypes were examined. Animals of the genotype $Dfd^{13}/Df(3R)Scr$ have been characterised by the presence of MHs (Merrill et al. 1987) (**Figure 2.4, D**). Here, they failed to move their MHs and 48.3 % of them died at the end of embryogenesis trapped within the eggshell, concluding that MH movements are critical for hatching (**Figure 2.4, A**).

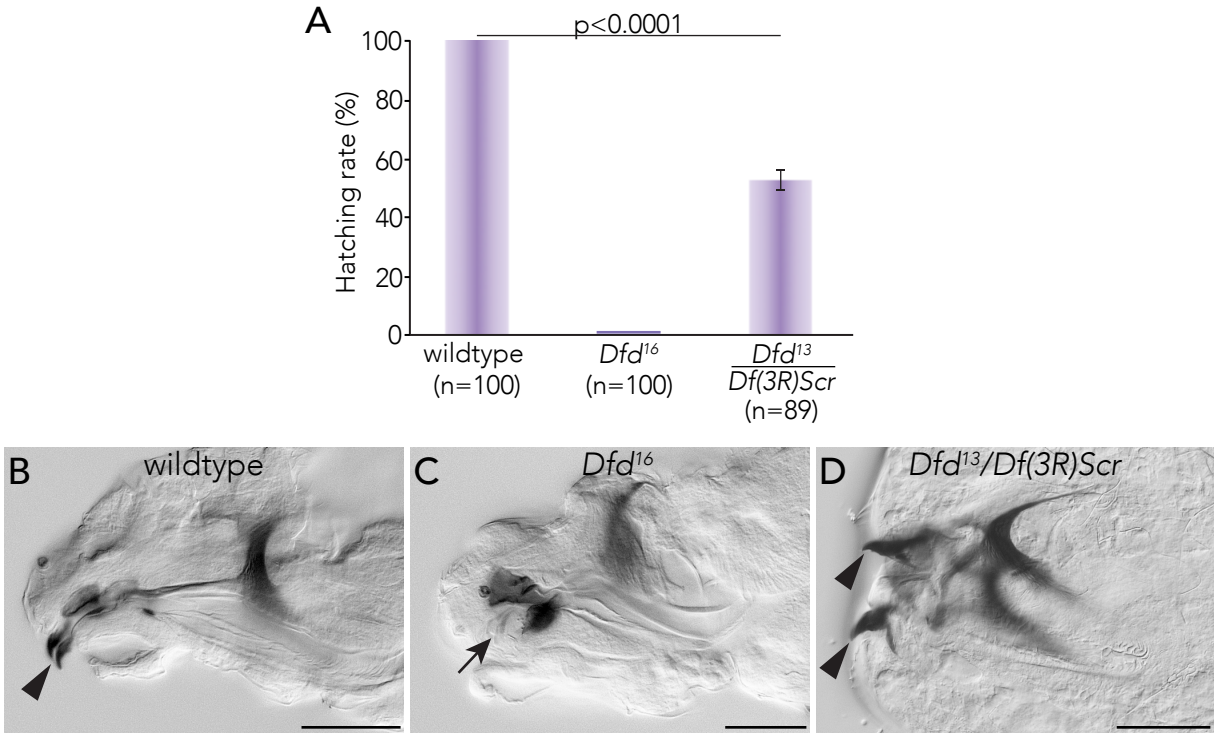

Figure 2.4: Coordinated movements of the MHs are critically required for MH-associated behaviours. (**A**) Hatching rates of wild-type, *Dfd* null mutants (*Dfd*^{16}) and *Dfd*^{13}/*Dfd(3R)Scr*-mutant embryos. Error bars indicate the standard deviation. (**B-D**) Lateral views of wild-type (B), *Dfd* null-mutant (*Dfd*^{16},C) and *Dfd*^{13}/*Dfd(3R)Scr*-mutant (D) embryonic head. The presence or absence of mouth hooks is indicated by arrowheads or arrows, respectively. Scale bars, 40µm.

Nevertheless, functioning motor systems depend on the action of neurons and muscles. In addition to the expression of Dfd in SEZ motoneurons, Dfd protein was also found to co-localise with the muscle-specific TF Myocyte enhancer factor 2 (Mef2) in nuclei of internal head muscles of stage 16 wild-type embryos (**Figure 2.5, A-C**). Noteworthy, *Dfd*^{16} mutants of the same age showed defects in the morphology and amount of these muscles (**Figure 2.5, D**). As muscle phenotypes were very diverse in *Dfd*^{16}-mutant embryos, they were classified into different categories according to the amount of muscles remaining, even if they were malformed (**Table 2.1**). In control embryos a total of four muscles was found clustered and attached to the presumptive cephalopharyngeal skeleton (CPS), most likely consisting of the MHE, MHD, Labial Retractor (LR) and a muscle of unknown origin on the most dorsal part of the cluster (**Figure 2.5, B and C**). The definite fate of single muscles could not be determined in detail as MHs are not fully developed and attachment sites not observable at embryonic stage 16. However, Dfd protein was not detected in the most dorsally (muscle of unknown origin) and ventrally (most likely the LR) located muscles of the cluster, but

confined to two muscles in the middle of the cluster (the MHE and MHD) (**Figure 2.5, B and C**). This suggests that the dorsal- and ventral-most muscles are specified independently of Dfd, or that expression of Dfd was lost during specification. In *Dfd*^{16}-mutant embryos the muscles in the middle of the cluster are malformed and in most cases lost (**Figure 2.5, D; Table 2.1**). Malformation of muscles might be in part due to the inability of *Dfd* mutants to involute their heads (Merrill et al. 1987), which again hampers further investigations on the fate of muscles remaining.

Muscles in the hypomorphic situation *Dfd*^{13}/*Df*(*3R*)*Scr* were not analysed as mutants showed a high variation in their life span, with a total of 51.7 % of embryos that were able to hatch.

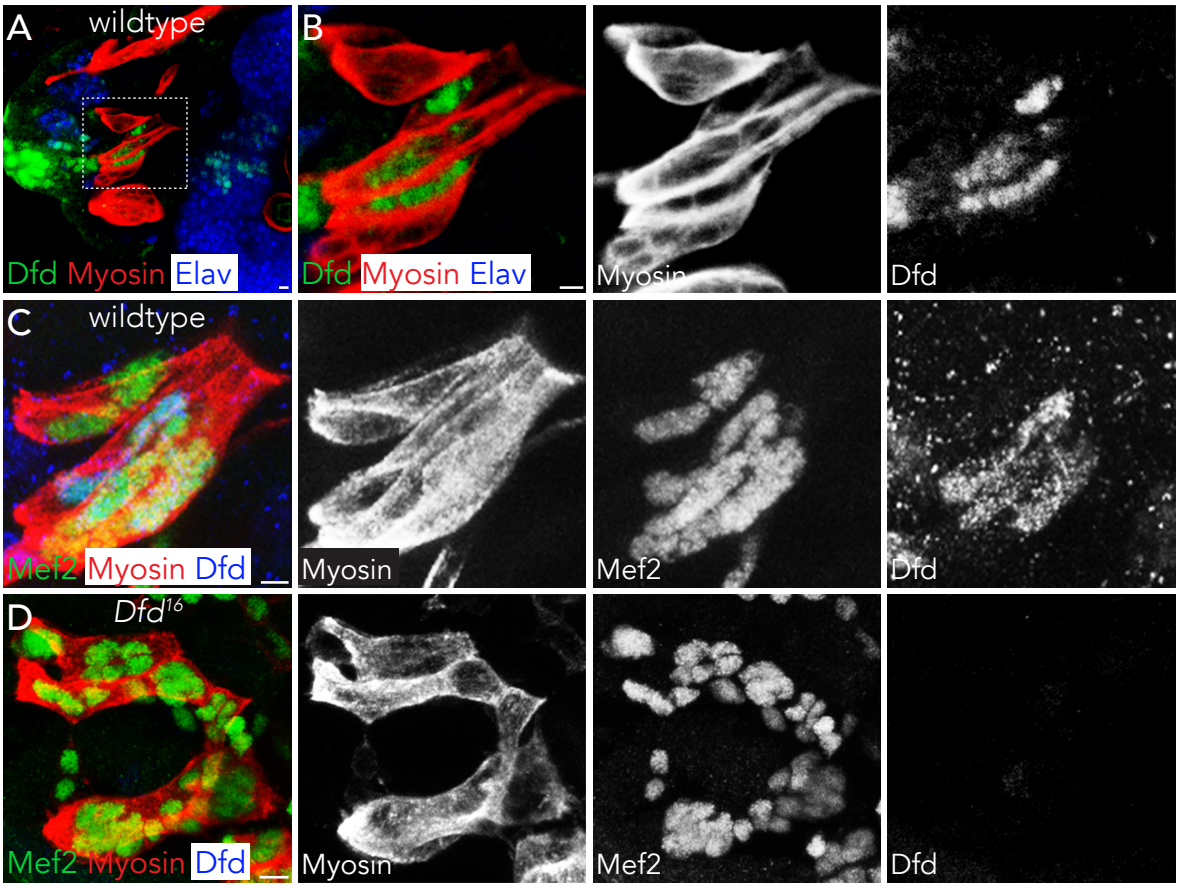

Figure 2.5: Dfd is expressed in embryonic muscles. (**A**-**D**) Lateral views of stage 16 embryos focussing on internal head muscles. (**A**) In addition to its localisation in neurons, Dfd protein (green) is also expressed in internal muscles of stage 16 embryos. Postmitotic neurons are marked by the expression of Elav (blue), muscles are stained by Myosin (red). (**B**) Enlarged view of A. (**C**) Whereas in total four muscles express the Myocite enhancer factor 2 (Mef2) (green), Dfd expression (blue) is confined to only two muscles of the cluster. (**D**) In *Dfd* null-mutant embryos the number of muscles is reduced. Muscles in the middle of the cluster are missing, indicated by the absence of Myosin and Mef2 staining. Scale bars, 5µm.

These results demonstrate that rhythmic MH movements are dependent on the *Hox* gene *Dfd* and critical for feeding-like behaviours. A loss of motor activity can be either explained by neural malfunction and/or the loss of muscles as the presence of MHs alone is not pivotal for MH mobility.

Table 2.1: Quantification of muscle phenotypes observed in *Dfd*^{16} homozygous mutants in comparison to the control (*Dfd*^{16}*/TM3*).

Muscle phenotype	Number of embryos	
	Dfd^{16}	*Dfd*^{16}*/TM3*
Severe defects (1-2 muscles, malformed)	10/36	0/20
Intermediate defects (2-4 muscles, malformed)	22/36	0/20
Weak defects (4 muscles, malformed)	4/36	0/20
No defects (4 muscles, normal)	0/36	20/20

2.5 Deformed-positive Motoneurons control Mouth Hook Elevation

To test whether MH movements are influenced by the manipulation of Dfd-expressing neurons and their neuromuscular connections, synaptic transmission was blocked in Dfd-positive neurons within the SEZ. Neurotransmitter exocytosis at NMJs was prevented by expressing the active form of the clostridial neurotoxin tetanus toxin (TNT-R) (Sweeney et al. 1995) under the control of *Dfd*^{NAE667}*-Gal4*. TNT proteolytically cleaves neural Synaptobrevin (n-Syb), an intrinsic membrane protein that is known to target synaptic vesicles to the plasma membrane (Trimble et al. 1988). Control animals expressed an inactive version of tetanus toxin (IMPTNT-V1) (Sweeney et al. 1995). As this approach aimed to focus on manipulating the output of motoneurons, input from interneurons and cholinergic sensory neurons was blocked by expressing in addition a choline-acetyltransferase (*Cha*)-*GAL80* transgene in the embryonic background (Pulver et al. 2009).

First, MH movements were monitored prior to hatching at the end of embryogenesis, with hatching rates determined 24 hours afterwards (**Figure 2.6, A**). Animals of the genotype *Cha-GAL80*, *Dfd*^{NAE667}*::TNT-R* were completely unable to perform any MH movements in comparison to control animals (*Cha-GAL80*, *Dfd*^{NAE667}*::IMPTNT-V1*) and

died trapped in their eggshells at the end of embryogenesis. Peristalsis of posterior body parts remained unaffected. The same experiment was carried out at larval stages in order to analyse the requirement of Dfd-positive neurons during larval feeding subsequent to hatching (**Figure 2.6, B-F**). To prevent transcription of TNT-R during embryogenesis and hence circumvent embryonic lethality, a temperature-sensitive GAL80 (Suster et al. 2004) was introduced.

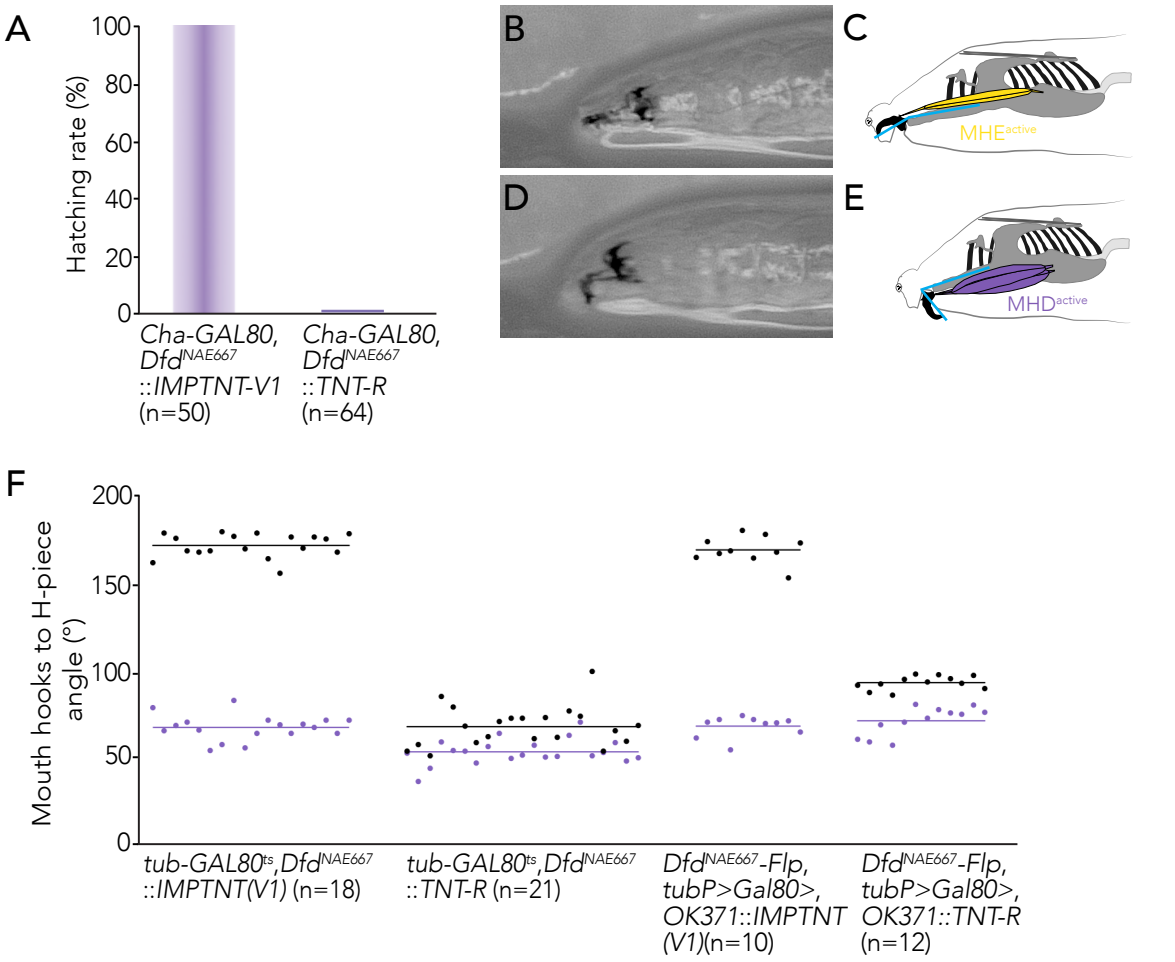

Figure 2.6: Dfd-expressing neurons control MH-related movements. (**A**) Hatching rates of *Cha-GAL80,Dfd*^{NAE667}*::IMPTNT-V1* and *Cha-GAL80,Dfd*^{NAE667}*::TNT-R* larvae at the end of embryogenesis. (**B**-**E**) Maximum elevation (B and C) and depression (D and E) of the MHs during one feeding cycle in an exemplary larva are shown. In the schematic drawing the yellow line indicates differences in the angle between the MHs and the H-piece. (**F**) Measurement of angles between the MHs and the H-piece in *tub-GAL80*^{ts}*,Dfd*^{NAE667}*::IMPTNT-V1* versus *tub-GAL80*^{ts}*,Dfd*^{NAE667}*::TNT-R* larvae, and *Dfd*^{NAE667}*-flp,tubP>GAL80>,OK371::IMPTNT-V1* versus *Dfd*^{NAE667}*-flp,tubP>GAL80>,OK371::TNT-R* larvae during one cycle of MH elevation and depression. Black and purple dots indicate individual larvae and black and purple lines represent the means of the measurements.

Experimental settings were adapted by F. Bujupi in order to determine the correct time point of Gal4-release by GAL80 (Bujupi 2016). For quantification of MH mobility the angle between the MHs and the H-piece was measured during one feeding cycle in first-instar larvae (**Figure 2.6, B-E**), a method invented by F. Bujupi. This angle varied between 70° and 170° in the control situation (*tub-GAL80^{ts}*, *Dfd^{NAE667}*::*IMPTNT-V1*), corresponding to the average depression and elevation of the MHs (Schoofs et al. 2010), respectively (Experiment performed by F. Bujupi; (Bujupi 2016) (**Figure 2.6, F**). In contrast, larvae of the genotype *tub-GAL80^{ts}*, *Dfd^{NAE667}*::*TNT-R3* expressing active tetanus toxin under the control of *Dfd^{NAE667}-Gal4* were unable to elevate their MHs while depression was slightly stronger compared to control animals with average angles varying between 57° and 71° (Experiment performed by F. Bujupi; (Bujupi 2016) (**Figure 2.6, F**).

Next, TNT-R was expressed in *Dfd^{NAE667}-Flp, tubP>GAL80>, OK371-Gal4* first-instar larvae blocking synaptic transmission exclusively in Dfd-expressing motoneurons and a few glutamatergic interneurons (Mahr & Aberle 2006). Execution of MH elevation movements was severely affected in *Dfd^{NAE667}-Flp, tubP>GAL80>, OK371-Gal4*::*TNT-R3* larvae in contrast to control animals (*Dfd^{NAE667}-Flp, tubP>GAL80>, OK371-Gal4*::*IMPTNT-V1*). The average angle between the MHs and the H-piece varied between 74° and 95° in the test group, whereas angles of control larvae reflected a normal depression, on average 71°, and elevation phase, on average 169° (**Figure 2.6, F**).

In sum, these results show that Dfd-expressing motoneurons control MH elevation movements that are essential for embryonic hatching and larval feeding and support the exclusive innervation of the MHE by Dfd expressing SEZ neurons.

2.6 Deformed-mutant Cells are defective in their Developmental Program

MH elevation is governed by Dfd-expressing motoneurons, and manipulation of these motoneurons results in the inability of animals to hatch or perform accurate MH elevation movements. Tetanus toxin has an effect on presynaptic endings of neurons that are completely matured, but what happened to the motoneurons in *Dfd* mutants that were shown to have comparable behavioural defects to those observed in TNT-R animals? To address this question *Dfd* mutants were analysed in more detail with regard to neural cell death, mis-specification of neural cells and failures in axon outgrowth and/or muscle innervation.

First, PCD in postmitotic neurons was analysed using terminal deoxynucleotide transferase-mediated dUTP end labelling (TUNEL) (Gavrieli et al. 1992) in addition to Elav-antibody staining in stage 13 embryos (**Figure 2.7, A and B**). TUNEL labels apoptotic cells in which the DNA has been cleaved. No additional apoptotic cells were detected within the mandibular and maxillary neuromeres in Dfd^{16} mutants compared to wildtype. Instead, the number of cells labelled by TUNEL was slightly decreased in *Dfd* null-mutant embryos, suggesting that PCD in neurons is usually induced by Dfd. This is in line with recent findings revealing the presence of ectopic NBs in Dfd^{16}-mutant embryos and in *Dfd*-mutant clones during larval stages (Urbach et al. 2016; Kuert et al. 2014; Kuert et al. 2012) In addition, these findings resemble apoptotic events in cells of the epidermis, being normally eliminated upon the action of the cell death promoting gene *reaper*, but survive in *Dfd* mutants (Lohmann et al. 2002).

To address the question whether mis-specification of neural cells in Dfd^{16} mutants accounts for the inability of embryos to perform proper MH-elevation movements, immunolabelling experiments using NB lineage markers were carried out. It has been shown recently that mutations in *Dfd* lead to homeotic transformations of the maxillary NB6-4 (Becker et al. 2016).

Interestingly, Dfd^{16} mutants showed a lack in the expression of the neural sublineage marker *even skipped* (*eve*) in progenitor neurons of specific NBs in the mandibular and maxillary neuromeres (**Figure 2.7, C-F**). Normally, *eve* is expressed in the NBs 1-1, 3-3, 4-2 and 7-1, which give rise to the aCC and pCC neurons (derived from GMC1-1a), EL-neurons (from NB3-3), RP2 and RP2-sibling neurons (from GMC4-2a), and the U/CQ neurons (generated by several GMCs in the NB lineage 7-1) (Dormand & Brand 1998; Fujioka et al. 2003). The aCC, RP-2 and U/CQ neurons are motoneurons, whereas pCC

and EL neurons are interneurons (Fujioka et al. 2003). Despite the presence of the mandibular NB4-2 in wild-type embryos, RP2-neurons are missing (Urbach et al. 2016). However, RP2 neurons are formed in the maxillary neuromere, but are assigned to undergo PCD at late stages of embryogenesis. NBs 1-1 and 3-3 and their progenies, the aCC and pCC neurons and the mandibular EL-neurons, are not formed in the mandibular neuromere (Urbach et al. 2016). Nevertheless, it has been shown that Eve-positive cells of unknown origin reside within the mandibular neuromere (Urbach et al. 2016).

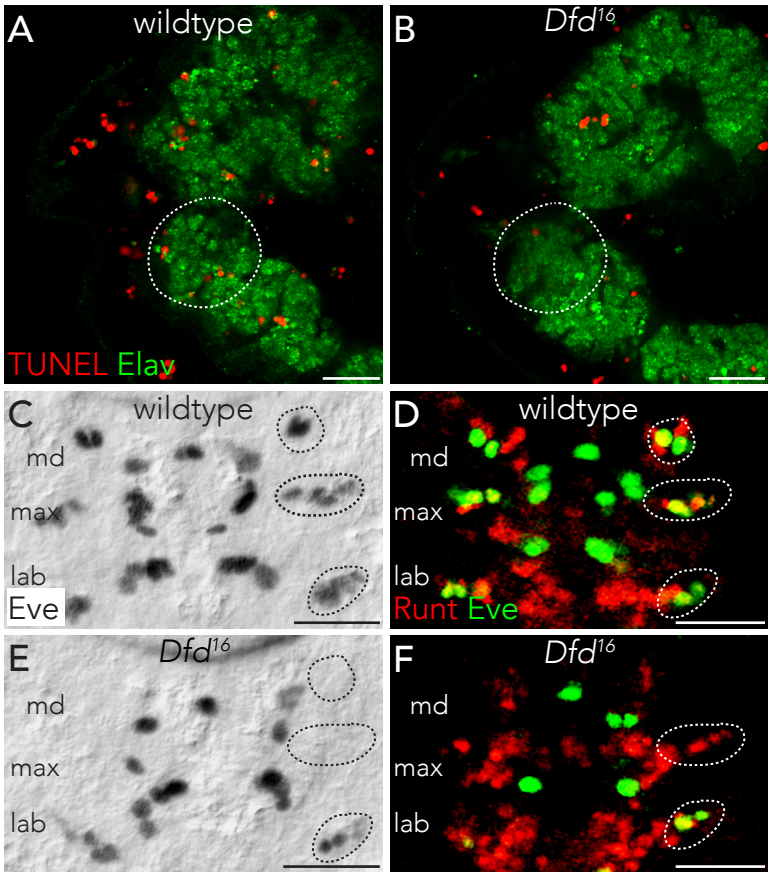

Figure 2.7: Dfd is crucial for the induction of PCD and cell-fate specification. (**A** and **B**) Programmed cell death (PCD) is indicated by TUNEL staining (red) in stage 13 wild-type and *Dfd*^{16}-mutant embryos. Postmitotic neurons are labelled with Elav (green). Lateral views. (**C**-**F**) Expression of Even-skipped (Eve) in wild-type and *Dfd* null-mutant embryos in specific neurons within the md, max and lab neuromeres. Neurons within the EL-cluster are highlighted by dashed circles. Ventral views. (D and F) Co-staining of Runt and Eve to indicate the presence of neurons at the position of the EL-cluster in *Dfd*^{16} mutants. Scale bars, 20µm.

In immunostainings with an Eve-specific antibody on *Dfd*^{16}-mutant embryos, no staining was detectable at positions within the maxillary neuromere where EL-neurons usually cluster in wild-type embryos (**Figure 2.7, E**). To indicate whether EL-neurons were completely missing in *Dfd*^{16} mutants, or simply lost Eve-expression, co-stainings with Eve- and Runt-specific antibodies were conducted as the pair rule gene *runt* was shown to be expressed in NB3-3 and its progenies (Dormand & Brand 1998) (**Figure 2.7, D and F**). These stainings revealed an overlap of Eve and Runt expression in neurons within the EL-cluster in the maxillary neuromere of wild-type embryos (**Figure 2.7, D**). However, in *Dfd*^{16}-mutant embryos Eve staining is lost from these cells indicating that these neurons developed, but did not express Eve (**Figure 2.7, F**). EL-neurons located within the labial neuromere were characterised by the expression of Eve and Runt in both, wild-type and *Dfd* null-mutant embryos. Furthermore, Eve-positive cells of unknown origin described in Urbach et al., which are usually located within the mandibular neuromere, were not labelled by the Eve-antibody in *Dfd*^{16} mutants (**Figure 2.7, E and F**). In addition to these cells and the maxillary EL-neurons, Eve-staining could not be detected in other neurons, most likely RP2 and/ or aCC, within the maxillary neuromere in *Dfd*^{16}-mutant embryos (**Figure 2.7, E and F**). Noteworthy, maxillary and labial RP2 neurons were shown to loose Eve-expression at later stages of embryogenesis and finally undergo PCD (Urbach et al. 2016). Thus, the absence of Eve-Signal in those cells in *Dfd*^{16} mutants could simply be explained by the natural elimination of maxillary RP2 cells.

Next, axon outgrowth was analysed in more detail in *Dfd* mutant backgrounds by making use of the common axon markers Fasciclin II (Fas II) and BP102, both labelling CNS axons (**Figure 2.8**). It has been shown that in *Drosophila* the maxillary nerve carries sensory axons from two major chemosensory organs, the terminal (maxillary) organ (TO) and the ventral organ (VO) (R. F. Stocker 1994). To distinguish between afferent sensory connections, entering the SEZ via the maxillary nerve, and efferent axons of motoneurons leaving the SEZ, 22C10 antibody stainings were carried out in addition. In principle, sensory neurons continued to project through the maxillary nerve in stage 16 *Dfd*^{16}-mutant embryos, although the overall number of afferent projections was slightly decreased compared to the wild-type control, apparent from a thinner maxillary nerve (**Figure 2.8, B**). This observation strongly supports phenotypic descriptions of *Dfd* mutants lacking two papilla sensilla of the TO (Regulski et al. 1987; Merrill et al. 1987), a phenomenon that could be explained by the lack of sensory neurons of the TO.

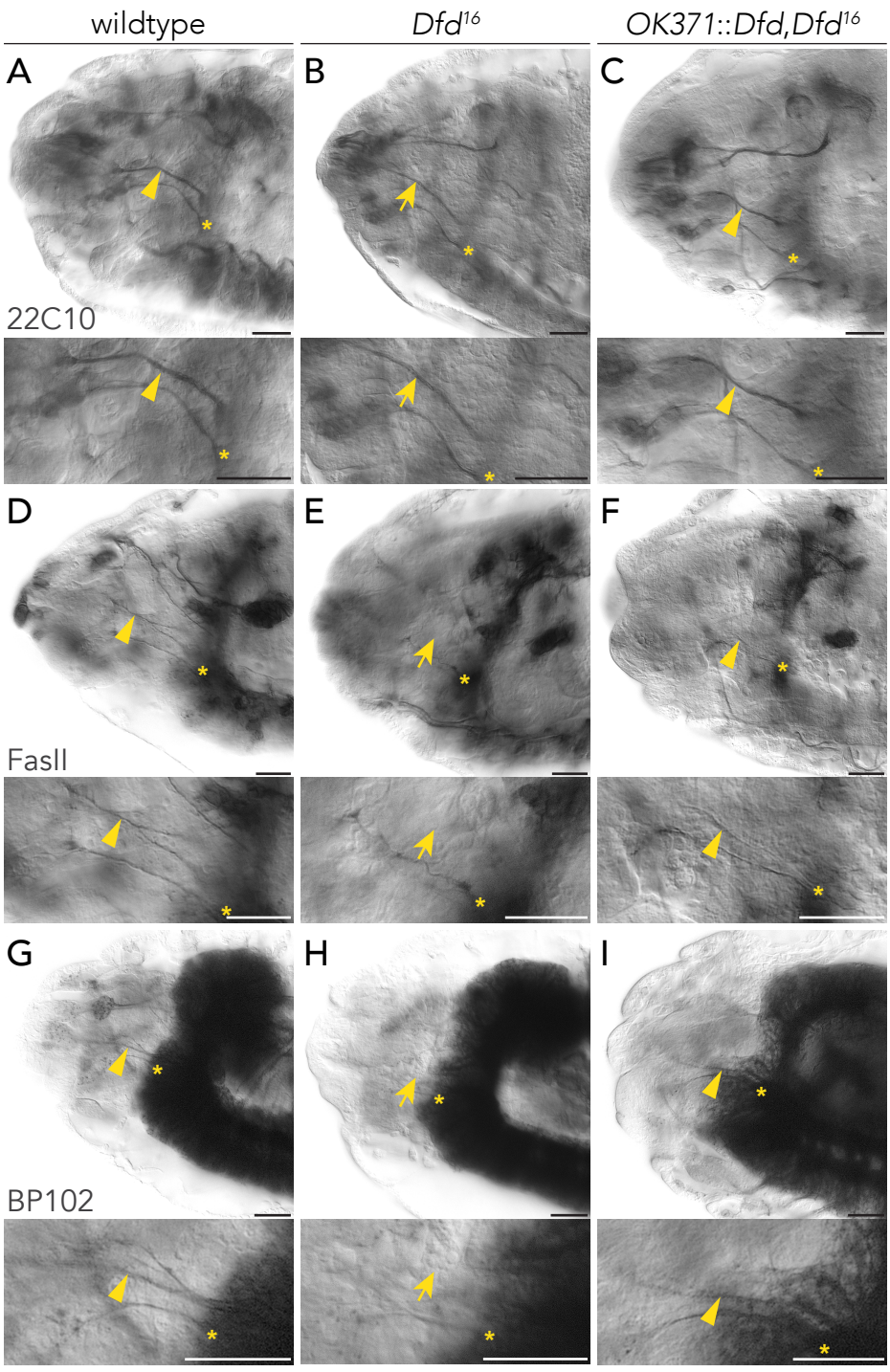

Figure 2.8: Axon outgrowth can be restored in *Dfd* null-mutant embryos. (**A-I**) Lateral views of stage 16 embryonic heads stained with the PNS axon marker 22C10 that labels the MAP1B/Futsch protein (A-C), and the CNS axon markers Fasciclin II (FasII) (D-F) or BP102 (G-I). (**A**, **D** and **G**) Wild-type embryos are marked by the presence of PNS and CNS axon projections that converge into the maxillary nerve (arrowhead). The asterisks mark the exit point of the control nerve, the labial nerve, from the CNS. (**B**, **E** and **H**) In *Dfd*^{16}-mutant embryos CNS axon projections, most likely motoneuronal projections, are completely missing (arrow in E and H), while PNS axons are reduced in number, yet present. The formation of the labial nerve is not affected (asterisks). (**C**, **F** and **I**) Axon projections from the CNS are partially restored (arrowheads in F and G) upon re-introduction of Dfd into motoneurons using the *OK371-Gal4* driver. Scale bars, 20µm.

Compared to afferent sensory projections, efferent motor projections were completely lost in *Dfd*^{16}-mutants (14/14 embryos, statistics performed by S. Sorge) (**Figure 2.8, E and H**), as well as in *Dfd*^{16}*/Df*(*3R*)*Scr* embryos (15/15 embryos, statistics performed by S. Sorge) (data not shown). The presence of CNS axons within the maxillary and labial nerve was marked by Fas II and BP102 antibody stainings on stage 16 wildtype embryos (15/15 embryos, statistics performed by S. Sorge) (**Figure 2.8, D and G**). The same stainings on *Dfd* mutants uncovered the presence of labial projections, while those converging into the maxillary nerve were not detectable (**Figure 2.8, E and H**).

In addition, drastic defects were observed in flat preparations of stage 14 *Dfd* loss-of-function mutants, augmenting the results obtained by Hirth et al. (Hirth et al. 1998). In wild- type embryos, axon tracts of the fly CNS were organised in an orthogonal manner, with longitudinal tracts alongside the midline, and segmentally reiterated pairs of commissures crossing the midline (**Figure 2.9, A**). However, in *Dfd*^{16} mutants, longitudinal and commissural axon projections within both, the mandibular and maxillary neuromeres, were reduced or disrupted (10/10 embryos) (**Figure 2.9, B**). In addition, thickening at the junctions between the connectives and commissures occurred. In severe cases the mandibular commissure was completely missing, whereas the posterior located tritocerebral commissure and the paired labial commissures were present with correct projections patterns (3/10 embryos) (**Figure 2.9, B**), indicating that the defects caused by loss of functional Dfd protein were specific and restricted to the mandibular and maxillary neuromeres. Noteworthy, the maxillary neuromere has been shown to comprise a pair of commissures and the maxillary nerve, which leaves the CNS at the level of the anterior most commissure (Nassif et al. 1998). Therefore, at least one of the maxillary commissures, the mandibular commissure, as well as efferent projections of the maxillary nerve were affected in *Dfd* loss-of-function embryos.

Afferent sensory projections entering the SEZ via the maxillary nerve were present, although reduced in number in *Dfd*^{16} mutants compared to wildtype (**Figure 2.8, A and B**).

Comparable defects to those seen in flat preparations of *Dfd*^{16}-mutant embryos were found in null mutants of the *Hox* genes *Antp* and *Abd-B*. *Antp* is predominantly expressed in the thoracic neuromeres, while strongest expression of *Abd-B* is localised to the terminal neuromeres (Hirth et al. 1998). Thus, in *Antp* and *Abd-B* mutants defects in the pattern of longitudinal connectives and commissures occurred within domains where both genes usually show the most intense expression (**Figure 2.9, C and D**).

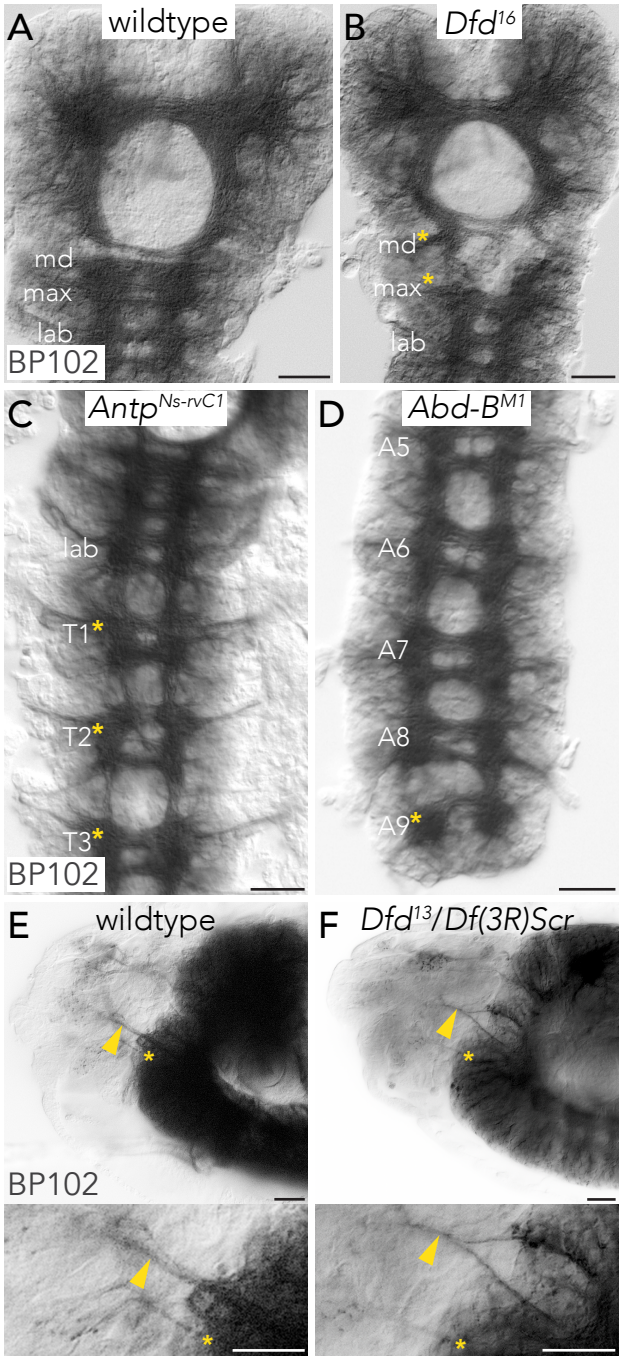

Figure 2.9: Dfd and related Hox-proteins are crucial for axonal patterning. (**A**-**D**) Flat preparations of the CNS. Axon trajectories are labelled by BP102-antibody. (**A**) In wild-type embryos the CNS is organised in a ladder-like structure, comprising longitudinal connectives and commissures. Mandibular (md), maxillary (max) and labial (lab) neuromeres are indicated. (**B**) In *Dfd* null-mutant embryos axon-patterning defects occur within the md and max neuromeres (asterisks), whereas in the lab neuromere the structure of the CNS is not affected. (**C** and **D**) Axon projections within the thoracic neuromeres (T1-T3) and abdominal neuromeres (A8 and A9) are disorganised and disrupted in *Antp* (*Apt*$^{NS\text{-}rvC1}$) (C) or *Abd-B* (*Abd-B*^{M1}) (D) null-mutant embryos, respectively. Asterisks mark the affected neuromeres. (**E** and **F**) Ventral views of stage 16 wild-type and *Dfd*^{16}-mutant embryos. Axonal projections of the CNS are marked by BP102-antibody staining. Efferent CNS, most likely motoneuronal, connections are not affected in the majority of hypomorphic *Dfd*^{13}/*Df(3R)Scr* mutant embryos as highlighted by the presence of the maxillary nerve (arrowhead in F). The asterisks mark the exit point of the labial nerve. Scale bars, 20µm.

Next, the capacity of Dfd to restore motor projections in a *Dfd* null-mutant background was analysed. For this purpose, Dfd expression was re-introduced in motoneurons of Dfd^{16}-mutant embryos using the *OK371-Gal4* driver, but not the more restricted Dfd^{NAE667}*-Gal4* driver as the neural enhancer of *Dfd* has been shown to be autoregulated (Lou et al. 1995). As visualised by Fas II and BP102 antibody stainings, motor projections of the maxillary nerve were partially recovered when *Dfd* was transgenetically expressed in motoneurons (8/16 embryos, statistics performed by S. Sorge) (**Figure 2.8, F and I**). Projections of motor neurons within other nerves were not affected in this genetic background. In rare cases additional axon projections were found deriving from the more posterior located labial neuromere instead of being exclusively recovered within the maxillary neuromere.

These results show that Dfd is crucial for the specification of neural cells in addition to inducing neural cell-death. Moreover, the competence of Dfd to restore motor projections in *Dfd* null-mutant embryos, even after cells have been initially specified, suggests that Dfd function is independently required at subsequent steps of motoneuronal development.

Supporting the temporal requirement of Dfd in motoneuronal development, efferent motor projections within the maxillary nerve were present in the majority of hypomorphic embryos (Dfd^{13}*/Df(3R)Scr)* analysed (14/19 embryos, statistics performed by S. Sorge) (**Figure 2.9, F**) even though MH movements and hatching rates were severely affected in almost 50 % of embryos. The fact that axon outgrowth was normal in animals with reduced Dfd levels, but behavioural defects remained, points towards a function of Dfd in the regulation of muscle innervation or even later in synapse related processes.

2.7 Regulation of Target Genes by Deformed

Dfd is a TF with specific DNA binding preferences encoded in *cis*-regulatory Hox response elements (HREs) (Slattery et al. 2011; Sorge et al. 2012). Genome-wide mapping of Dfd-binding sites *in vivo* using Chromatin immunoprecipitation coupled to massively parallel sequencing (ChIPseq) on stage 10-12 *Drosophila* embryos uncovered a total of 1079 HREs (Sorge et al. 2012), amongst them a significant number associated with genes that are known to function in the nervous system. In the context of this thesis these neural genes, referred to as neural Dfd target genes, were classified based on gene ontology (GO) annotation (by N. Ha) and subsequently grouped according to similar GO-terms into three major groups, reflecting sequential phases of neural

development. The first group (group 1) contained genes related to early processes in nervous system development, including NB and ganglion mother cells (GMC) fate determination and development, or the differentiation of neurons (32/182 genes). Within the second group (group 2), genes implicated in axon outgrowth and guidance were clustered (86/182 genes) and the third group (group 3) comprised of genes with known functions at the synapse (85/182 genes). Three independent lists of GO-terms used for the classification of neural Dfd target genes and the lists of genes belonging to the respective groups are deposited in the appendix of this thesis.

With this, HREs for Dfd have been identified (Sorge et al. 2012) and concomitant neural genes that are putative direct targets of Dfd. Most interestingly, grouping of these genes revealed that they operate at different phases of neural development, pointing again towards a temporal requirement of Dfd in motoneuronal development. Further experiments aimed to verify candidate neural target genes and their stage specific control by Dfd.

2.8 Neural Specification and Axon Guidance are affected in *Dfd* Mutants

First, the Dfd-dependent regulation of genes required at the beginning of neural development and of genes important for axon outgrowth and guidance was analysed by comparing their expression patterns in wild-type embryos versus Dfd^{16}-mutant embryos.

The homeodomain TF Pros is inherited to GMCs during asymmetric NB divisions (Spana & Doe 1995). In Pros antibody stainings on stage 13 wild-type embryos, Pros-Protein was localised at the basal cortex of Dfd-positive NBs and within Dfd-expressing GMCs, whereas *Dfd* null-mutant embryos showed an aberrant distribution of Pros-Protein (**Figure 2.10, A and B**). Pros was found distributed alongside the cell-membrane of affected NBs in Dfd^{16} mutants, including apical domains. In addition Pros segregated to the whole cell body of budding GMCs. However, the position of some of these daughter cells was random with respect to the apical-basal axis of the NB, indicative of defects in spindle orientation in *Dfd*-mutant NBs.

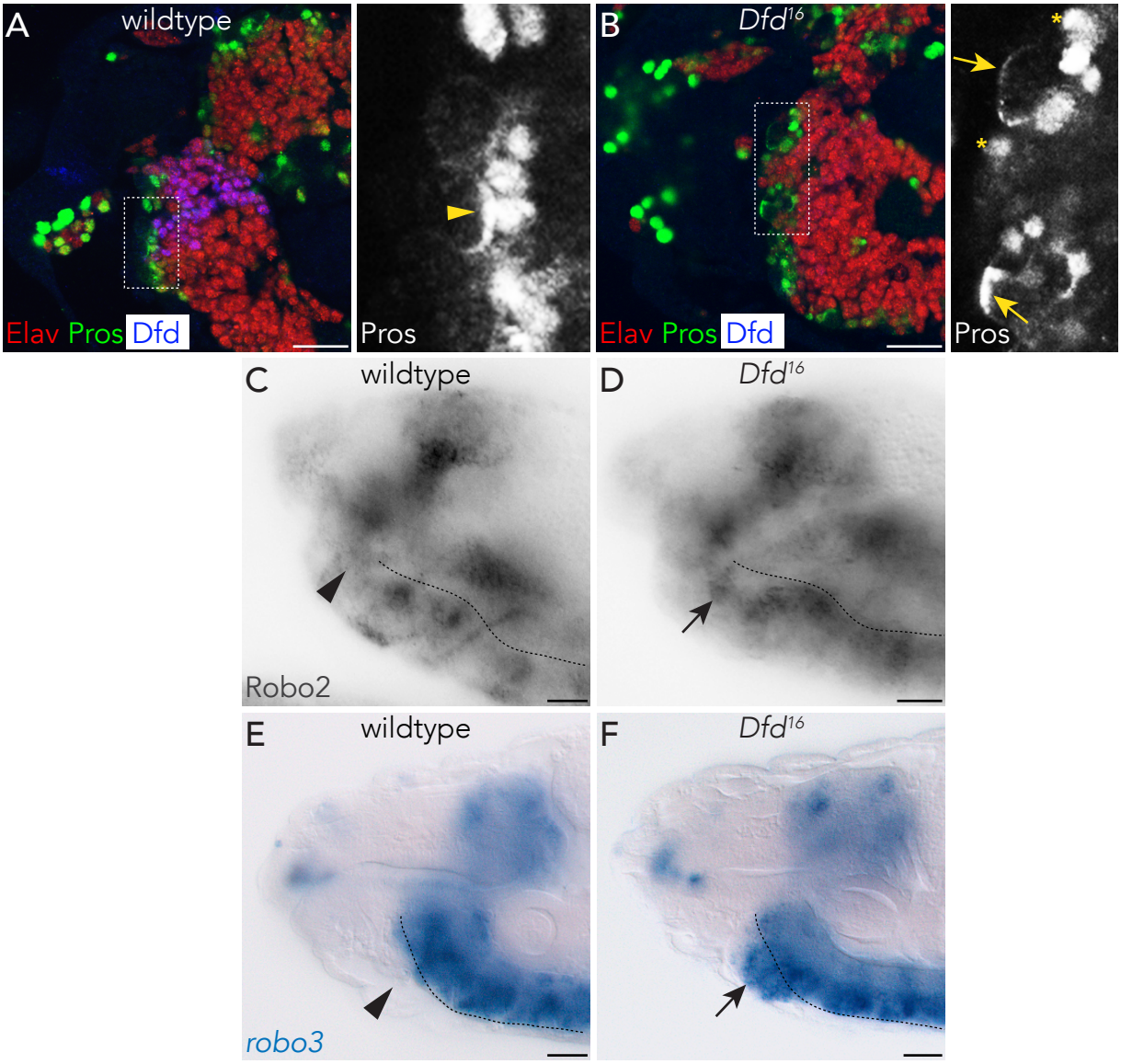

Figure 2.10: Dfd dependent regulation of target genes required for neural specification and axon guidance. (**A** and **B**) Ventral view of stage 13 embryos. The expression of Pros (green), Elav (red) and Dfd (blue) is depicted. (**A**) In wild-type embryos Pros is building a basal crescent in Dfd expressing NBs as indicated by an arrowhead in the magnification. NB progenies are situated at the basal side of NBs and are characterised by nuclear Pros protein (green). (**B**) *Dfd*^{16}-mutant embryos show an abnormal localisation of Pros, spreading towards the apical side of the NB cortex (arrows in the magnification). Note that the position of NB daughter cells is random and some of the cells occupy apical areas of the embryo (asterisks). (**C**-**F**) Protein and mRNA expression of the Roundabout receptors Robo2 and *robo3* in wildtype and *Dfd* loss-of-function mutants. (**C**) In wild-type embryos, Robo2 protein is detectable at high levels in clusters of cells in every segment, except of the mandibular cluster where only faint levels of Robo2 are recognised by the antibody. (**D**) Robo2 is de-repressed in the mandibular neuromere in *Dfd*^{16}-mutant embryos indicated by an arrow. (**E** and **F**) Compared to wildtype (E), robo3 is ectopically expressed in cells located ventral to the SEZ (arrow in F). Scale bars, 20µm.

Pros-expressing progeny cells, most likely GMCs, were located at inappropriate positions close to the apical surface of the embryo.

The second and most comprehensive group of neural Dfd target genes identified by ChIPseq analysis (Sorge et al. 2012) comprised of molecules known to guide the formation of axon pathways and to navigate axons to specific target sites, which are finally recognized by the axon. Axon guidance molecules in vertebrates can be classified into secreted ligands, cell surface proteins or intracellular proteins (reviewed by Araújo & Tear 2003). Whereas intracellular proteins are often part of main signalling systems, soluble molecules that act as guidance cues to attract or repel axons and their corresponding receptors can play distinct roles in midline, longitudinal or motoneuron axon guidance (reviewed by Araújo & Tear 2003). Interestingly, molecules covering all different classes of axon guidance factors were uncovered to be candidate targets of Dfd (Sorge et al. 2012), amongst them Robo, Robo2 and Robo3 (Kidd et al. 1998; Simpson et al. 2000; Rajagopalan et al. 2000), receptors that are part of a major and conserved signalling system at the midline, the Robo/Slit pathway (Kidd et al. 1999; K. Brose et al. 1999). Robo1 and Robo2 play a role in commissure formation while Robo2 and Robo3 regulate the formation of ipsilateral pathways (Rajagopalan, et al. 2000).

Previous analysis on the mRNA-expression of *robo2* revealed a de-repression of *robo2* expression within the mandibular neuromere in Dfd^{16}-mutant embryos (personal communication). As part of this thesis, the expression of at least two of the *Drosophila* roundabout (Robo) family of receptors, Robo2 and Robo3 was found to be altered in Dfd^{16}-mutant embryos. Immunostainings on stage 12 embryos using a Robo2-specific antibody revealed clusters of cells expressing Robo2 at the boundaries between the maxillary and labial neuromere and the deuterocerebral and tritocerebral neuromere in wild-type embryos (**Figure 2.10, C**). In addition, an extremely reduced cluster of only a few Robo2-positive cells was found located between the mandibular and maxillary neuromere. These observations match the described pattern of Fasciclin II (Fas2) expressing founder clusters, which are composed of neurons that pioneer commissures and connectives within the appropriate segments (Nassif et al. 1998). As an example, the maxillary nerve is usually pioneered by cells of the mandibular/maxillary founder cluster. Furthermore, the level of Robo2 protein in cells of the mandibular/maxillary cluster appeared to be very low, evident from a weak Robo2 antibody staining (**Figure 2.10, C**). A remarkable strong Robo2 staining was found in the same cluster in Dfd^{16} mutants, indicative of elevated levels of Robo2 protein in cells of this cluster compared to wildtype (**Figure 2.10, D**). This result suggests, that Robo2 expression in cells of the

mandibular/maxillary founder cluster is tightly regulated by Dfd. Interestingly, Robo2 has been shown to govern distinct axon guidance decisions, among others it promotes the midline crossing of commissural axons. Moreover, overexpression studies using transgenic *UAS-robo2* responder lines in combination with *elav-Gal4* driver stocks of various strength revealed that increasing levels of Robo2 generate a phenotype in which high expression of Robo2 causes axons to completely fail to cross the midline (Simpson et al. 2000; Jhaveri et al. 2004). The capacity of Robo2 to mediate midline repulsion and thus prevent axons from crossing the midline at high expression levels can therefore be linked to the drastic defects in the formation of the mandibular commissure observed in Dfd^{16}-mutant embryos.

Due to the absence of an antibody against Robo3, *in-situ* hybridisations using an antisense RNA-probe against *robo3*-mRNA were performed. As *robo3* is expressed later than *robo2* and not before late stage 13 (Simpson et al. 2000), wild-type and *Dfd* null-mutant embryos were analysed at maximum expression levels of *robo3* around stage 15 of embryonic development (**Figure 2.10, E and F**). Compared to wildtype, *robo3*-mRNA was detected in an ectopic cluster of cells located ventral to the SEZ in Dfd^{16} mutants (**Figure 2.10, F**), suggesting that Dfd normally suppresses the transcription of *robo3* in these cells. A detailed list of the ChIPseq-identified neural Dfd target genes that were confirmed to be differentially expressed in Dfd^{16}-mutant embryos is attached in the appendix of this thesis.

In summary, these results show that Dfd directly regulates genes involved in early processes of nervous system development, as well as factors that are pivotal for the establishment of axon pathways subsequent to neuronal specification. Defects already occur in neural stem cells in *Dfd*-mutant embryos and consequently affect early cell fate decisions, leading to mis-specification of neural cells. Therefore, it is conceivable that the failures in axon guidance decisions observed in Dfd^{16} mutant cells are based on an incorrect assignment of cell fates earlier in the development of these cells. To overcome these "secondary" effects and specifically interfere with Dfd activity at later time points of development, when the basic framework of neural connections is completely set up, the temperature-sensitive (ts) loss-of-function allele of *Dfd* (Dfd^{3}) (Merrill et al. 1987) was used for later analysis.

2.9 Deformed controls the Synaptic Targeting Molecule Connectin

Interestingly, 27 out of 182 identified neuronal ChIPseq genes are expressed by one or few muscle fibres and motor neurons. Several of these genes code for target recognition molecules that have been shown to promote specific connectivity between motoneurons and muscles by attractive or adhesive mechanisms, amongst them Capricious (Caps) (Kurusu et al. 2008; Kohsaka & Nose 2009) and Connectin (Con) (Nose et al. 1992; Nose et al. 1997; Raghavan & R. A. White 1997).

Here, neurons expressing the homophilic cell adhesion molecule (CAM) Con were detected within the mandibular/maxillary neuromere by immunostainings on stage 16 wild-type embryos using Con-specific antibodies (**Figure 2.11, A and B**). However, despite their location within the normal expression domain of *Dfd*, these Con-positive cells lacked Dfd protein, indicated by the absence of Dfd signal. In addition, tracking axon connections of the identified Con-positive neurons unravelled the innervation of Con-expressing head muscles that were devoid of Dfd protein as well (**Figure 2.11, C and D**). Con expression was found on the surface of muscles. However, highly concentrated protein levels were obvious at the innervation sites. These findings pointed towards a role of Dfd in suppressing the expression of *Con* within the Dfd expression domain. This assumption was approved by the detection of *Con* mRNA in *Dfd*-mutant neural cells, which were marked by the presence of *Dfd* mRNA, demonstrating that Dfd normally acts as a suppressor of *Con* (**Figure 2.11, E and F**). Labelling of cells mutant for Dfd is possible since Dfd^{16} mutants still express *Dfd* mRNA, but lack the functional protein. This is in line with the results obtained by Gould and White, showing that *Con* RNA expression is regulated in the CNS by Ubx and other abdominal Hox transcription factors (Gould et al. 1990). Moreover, expression of a regulatory element of *Con*, which directs expression predominantly in the somatic mesoderm, has been shown to be de-repressed in the abdominal segments A1 and A2 in *Ubx*-mutant embryos where *Ubx* function is usually required in the somatic musculature (Gould & R. A. White 1992).

In summary, it can be stated that Dfd negatively regulates the expression of the target recognition molecule Con in neural cells of the mandibular/maxillary neuromere. Further, Con protein localization is confined to Dfd negative muscles, assuming that Dfd suppresses the expression of Con in adjacent muscles, thus ensuring specificity in the matching of partner cells.

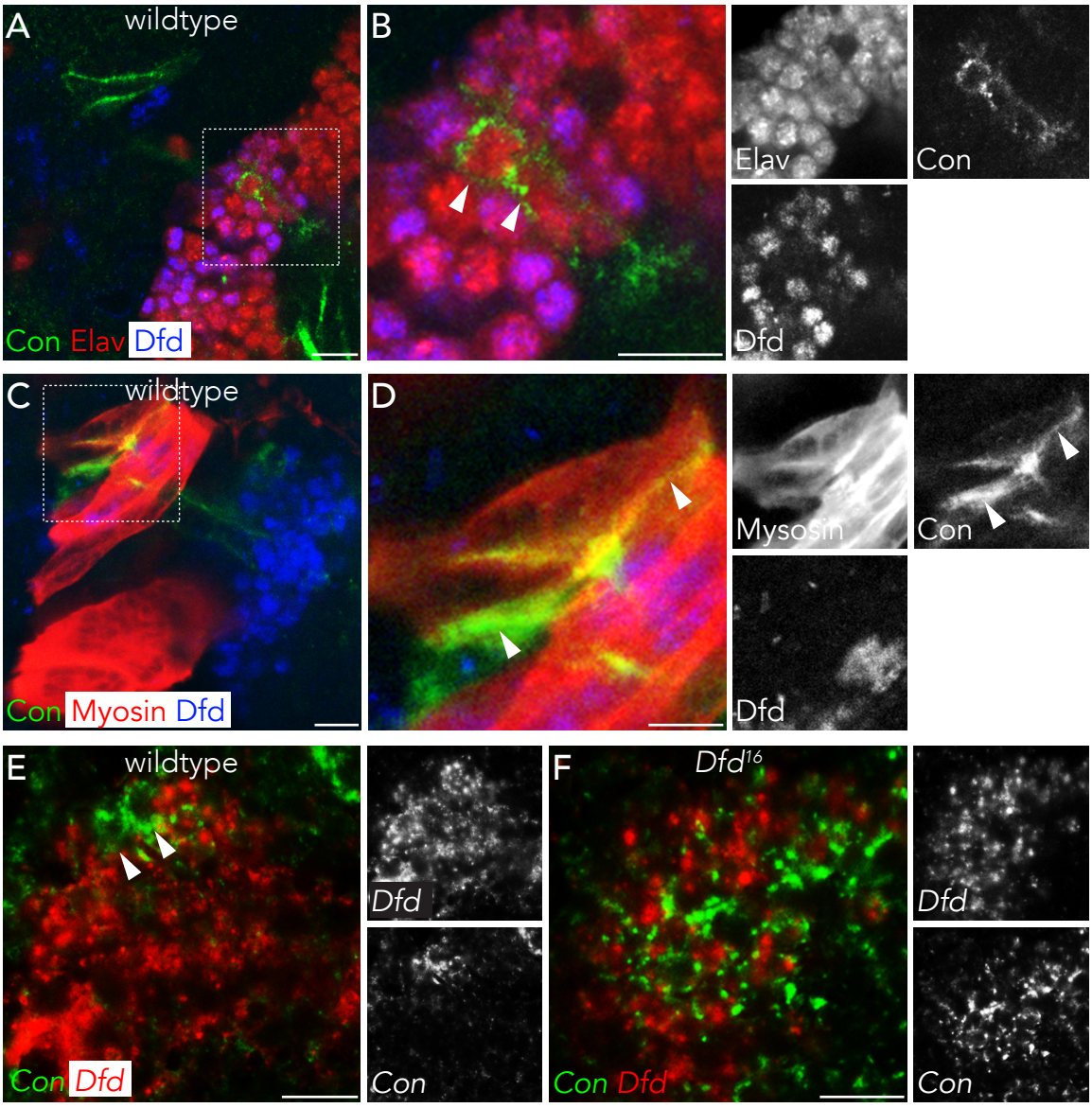

Figure 2.11: Dfd negatively regulates the synaptic target recognition molecule Connectin. (**A-D**) Expression of the homophilic cell adhesion molecule Connectin (Con) in the head of stage 16 embryos. (**A**) Con protein (green) co-localises with Elav (red) in postmitotic neurons located within the domain of Dfd (blue). (**B**) Enlarged view of (A). Note that cells expressing Con are devoid of Dfd protein (arrowheads). (**C**) Localisation of Con (green) on the surface of internal head muscles, which are marked by Myosin-antibody staining (red). (**D**) Enlarged view of (C). Note that Con-positive motor projections innervate Con-positive, yet Dfd-negative muscles. Highest levels of Con protein appeared at the innervation sites (arrowheads). (**E** and **F**) *Con* and *Dfd* mRNA expression in cells of the SEZ of stage 16 wild-type and Dfd^{16}-mutant embryos. Arrowheads in (E) mark *Con* mRNA-expressing cells in the SEZ. Note that these cells are devoid of *Dfd* mRNA. Lateral view. Scale bars, 10µm.

2.10 Inactivation of Deformed during late Embryogenesis affects Mouth Hook-associated behaviour

In the two chapters before, the stage-specific regulation of selected genes identified by Dfd-ChIPseq analysis (Sorge et al. 2012) was shown. Amongst them there are genes that are initially required at the onset of axogenesis or even later for axon target recognition. For this purpose *Dfd*^{16}-mutant embryos were analysed, but precise investigation on the temporal requirement of Dfd was difficult as defects in axon guidance or outgrowth were assumed to be "secondary" and the consequence of defects occurring earlier.

In order to shed light on the role of Dfd in regulating synaptic processes, rapidly reversible *ts*-mutants of *Dfd* were characterised in more detail. Flies carrying the *ts*-allele *Dfd*^{3} and raised at a permissive temperature of 18 °C (*Dfd*$^{3\ (18°C)}$) were fully viable and developed like wild-type individuals with no gross abnormalities (**Figure 2.11, C**). In contrast, animals raised at 31 °C, the restrictive temperature (*Dfd*$^{3\ (31°C)}$), resembled *Dfd*^{16} mutants in various aspects. They failed to hatch due to their inability to perform proper MH movements and died at the end of embryogenesis as completely developed first-instar larvae (**Figure 2.11, C**). Moreover, they exhibited the same and drastic head defects as described earlier for *Dfd* null-mutant embryos (**Figure 2.4, C; Figure 2.11, A**).

Early muscle contractions in the embryo are not driven by the activity of motoneurons, but rather are unrhythmic and occur spontaneously within muscles of one segment or hemisegment (Pereanu et al. 2007). The first coordinated movements appear at stage 17b of embryonic development, the time when synapses have formed and neurons have developed the capacity to generate action potentials to trigger muscle contractions (Prokop 1999; Crisp et al. 2008). When raised at a temperature of 18 °C and shifted to the restrictive temperature at stage 17b of embryogenesis (28 hours AEL), a high percentage (40.3 %) of homozygous *Dfd*$^{3\ (18°C/31°C,17b)}$ mutant first-instar larvae were found dead in their eggshell 48 hours AEL (**Figure 2.11, C**). Moreover, monitoring MH mobility 5 hours after the temperature shift uncovered the inability of *Dfd*$^{3\ (18°C/31°C,17b)}$ mutants to perform any movements of the MHs in comparison to the control, heterozygous *Dfd*^{3} animals balanced by a fluorescently marked chromosome (*Dfd*$^{3\ (18°C/31°C,17b)}$/*TM3*, *Act-GFP*).

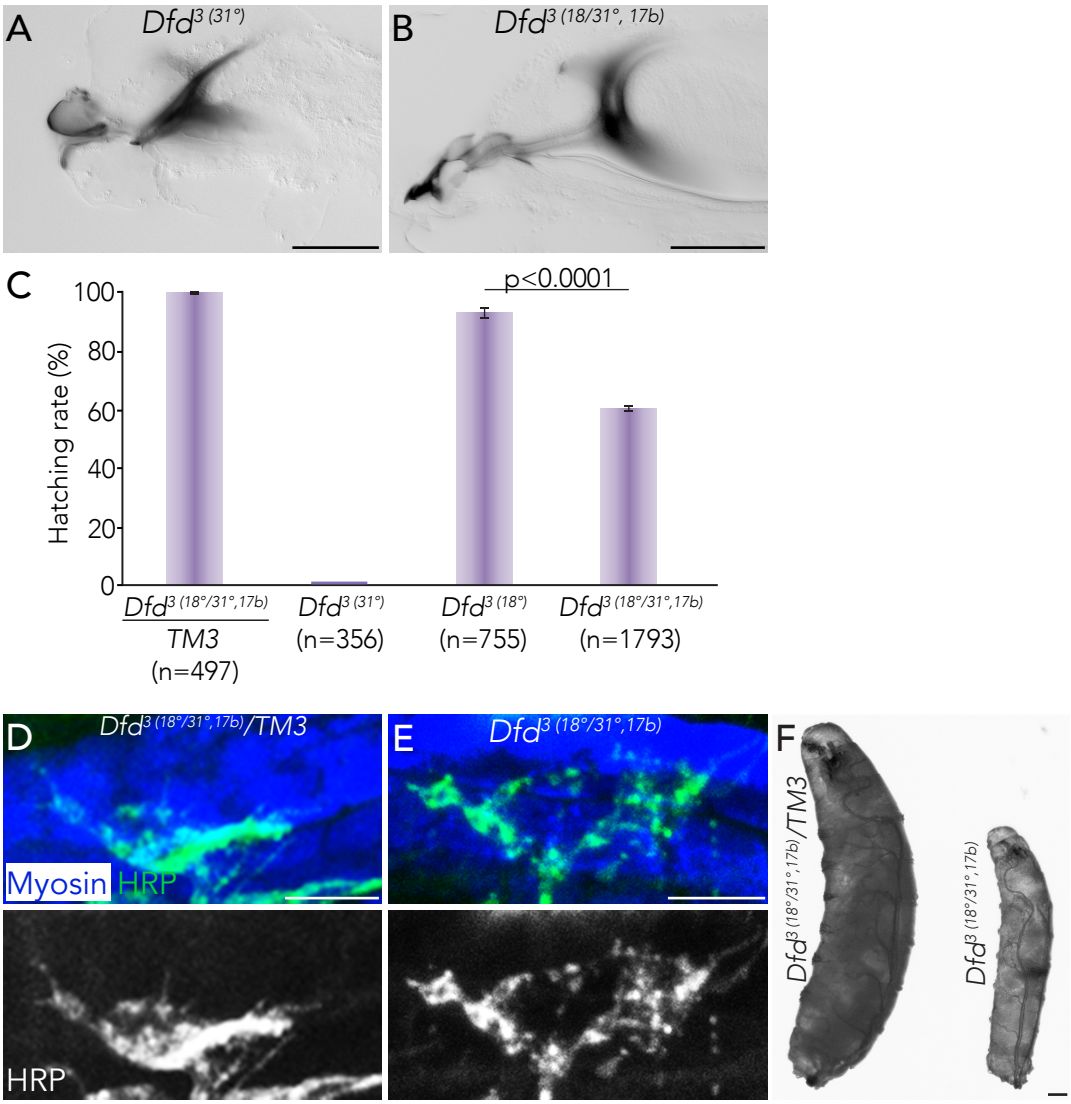

Figure 2.12: Feeding-related behaviours are disrupted upon inactivation of Dfd. (**A** and **B**) Lateral views of the head of first-instar larvae carrying the temperature-sensitive allele *Dfd*^{3} shortly before hatching. (**A**) Animals constantly raised at the restrictive temperature of 31°C show severe defects in head structures. Note the absence of the MHs. (**B**) In *Dfd*^{3}-mutant animals subjected to a temperate shift (18°/31°C) at late stages of embryogenesis (stage 17b) head structures are unaffected. (**C**) Hatching rates of *Dfd*^{3}-mutant embryos raised at the permissive (18°C) or restrictive (31°C) temperature throughout embryogenesis, as well as of homozygous and heterozygous *Dfd*^{3}-mutants subjected to the temperature shift. The mean of three individual experiments is represented. Error bars indicate the standard deviation. (**D** and **E**) Neuromuscular junction, marked by the expression of the neuronal membrane marker HRP (green), on the mouth hook elevator (MHE, blue) of heterozygous (D) and homozygous (E) *Dfd*^{3}-mutant first-instar larvae. (**F**) Example larvae depicting heterozygous (left) and homozygous (right) *Dfd*^{3}-mutant larvae 60 hours AEL. Note the size differences in heterozygous animals, which already reached second instar stages, compared to homozygous larvae that die before the first moult. Scale bars, 40µm in A and B, 10µm in D and E, and 50µm in F.

2.11 Partial deletion of *Dfd* causes Lethality during postembryonic Development

Another piece of evidence emphasizing the requirement for Dfd during the lifetime of *Drosophila* is depicted by the life span of hypomorphic *Dfd* mutants (*Dfd*^{13}/*Df*(*3R*)*Scr*) that have reduced levels of Dfd. As shown in this thesis, 48.3 % of animals died at the end of embryogenesis as completely developed first-instar larvae trapped in their eggshells (**Figure 2.4, A**). Those *Dfd*^{13}/*Df*(*3R*)*Scr* mutants who were able to hatch (51.7 %) were analysed in detail to determine their life span and the time point of death (**Figure 2.13, A**). As illustrated in (**Figure 2.13, A**), 11.8 % of animals that survived hatching died as first or second instars (**Figure 2.13, B**), and 16.4 % of larvae survived until third-instar larval stages before lethality occurred. Apart from embryogenesis, were the majority of *Dfd*^{13}/*Df*(*3R*)*Scr* mutants lost their life, a high number of animals died during pupal stages (19.6 %), either at the very end as a completely developed adult fly unable to eclose, or strikingly early as an incompletely developed larvae of small size (**Figure 2.13, A, C and D**). Adult survivors were only detected in 3.9 % of the cases (**Figure 2.13, A, E-J**). They were delayed in development as they eclosed subsequent to the control (*Df*(*3R*)*Scr*/*TM6*), but were fertile and viable for several days. Different from this thesis, Merril and colleagues claimed that *Dfd*^{13}/*Df*(*3R*)*Scr* mutant adult survivors are unable to inflate their wings (Merrill et al. 1987). Here, all of the surviving adults showed fully inflated wings as well as defects in head structures, like the absence of the maxillary palps, a characteristic phenotype of *Dfd*-mutant adults that has been described earlier (Merrill et al. 1987) (**Figure 2.13, F**). In contrast to what has been published (Merrill et al. 1987), *Dfd*^{13}/*Df*(*3R*)*Scr* adult flies were also able to fully extend their proboscises, a movement required to take up food (**Figure 2.13, H**). Food uptake was proven by rearing flies on red-coloured yeast to document their ability to ingest the yeast. Both, flies of the test group (*Dfd*^{13}/*Df*(*3R*)*Scr*) and of the control group (*Df*(*3R*)*Scr*/*TM6*) were able to take up the food as displayed by their red coloured abdomen (**Figure 2.13, I and J**). However, the amount of food taken up by flies of the different groups was not measured quantitatively and, therefore, feeding defects cannot be entirely excluded.

These results point to the fact that Dfd function is essential throughout the development of a fly. Reduced levels of *Dfd* lead to lethality at different stages of development and, amongst other defects, the inability to perform efficient motor programs required for embryonic hatching, feeding or adult eclosion. Nevertheless, maxillary nerve projections were shown to be present in hypomorphic *Dfd*-mutant

embryos (**Figure 2.9, F**) and, thus, the role of Dfd in the regulation of more intrinsic and synapse related processes needed further exploration in order to be confirmed.

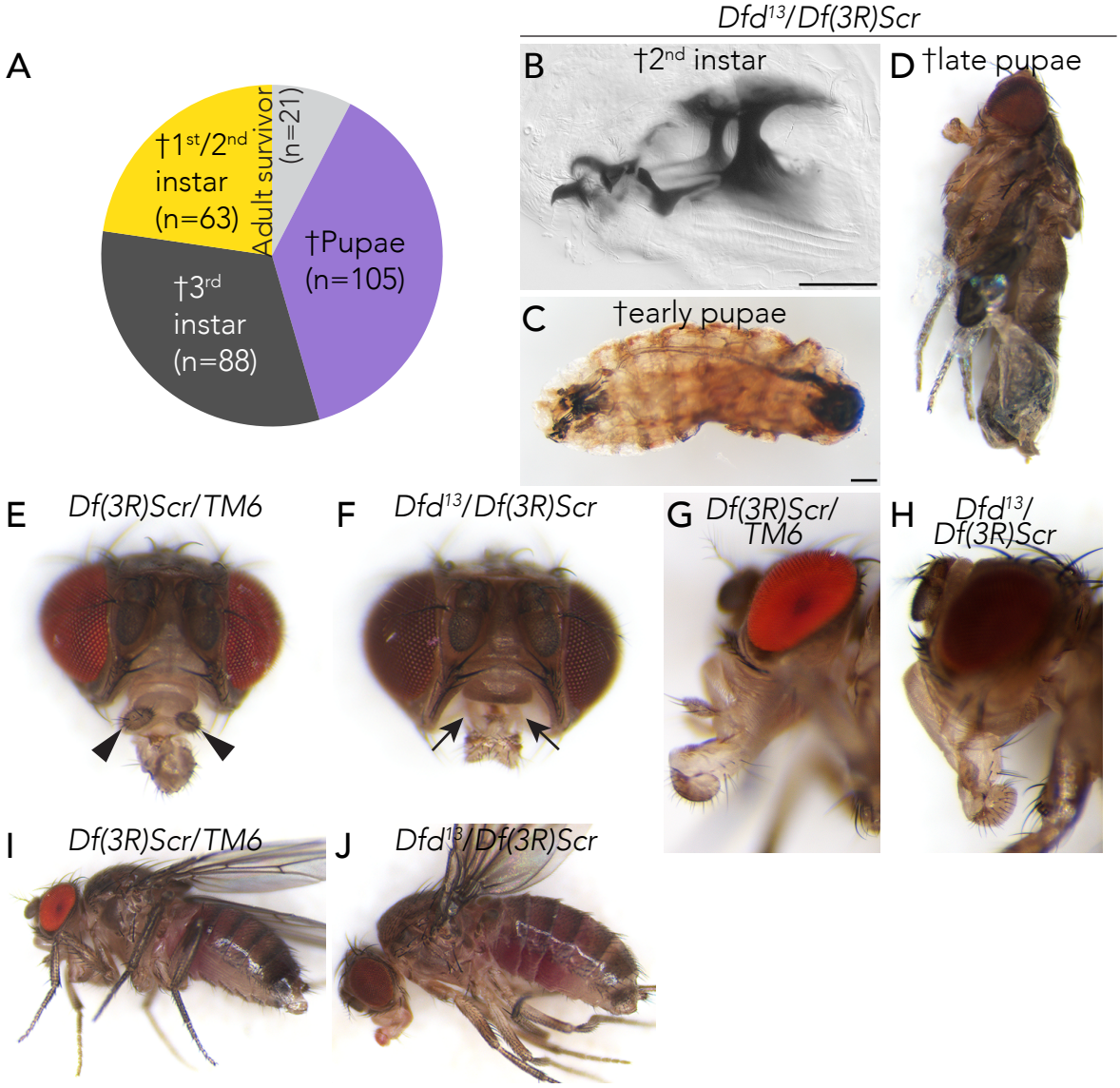

Figure 2.13: Effects of *Dfd* hypomorphic mutations on the life span of *Drosophila*. (**A**) Representation of the 51,7% *Dfd*^{13}/*Df(3R)Scr* animals that survive embryogenesis. Animals die at different stages of life as first, second (**B**) or third-instar larvae or during pupal stages (**C** and **D**). (**E**) Head of a control heterozygous balanced *Df(3R)Scr* fly. The presence of the maxillary palps is indicated by arrowheads. (**F**) Adult *Dfd*^{13}/*Df(3R)Scr* survivors do not develop maxillary palps (arrows in. (**G** and **H**) Proboscis extension of a heterozygous balanced *Df(3R)Scr* fly (G) and *Dfd*^{13}/*Df(3R)Scr* survivor (H). (**I** and **J**) Hypomorphic mutants are able to extend their proboscis and ingest red coloured food. The ingested yeast can be traced by the red-coloured abdomen of the fly. Scale bars, 40µm.

2.12 Loss of Deformed results in Defects in NMJ Morphology

Temperature-induced loss of functional Dfd protein, elicited after the onset of propagated action potentials (Baines et al. 2001), was shown before to influence the capacity of larvae to perform proper movements of the MHs in order to hatch and feed, leading to embryonic and larval death. In fact, the overall structure of the nerve-muscle connections and the innervation of the MHE by maxillary nerve projecting neurons was found to be intact regardless of the time point of examination in affected first- or third-instar larvae. This leads to the conclusion that Dfd directly regulates genes important for synaptic function.

More precise investigations on the morphology of synaptic boutons on the MHE of third-instar larvae revealed an abnormal increase in size and aberrant spacing between single boutons in homozygous *Dfd*^{3} mutant animals shifted as early third-instar larvae to the restrictive temperature (**Figure 2.14, B and G**). Normally, boutons are rounded or oval in shape and, dependent on their type, of specific size (Menon et al. 2013). They are separated from one another by well-defined axon processes in wild-type larval backgrounds (**Figure 2.14, A, C and E**).

In order to quantify the differences in bouton size observed upon removal of functional Dfd protein, control (*Dfd*$^{3\ (18°C/31°C,L3e)}$/*TM3*) and *Dfd*$^{3(18°C/31°C,L3e)}$ mutant third-instar larvae were stained with HRP to visualise NMJs and all boutons on the MHE (**Figure 2.14, A-F**). Five NMJs of each genotype were examined and the size of individual boutons was measured (**Figure 2.14, G**). Although variable, ranging from very small to very large, the majority of boutons was extremely enlarged in NMJs of *Dfd*$^{3(18°C/31°C,L3e)}$ mutants compared to the control. The increase in bouton size in *Dfd*$^{3(18°C/31°C,L3e)}$ mutant larvae was accompanied by a significant reduction in the number of boutons per NMJ. Whereas, control NMJs harboured on average 41 boutons, the average number of boutons within NMJs in *Dfd*$^{3(18°C/31°C,L3e)}$ mutants was only 25. One possible explanation for the diminished number of boutons and their gain in size is the fusion of individual boutons, which is also reflected by the loss of spacing between single boutons observed in NMJs of *Dfd*$^{3(18°C/31°C,L3e)}$ mutant larvae (**Figure 2.14, A-G**).

The defects observed on NMJs of the MHE are unique to this single muscle and are not driven by side effects due to prolonged exposure to a higher temperature. To test this, NMJs on a control muscle, the CDM, of third-instar larvae were analysed in terms of bouton size and bouton spacing. No obvious differences were detected in *Dfd*$^{3(18°C/31°C,L3e)}$ mutants compared to the control (cf. Figure 2.15).

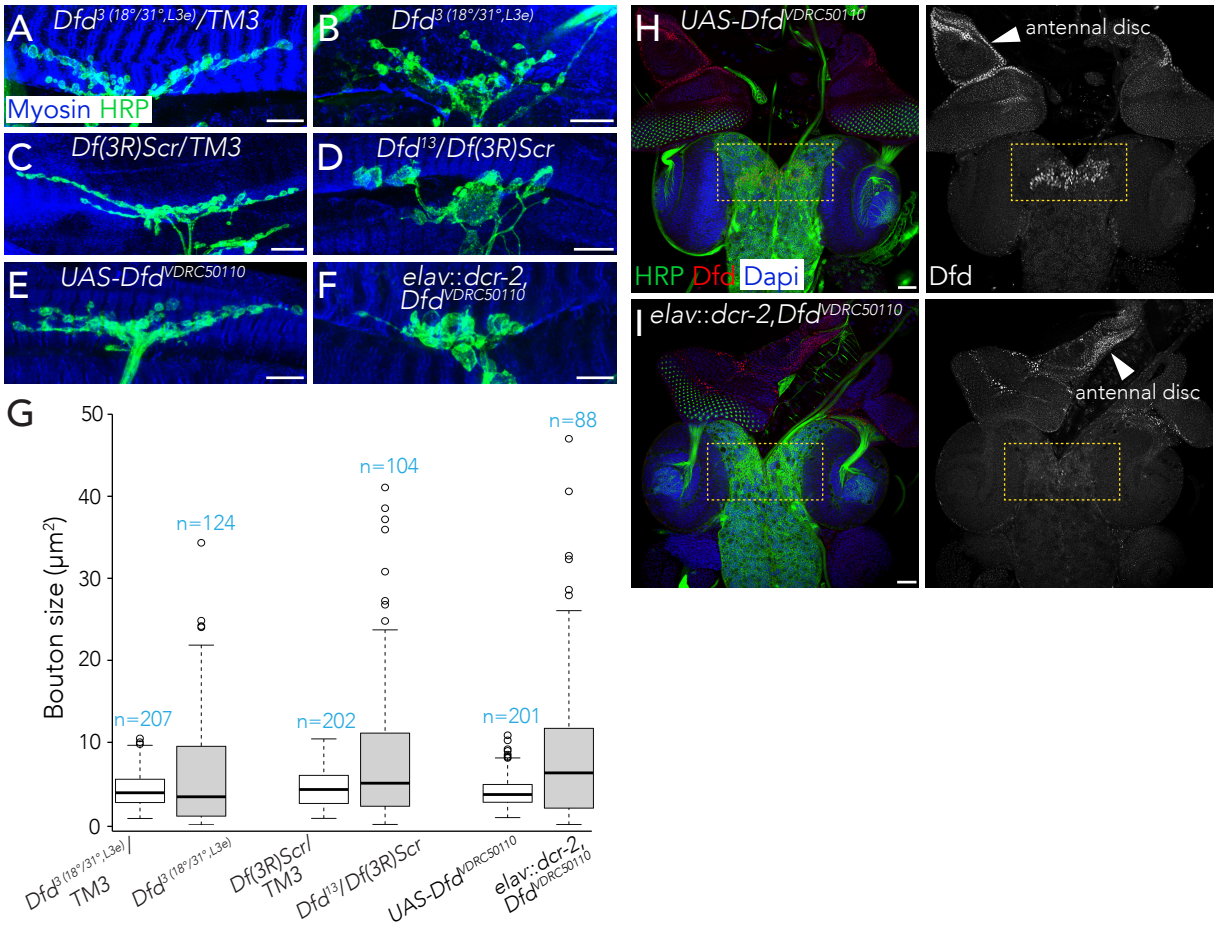

Figure 2.14: Loss of functional Dfd affects synapse morphology. (**A-F**) NMJs on the MHE of third-instar larvae. Muscles are visualised by Myosin-antibody staining (blue), neuronal membranes and synapses by HRP (green). (**A** and **B**) Temperature-sensitive heterozygous control (A) and homozygous (B) *Dfd*^{3}-mutants subjected to the restrictive temperature at early third-instar larval stages (L3e). Note the perturbations in the size of single boutons in homozygous animals. (**C** and **D**) NMJ morphology in control *Df(3R)Scr/TM3* (C) and hypomorphic *Dfd*^{13}*/Df(3R)Scr* (D) larvae. (**E** and **F**) Effect of *Dfd* knockdown on the size and spacing of boutons. The *UAS-Dfd*^{VDRC50110}-line serves as a control (E). *UAS-Dfd*^{VDRC50110} is driven in postmitotic neurons by *elav-Gal4* (F). (**G**) Tukey boxplot representing the quantification of bouton size from five individual NMJs per genotype (n=88-207 boutons). (**H** and **I**) Expression of Dfd (red) in control larvae (*UAS-Dfd*^{VDRC50110}, H) and upon RNAi knockdown in *elav::dcr-2,Dfd*^{VDRC50110} larvae (I). Note that Dfd protein can be detected in the antennal disc in both genetic backgrounds. Scale bars, 10µm in A-F, 40µm in H and I.

Hypomorphic *Dfd* mutants of the genotype *Dfd*^{13}*/Df(3R)Scr* were shown in one of the previous chapters to survive at least partially until third-instar larval stages. Thus, NMJs of third-instar larvae were examined in more detail. Here, too, obvious defects in bouton morphology and spacing were visible in *Dfd*^{13}*/Df(3R)Scr* larvae, but not in the *Df(3R)Scr/TM3* control larvae (**Figure 2.14, C and D**). Further quantification on the size of boutons revealed the same drastic effects described for temperature-sensitive *Dfd*$^{3(18°C/31°C,L3e)}$ mutant larvae (**Figure 2.14, G**). This was reflected again by the average

number of boutons per NMJ, estimated to be 21 for the test group and 40 for the wild-type control.

To refer the abnormalities observed in bouton morphology to motoneuron-specific defects on the presynaptic terminal, Dfd activity was specifically knocked down in neurons. To this end the postmitotic *elav-Gal4* driver line was used to drive the expression of two independent *Dfd*-RNAi transgenes: one of them encoding a long hairpin RNA (Vienna line 50110, referred to as *UAS-Dfd*^{50110}), the other a small interfering RNA (made by S. Sorge), both triggering sequence-specific degradation of *Dfd*-mRNA. Nervous system specific loss of Dfd-protein expression caused by the activity of these constructs, was demonstrated in third-instar larval brains, where Dfd protein is normally detected in neurons of the SEZ (**Figure 2.14, H and I**). However, Dfd levels on the ventral most side of the antennal disc (Diederich et al. 1991), an imaginal tissue giving rise to the adult antenna, remained unchanged as *elav*-Gal4 is not active in cells of this tissue.

NMJs of third-instar larvae of the genotype *elav-Gal4*;*UAS-dcr-2*;*UAS-Dfd*^{50110} showed the most drastic defects in bouton morphology compared to the control (*UAS-Dfd*^{50110}), depicted by HRP-antibody staining and bouton size quantification (**Figure 2.14, E, F and G**). Boutons within NMJs of this group were largest in size compared to the control and to those of the remaining groups tested (*Dfd*$^{3(18°C/31°C,L3e)}$; *Dfd*^{13}*/Df*(*3R*)*Scr*). In addition, the overall number of boutons within affected NMJs was on average 18, whereas control NMJs had on average 40 boutons. Thus, *elav-Gal4*;*UAS-dcr-2*;*UAS-Dfd*^{50110} animals displayed the most severe phenotype with regard to bouton morphology and number. Noteworthy, muscle morphology was completely normal in this genetic background, indicating that all defects observed in the structure of NMJs are of presynaptic and thus motoneuronal origin.

2.13 Ankyrin2-XL, a synaptic Protein, is regulated by Deformed

Loss of Dfd has been shown to cause severe defects in synaptic structure, indicating that genes required for synaptic organisation, stability and/or maintenance are under the control of Dfd. This is in line with an overrepresentation of synaptic genes uncovered in the Dfd-ChIPseq analysis (Sorge et al. 2012). To further prove this assumption, expression analysis on putative Dfd targets with known functions at the synapse were carried out using different genetic backgrounds.

Amongst the relevant genes was *ankyrin2* (*ank-2*), which encodes a membrane-associated adaptor protein, Ankyrin2-XL (Ank2-XL), present at NMJs and implicated in

the organisation of the presynaptic microtubule-cytoskeleton, was found and analysed further. Ank2-XL has been demonstrated to function in complex with the microtubule associated protein (MAP)1B-homolog Futsch (Roos et al. 2000; Hummel et al. 2000) and a second giant isoform encoded in the *ank2*-locus, namely Ank2-L (Stephan et al. 2015). Here, expression of Ank2-XL was found to be altered in all genetic backgrounds analysed when compared to the controls (**Figure 2.15**). First, antibody stainings were performed using a Ank2-XL-specific antibody in combination with HRP staining to visualize neuronal membranes in third-instar larvae. The following genetic backgrounds, in which Dfd function was modified, were tested versus the corresponding controls: (a) *Dfd* $^{3(18°C/31°C,L3e)}$ versus *Dfd*$^{3\ (18°C/31°C,17b)}$*/TM3*, (b) *Dfd*^{13}*/Df*(*3R*)*Scr* versus *Df*(*3R*)*Scr/TM3*, and (c) *elav-Gal4*; *UAS-dcr-2*; *UAS-Dfd*^{VDRC50110} versus *UAS-Dfd*^{VDRC50110}.

A significant reduction in Ank2-XL protein levels was observed in synaptic boutons, axons and especially in axon terminals on the MHE in all the genetic backgrounds with modified Dfd expression analysed (**Figure 2.15, B, D and F**), whereas expression in NMJs on the CDM, which served as a control muscles in (a), appeared to be normal (**Figure 2.15, G and H**).

It has been shown that Ank2-XL controls the organisation of microtubules synergistically with MAP1B/Futsch (Stephan et al. 2015). In order to investigate if changes in the expression of Ank-2XL also affect MAP1/Futsch protein levels, additional antibody stainings using anti-22C10 to detect MAP1B/Futsch, anti-Ank2-XL and anti-HRP were conducted in *Dfd*$^{3(18°C/31°C,L3e)}$ versus *Dfd*$^{3\ (18°C/31°C,17b)}$*/TM3* larvae (**Figure 2.16, A and B**). These revealed a close association of Ank2-XL and MAP1B/Futsch in control axons and synaptic terminals (**Figure 2.16, A**). In contrast, expression of MAP1B/Futsch was reduced after inactivation of Dfd in *Dfd*$^{3(18°C/31°C,L3e)}$-mutant larvae (**Figure 2.16, B**), accompanying the reduction in Ank2-XL protein levels.

Moreover, *ank2*-XL-mRNA expression was examined in the SEZ by fluorescent *in-situ* hybridisation on third-instar larval brains using an *ank2-XL*-specific antisense probe. Again, expression of *ank2-XL* in the larval SEZ was found to be strikingly reduced at a position where the cell bodies of Dfd-positive motoneurons usually reside in (**Figure 2.16, C and D**).

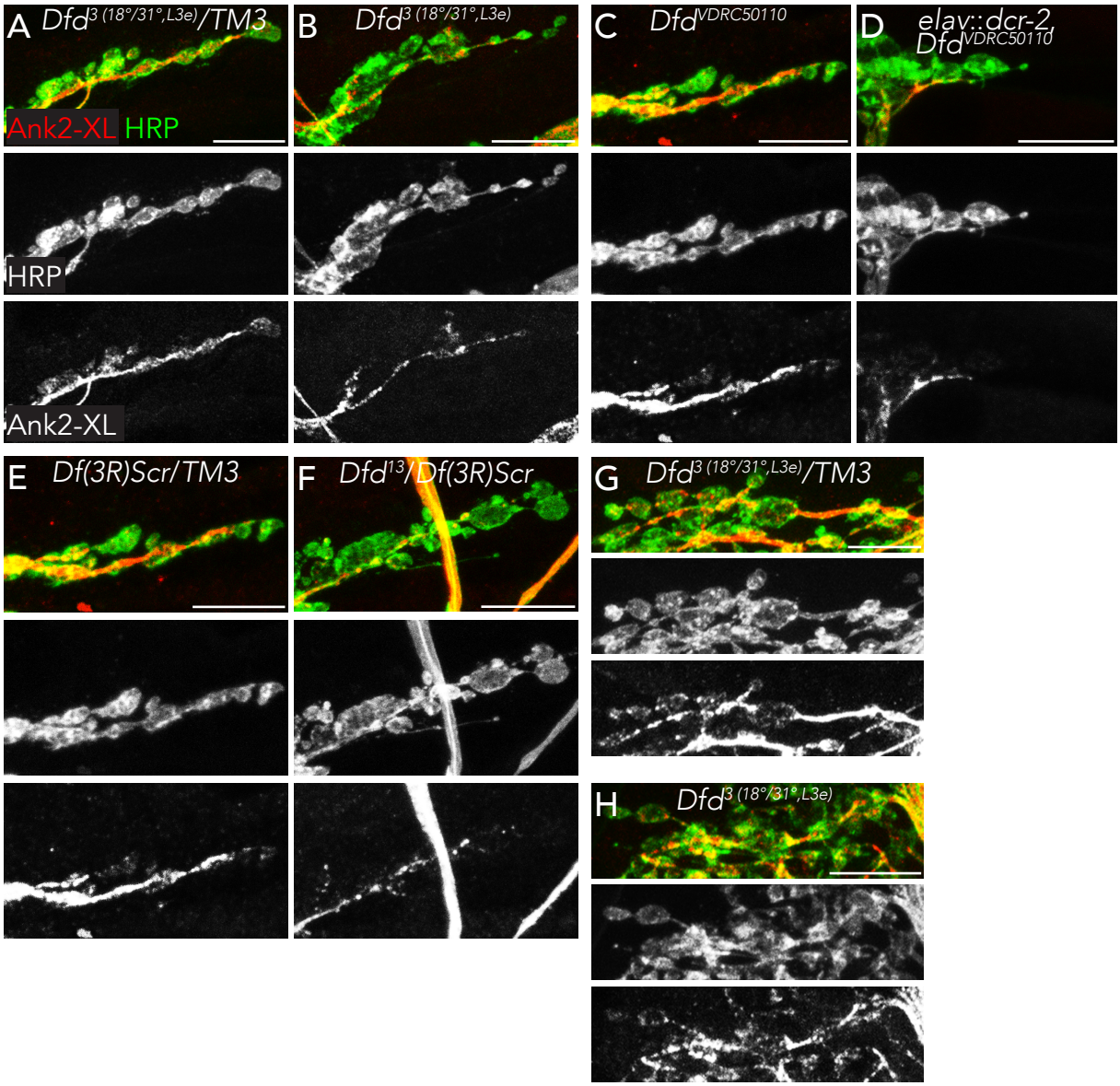

Figure 2.15: Dfd controls the expression of Ankyrin2-XL at presynaptic terminals. (**A-H**) Expression of Ankyrin2-XL (Ank2-XL) in NMJs on the MHE in various genetic backgrounds. Ank2-XL protein is labelled in red and HRP, which stains neuronal membranes and synapses, in green. (**A** and **B**) Temperature-sensitive control (*Dfd*$^{3(18°/31°,L3e)}$/TM3, A) and *Dfd*$^{3(18°/31°,L3e)}$ (B) mutants shifted to the restrictive temperature at early third-instar larval stages. Note that expression of Ank2-XL is reduced especially in terminal boutons and axons of homozygous animals (A) compared to the control (B). (**C** and **D**) Knockdown of *Dfd* in postmitotic neurons using *elav-Gal4*, which drives the expression of *UAS-dcr-2,Dfd*^{VDRC50110} (**C**). *UAS-Dfd*^{VDRC50110} serves as a control (D). (**E** and **F**) Ank2-XL protein expression in control *Df(3R) Scr/TM3* (E) and hypomorphic *Dfd*^{13}/*Df(3R)Scr* (D) larvae. (**G** and **H**) Expression of Ank2-XL in the control cibarial dilator muscle of heterozygous control (G) and homozygous (H) *Dfd*$^{3(18°/31°,L3e)}$-mutants. Note that Ank2-XL protein is uniformly distributed in boutons and axons in both genetic backgrounds. Scale bars, 10µm.

Due to the high background in antibody stainings using the Ank2-L antibody, evaluation on the levels of Ank-L in *Dfd*$^{3(18°C/31°C,L3e)}$ larvae were not possible. However, two additional putative Dfd targets were tested in the scope of this thesis.

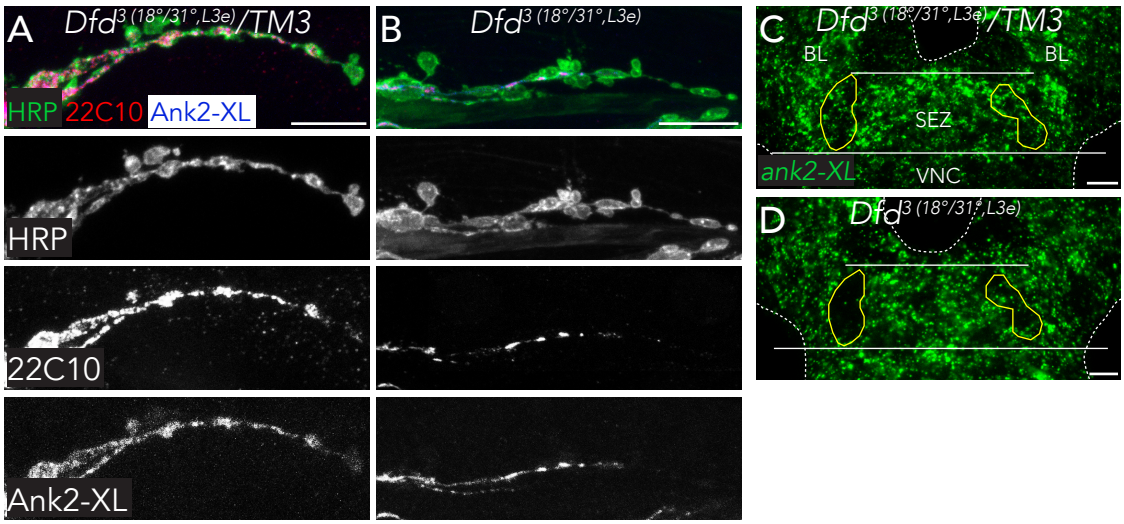

Figure 2.16: The expression of MAP1B/Futsch is altered upon inactivation of Dfd. (**A** and **B**) Expression of MAP1B/Futsch (red) is visualised by anti-22C10 staining on NMJs on the MHE of third-instar heterozygous control (A) and homozygous (B) *Dfd*$^{3(18°/31°,L3e)}$mutants shifted to the restrictive temperature at early third-instar larval stages. Neuronal membranes and synapses are marked by the expression of HRP (green). Ank2-XL protein staining is overlapping with MAP1B/Futsch. Expression of both proteins is diminished in axons and boutons in homozygous *Dfd*^{3}-mutant larvae (B). (**C** and **D**) *Ank2-XL* transcripts in *Dfd*$^{3(18°/31°,L3e)}$/*TM3* (C) and *Dfd*$^{3(18°/31°,L3e)}$ (D) mutants. The SEZ, brain lobes (BL) and the ventral nerve cord (VNC) are indicated. The area where Dfd-positive motoneurons usually reside in is outlined in yellow. Scale bars, 10µm.

The presynaptic vesicle protein Synaptotagmin-1 (Syt1) functions as a calcium sensor and plays an important role in triggering the secretion of neurotransmitters on the one hand and clamping vesicle fusion on the other (N. Brose et al. 1992; DeBello et al. 1993). It has been shown recently that expression of *Syt1*-mRNA is reduced in the SEZ of *Dfd*^{16}-mutant embryos compared to the wild-type control (Bujupi 2016). However, considering the early occurring defects in the mutant background, this phenotype is questionable. The levels of Syt1-protein in NMJs on the MHE were equal in *Dfd*$^{3(18°C/31°C,L3e)}$ larvae compared the control (wildtype/*Dfd*$^{3(18°C/31°C,L3e)}$) (**Figure 2.17, A and B**), suggesting that Syt1 is not regulated by Dfd in motoneurons innervating the MHE, at least not during this developmental stage.

Another crucial factor at the synapse is Stoned-B (STNB) (Kelly & Phillips 2005; Phillips et al. 2009), which is assumed to regulate synaptic vesicle cycling at presynaptic terminals. Like Syt1, expression of STNB was not affected in *Dfd*$^{3(18°C/31°C,L3e)}$ mutant larvae (**Figure 2.17, C and D**), revealed by antibody stainings using a STNB-specific antibody.

In sum, these findings demonstrate that Dfd function is crucial for synapse stability and maintenance as it regulates the expression of *ank2-XL* in motoneurons on the transcriptional level, thus ensuring a proper assembly of the microtubule-organizing complex in presynaptic terminals. Other synaptic proteins like Syt1 or STNB are regulated independent of Dfd. Moreover, these results confirmed the role of this Hox transcription factor in the direct regulation of synaptic target genes.

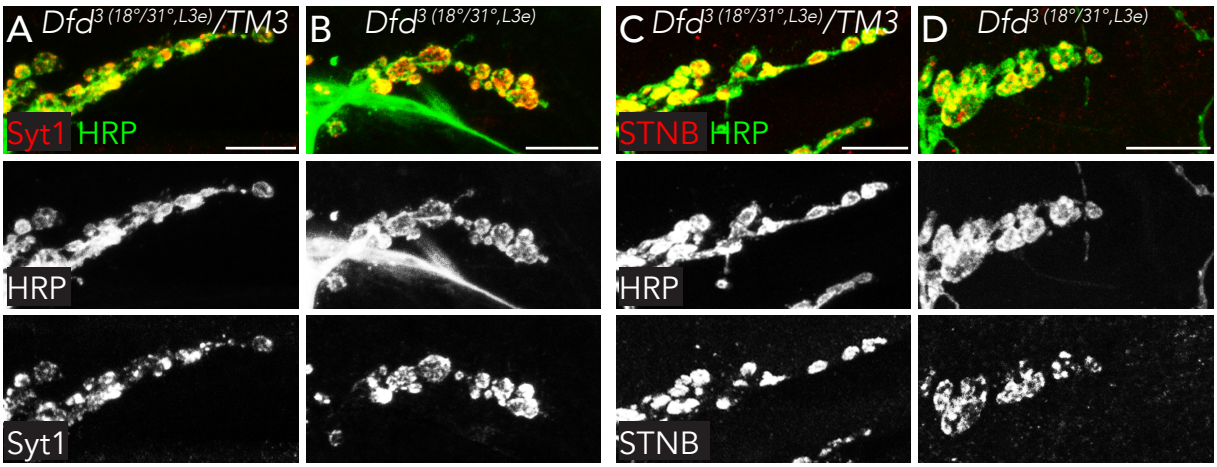

Figure 2.17: Inactivation of Dfd does not affect the expression of Synaptotagmin-1 and Stoned-B. (**A-D**) NMJs on the MHE of third-instar control (*Dfd*$^{3(18°/31°,L3e)}$/TM3, A and C) and *Dfd*$^{3(18°/31°,L3e)}$ mutant-larvae (B and D). Synaptotagmin1 (Syt1, **A** and **B**) and Stoned-B (STNB, **C** and **D**) are labelled in red, neuronal membranes by HRP-staining in green. The expression of both synaptic proteins is not altered in *Dfd*$^{3(18°/31°,L3e)}$ mutants compared to the control. Scale bars, 10µm.

2.14 Knockdown of *ankyrin-2* expression resembles the Defects in NMJ Morphology observed upon Loss of functional Deformed

Expression analysis on Ank2-XL protein and *ank2-XL* mRNA revealed their regulation by Dfd in motoneurons of third-instar larvae, respectively. Furthermore, the morphology of synaptic boutons was found to be dramatically altered in $Dfd^{3(18°C/31°C,L3e)}$ mutant larvae. To address the question whether silencing of *ank2* via RNAi has the same drastic effects on NMJs, a hairpin structure targeting *ank2*-RNA (referred to as $UAS\text{-}ank2^{03374}$) was specifically expressed in the SEZ using the Dfd^{NAE667}*-Gal4* driver line.

Intriguingly, Ank2-protein expression was completely lost from NMJs of the MHE, whereas expression in axons and boutons remained stable in motoneurons innervating the MHD, indicated by co-localization of Ank2-XL and HRP. Furthermore, the morphology of boutons was severely affected, resembling the phenotype of $Dfd^{3(18°C/31°C,L3e)}$ mutant larvae. Boutons appeared to be enlarged and not connected to one another, suggesting that silencing of *ank2* is sufficient to induce the same drastic defects as observed in *Dfd* mutant larvae.

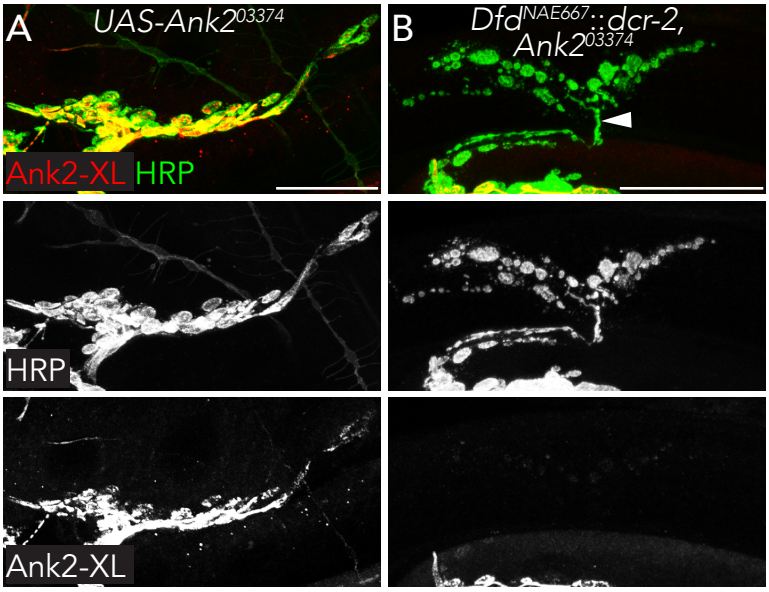

Figure 2.18: Synapse morphology is affected in *Dfd*-expressing neurons after knockdown of *ank2*. (**A** and **B**) NMJs of third-instar control larvae carrying the RNAi construct alone ($UAS\text{-}Ank^{203374}$, A) and Dfd^{NAE667}*::dcr-2*, Ank^{203374} (B) larvae in which an *ank2*-mRNA targeting hairpin structure is driven by the neural enhancer of *Dfd*. Expression of Ank2-XL (red) and HRP (green) is visualised. Note that Ank2-XL cannot be detected in synapses on the MHE and is retracted from the axon before it initially splits into the two trees of the junction (arrowhead in B). Scale bars, 10µm.

2.15 The *Drosophila* autoregulatory Enhancer of *Deformed* drives Expression in Hindbrain Neurons of the Teleost Fish Medaka (*Oryzias latipes*)

Hox genes confer positional identity to neural cell types along the body axis. In vertebrates, the homologs of *Drosophila Dfd*, *Hox4 genes*, are expressed in the hindbrain rhombomeres r7 and r8.

In order to shed light on the evolutionary conservation of Hox function in hindbrain neurons of vertebrates, the *Drosophila* neural enhancer of *Dfd*, Dfd^{NAE667}, was tested *in vivo* for its activity in the vertebrate model organism medaka (*Oryzias latipes*). To this attempt, 664 bp of the original *Drosophila* Dfd^{NAE667} enhancer including two ClaI restriction sites were subcloned into the p339-hsp70-EGFP reporter vector resulting in p339-Dfd^{NAE667}-hsp70-EGFP.

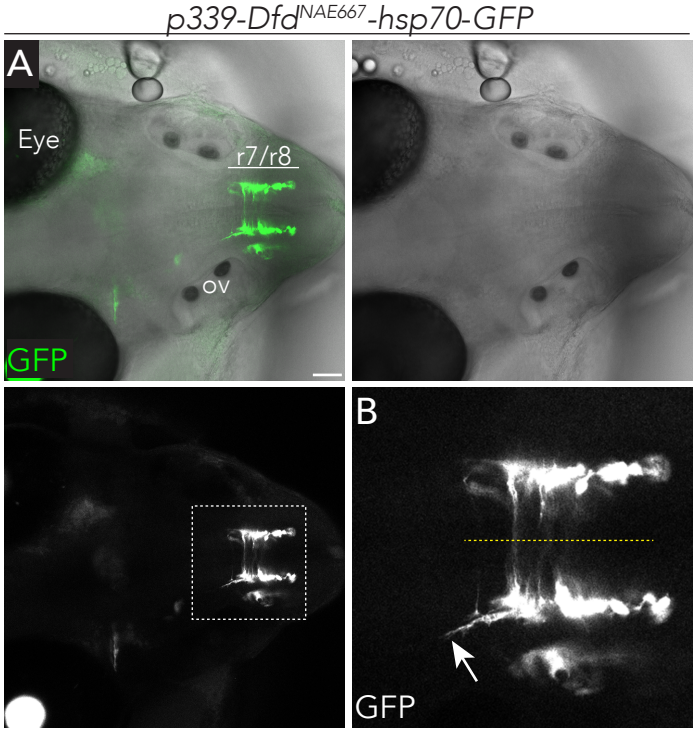

Figure 2.19: The *Drosophila* Dfd^{NAE667} enhancer is active in the hindbrain of the teleost fish medaka (*O. latipes*). (**A** and **B**) Dorsal views of a transgenic medaka embryo (4 dpf) expressing GFP under the control of the neural enhancer of *Dfd* (Dfd^{NAE667}). GFP-expression in the eye is due the p339-transgenesis vector used and indicates the successful genomic integration of the construct. ov, otic vesicles. (**A**) Confocal imaging revealed a distinct set of GFP-positive neurons in the hindbrain rhombomeres 7 and 8 (r7/r8). (**B**) Enlarged view of (A). Note that neurons extend their axons across the midline (yellow dashed line) and towards more anterior regions of the animal (arrow in B). Images were acquired by Dr. Michael P. Eichenlaub. Scale bars, 10µm.

In *Drosophila*, two high affinity binding sites for Dfd (10 basepairs in length), located within the neural enhancer, have been identified and shown to be essential for the binding of Dfd *in vitro*, enabling the expression of target genes *in vivo*. Interestingly, sequence analysis on the medaka genome uncovered one binding site identical in sequence to one of the *Drosophila* Dfd binding sites within the *hoxb4* gene region.

Injection of p339-hsp70-EGFP vector DNA into one-cell stage medaka embryos resulted in transient EGFP-reporter gene expression detected four days post-fertilization (dpf) in cells located in the hindbrain rhombomeres r7 and r8. Obviously, these cells were of neural fate as axon projections towards more anterior regions of the embryo were visible. Later analysis on stable lines (performed by M. Eichenlaub) revealed the neural structure of these cells in more detail.

These results indicate that the fly's neural enhancer of *Dfd* is active in fish in a tissue specific manner and within the expression domain of the vertebrate *Dfd* homolog *Hox4* (A. Davis & Stellwag 2010), suggesting that (Hox4 group) regulatory/transcription factors in medaka are able to direct the expression of this enhancer element *in vivo*, most likely by binding to highly conserved *Hox* binding sites.

3__ Discussion

Rhythmic movements in the head region are common to all bilaterian animals. There is increasing knowledge about the composition of the underlying motor systems and the way neurons are connected to one another and to specific muscle targets. However, little is known about critical determinants regulating the establishment and functionality of such motor systems.

The fruit fly *Drosophila melanogaster* is a powerful model to study neuromuscular development because the nervous system is easily accessible for dissection and imaging and genetic tools to manipulate neuronal function have been widely used.

Here, one of the larval motor units in the head of *Drosophila* is used as a model to illustrate the importance of a particular key developmental regulator underlying the establishment of this vital system. Interestingly, not only the establishment, but also the maintenance of the motor system is tightly controlled by this key factor, which is the Hox transcription factor Deformed.

The objective of this thesis was to, first, characterise the expression of *Dfd* in the fly nervous system and within the motor unit, second, determine the critical steps in the development of the unit under the control of Dfd, and third, unravel the molecular basis of motor unit formation.

3.1 Deformed is expressed in Neural Cells of a Feeding Motor Unit in the Head of *Drosophila*

Neural stem cells in the developing CNS are adapted in number and type to the functional requirements of the regions, were they delaminate in. Within the gnathal neuromeres, which constitute the SEZ (between brain and thoracic neuromeres), the Hox transcription factor Dfd is expressed in all neural stem cells, called NBs in *Drosophila*, located in the mandibular and anterior-maxillary neuromere. Moreover, expression of Dfd is not confined to NBs, yet continued throughout embryonic development and beyond. At later stages of embryogenesis Dfd protein was detected in the majority of postmitotic neurons within the allocated neuromeres. However, not all postmitotic neurons within the *Dfd* domain expressed Dfd. Some of these Dfd-negative cells were identified in the anterior part of the mandibular neuromere in close proximity to the adjacent intercalary segment. Thus, Dfd, which is initially expressed in all NBs, probably gets lost in some of the postmitotic progenitor cells. Factors regulating the differentiation and subsequent steps in the development of these neurons remain unknown. Whether different Hox factors adopt the function of Dfd has not yet been determined.

A small number of Dfd-positive progenitors developed into motoneurons. These motoneurons were visualized during late embryonic stages, but due to limitations in the experimental readout, the correct number of these cells in the embryo could not be determined. The same problem hampered further investigations on the specific muscle targets of these motoneurons in the embryo. In fact, axons of Dfd-positive motoneurons projected into the maxillary nerve, a major nerve route that is known to innervate the MHE and MHD muscles in *Drosophila* larvae, thus enabling the elevation and depression of the MHs during larval feeding (Schoofs et al. 2010).

For the detailed characterisation of Dfd-expressing motoneurons and their muscle targets, analyses were pursued in the larval system where neurons and their connections are easily accessible and large in size. The known neural enhancer element, *Dfd*-NAE (Lou et al. 1995), was modified and approved in the embryo for its specificity to label *Dfd*-positive neurons. In the embryo, Dfd^{NAE667}-*Gal4* driven reporter gene expression was shown to recapitulate the endogenous expression of Dfd faithfully during neurogenesis, yet activity of this element extended towards more posterior segments and into the expression domain of the *Hox* gene *Scr* (Hirth et al. 1998), at later stages of embryonic development. This was reflected by staining of both nerve routes, the maxillary and labial nerve in the embryo. Importantly, the enhancer region of Dfd^{NAE667} contains two highly

conserved binding sites for Dfd and the dimeric co-factor Extradenticle-Homothorax (Exd) (Lou et al. 1995; Slattery et al. 2011). Hox proteins have been shown to bind DNA in complex with Exd, thereby increasing the degree of specificity through unique DNA binding site preferences (Slattery et al. 2011). Interestingly, different Hox-Exd heterodimers prefer distinct subsets of a generalized DNA binding site, which is GAYNNAY (where Y = T or C) (Slattery et al. 2011). On the molecular level, this suggested that differences in the amino acid sequences of distinct Hox transcription factors only have an impact on DNA recognition upon hetero-dimerisation with Exd (Slattery et al. 2011). Even more intriguingly, Dfd-Exd and Scr-Exd showed the highest relative binding affinity towards the DNA sequence TGATTAAT, which is exactly one of the sequences found in the Dfd^{NAE667}. Therefore, the binding of Scr to this sequence might explain the shift of *Dfd^{NAE667}-Gal4*-guided reporter gene expression into CNS neurons within the Scr expression domain. Moreover, the same binding site has been shown to be essential for proper activity of the Dfd^{NAE667} element as mutations within this sequence resulted in the complete loss of reporter gene expression in the entire embryo (Bujupi 2016). Certainly, the activity of the enhancer in cells of the PNS along the embryo is also dependent on this particular binding site. This is in line with the moderate relative binding affinity to this core motif reported for six other Hox proteins (Slattery et al. 2011).

Given the fact that the activity of the Dfd^{NAE667} element was strong in CNS cells within the normal Dfd expression domain, this element was used for further analysis. *Dfd^{NAE667}*-enhancer driven expression was restricted to Dfd-positive motoneurons applying an intersectional approach. Connections of these neurons could be traced up to their muscle targets in third-instar larvae. However, this system allowed tracing of motoneurons only at larval stages as reporter gene expression was detectable earliest in first-instar larvae. Another drawback of the *OK371-Gal4* line used in this approach became prominent at larval stages. In addition to Dfd-expressing motoneurons projecting into the maxillary nerve, other neurons, most likely glutamatergic interneurons located within the SEZ were labelled in the context of this experiment. These interneurons have to be considered for the interpretation of any result obtained by using this experimental setup.

Nevertheless, the aim of this experiment was to shed light on the components of the motor unit itself. As revealed by this approach, the unit consists of few motoneurons that projected via the maxillary nerve. The number of motoneurons in the SEZ of third-instar larvae reflects the number of neurons differentiating into motoneurons during embryogenesis (Kuert et al. 2014). Therefore, this experiment identified all Dfd-positive

motoneurons. Using 3D-reconstructions the number of motoneurons was narrowed down to two or three per half segment. However, the exact number of Dfd-positive motoneurons was not determined. One method that allows genetic labelling of the individual motoneurons is the mosaic analysis with a repressible cell marker (MARCM) technique (Lee & Luo 1999; Kim et al. 2009). Implementation of this technique in the future will enable a more detailed analysis on the number and identity of individual Dfd-positive motoneurons, as well as of their neuroanatomical features like the pattern of dendritic arborisation. Using the anatomy of these motoneurons, common resources of driver lines, for example FlyLight (Jenett et al. 2012), can be screened and suitable cell-type specific Gal4 lines identified. This will on the one hand render detailed analysis on the wiring of single Dfd-positive motoneurons within the feeding motor circuit, and on the other hand allow the functional modification of these particular neurons.

On the muscle side, one particular head muscle, the MHE, was identified as target of Dfd-positive motoneurons. This paired muscle has been described to be innervated by side branches of the maxillary nerve and is connected to the dorsal protuberance of the MH via a single tendon (Schoofs et al. 2010). Upon activation of the MHE, the MHs of the larva will be elevated, a motor behaviour required for proper feeding (Schoofs et al. 2010). All NMJs on the MHE were formed by Dfd-positive motoneurons as revealed by co-staining of the neurotransmitter reporter DVGlut. However, the Dfd^{NAE667}-enhancer was not active in motoneurons targeting the MHD muscle although this muscle was shown to be innervated by maxillary nerve projecting neurons residing within the SEZ (Hückesfeld et al. 2015). Presumably, different upstream factors might regulate the development of these motoneurons or even a different enhancer region. The cell bodies of motoneurons projecting via the maxillary nerve clustered together in close proximity (Hückesfeld et al. 2015). Thus it can be speculated whether these neurons eventually originated within the Dfd domain and somehow lost Dfd expression during their development, or if they developed next to the Dfd domain, most likely in the posterior part of the maxillary neuromere, where Scr is expressed. Like Dfd, Scr has been shown to be expressed in all NBs of the posterior maxillary and anterior labial neuromeres (Urbach et al. 2016). Nevertheless, both hypotheses await to be tested and the identity of the MHD innervating motoneurons clarified in more detail.

To summarise, Dfd-positive motoneurons were identified and assigned a place within a particular motor unit, which is known to direct MH elevation during feeding. However, motoneurons directing the counteracting behaviour, MH depression, were not trapped by this approach. This raises the question if these neurons, which innervate the MHD,

were simply not captured by the Dfd^{NAE667} enhancer, or express a different determinant throughout development, eventually the *Hox* gene *Scr*. Probably, they could also have lost expression of *Dfd* during their development, as their cell bodies are likely to be located in the *Dfd* domain and NBs delaminating within this region were shown to express Dfd.

3.2 Deformed is critically required for feeding-related Behaviours

Null mutants of *Dfd* are embryonic lethal (Regulski et al. 1987). They die as fully developed first-instar larvae before emerging from their eggshell. At first appearance Dfd^{16} mutants show severe defects in the structure of the head skeleton, which might alone be sufficient to force early death. In addition, *Dfd* null-mutant embryos show severe defects in the organisation of CNS axon tracts and internal head muscles. Dfd expression in neural cells of the embryo has been reported outside (Lou et al. 1995; Hirth et al. 1998; Urbach et al. 2016; Becker et al. 2016) and within this thesis. Yet unknown was the expression and function of Dfd in embryonic muscles. Dfd protein was detected in two defined head muscles, most likely representing the MHE and MHD. Possibly, a timeline of Mef2 expression could clarify the origin of specific muscles, like the MHE and MHD, in the embryo. Another approach to capture the developing internal head muscles in more detail would be life imaging. Nevertheless, Dfd^{16} mutants showed drastic defects in muscle formation and morphology, pointing towards a function of Dfd in muscle specification. Recently, it has been shown that Ubx/Abd-A contribute to muscle specification by controlling the segment-specific number of muscle progenitor cells allocated to each muscle. Moreover, they control the expression of identity transcription factors in specific muscle progenitors, such as Nautilus and Collier (Enriquez et al. 2010). Notably, in the absence of *Hox* input, *Col* expression was lost in these progenitors and the respective muscles did not form in *Hox* mutants.

However, this work shows that Dfd is crucial for head-associated motor activities as animals with normal developed head structures, yet reduced levels of Dfd, showed improper motor behaviour and were not able to hatch at the end of embryogenesis. Moreover, the loss of motor activity in these hypomorphic embryos can be attributed to neural defects, although the structure of muscles was not further examined in this mutant background. Future research must be undertaken to investigate the contribution of muscles to the loss of motor activity in *Dfd* mutants. A prerequisite to approach this is, however, that the identified head muscles can be specifically targeted by knock down of

Dfd. The ideal tool to tackle this question would be a *Dfd*-specific muscle enhancer. However, to date such an enhancer could not be identified. Extensive work has been carried out on RNA interference in the embryo, aiming towards tissue-specific *Dfd* interference. Nevertheless, any effort to get this technique working in the embryo failed and muscle directed *Dfd*-RNAi could not be applied. To overcome this problem, alternative methods that became available recently will be used in the future. One example is the deGradFP system (Caussinus et al. 2011). This system relays on the degradation of a GFP-tagged version of the protein, which already has been generated subsequent to the work presented here.

A main achievement of the present study was to assign functionality to the identified Dfd-positive motoneurons innervating the MHE. This was shown when controlling neuronal function. Blocking synaptic transmission artificially and exclusively in *Dfd*-expressing motoneurons led to the loss of feeding-associated motor behaviours in embryos and larvae, and concomitant to late embryonic or larval death, most likely due to starvation. The cause of death is debatable as MH mobility during crawling was investigated, yet feeding assays were missing. Anyhow, affected larvae were obviously inhibited in their ability to grow in size, suggesting that they failed to feed properly. Intriguingly, MH elevation movements were affected upon neuronal silencing of *Dfd*-positive neurons, but not the ability of animals to perform counteracting movements of the MHs. Here, depression was shown to be slightly stronger in test animals. Unfortunately, the intersectional approach used for the visualisation of the *Dfd* motor unit could not be applied in the embryo and hence input of interneurons and sensory neurons had to be eliminated differently by using the Cha-GAL80 transgene in addition. However, as mentioned earlier, input of glutamatergic interneurons cannot be completely excluded even when using the intersectional approach, so these cells might have contributed to the phenotypes observed.

In summary, feeding-like behaviours are controlled cell-autonomously by Dfd-expressing motoneurons. Nevertheless, the precise function of *Dfd* in the head musculature needs to be elucidated further. Moreover, the activity of the *OK371*-Gal4 line in non-motoneuronal Dfd-positive glutamatergic neurons might have contributed to the phenotypes observed as synaptic transmission has been blocked in all neurons.

3.3 Deformed determines the developmental Program of Neural Cells

Dfd null-mutant embryos show remarkable defects in the structure of the CNS. Probably, these are due to a combination of different cellular phenotypes that are discussed in the following section. First, the role of cell-death is explained, second, alterations in the localisation of neural fate determinants, and third, changes in the expression of axon guidance factors.

The results described here show that the number of apoptotic cells was not increased in Dfd^{16}-mutant embryos, but rather decreased, implying an excess of neurons in the mutants compared to wild-type embryos. This is in line with the function of Dfd in the regulation of the cell death promoting gene *reaper* (*rpr*) (Lohmann et al. 2002). Cell death-mutant embryos (*H99*), that are depleted of *reaper* and two other pro-apoptotic genes, *head involution defective* (*hid*) and *grim,* show supernumerary cells in the CNS, amongst them NBs (K. White et al. 1994). Whether additional cells, which are usually eliminated in the wildtype, affect the pattern of axon pathways in Dfd^{16} mutants has not yet been examined. Notably, blocking PCD in specific brain lineages of *Drosophila* revealed an abnormal arborisation and perturbed innervation pattern of neurons (Jiang & Reichert 2012). Moreover, the organisation of the nervous system in *H99*-mutant embryos was shown to be impaired in that junctions of longitudinal and commissural bundles were thickened (L. Zhou et al. 1995), a phenotype reminiscent of Dfd^{16}-mutant embryos. The authors of this publication have proposed that excess neurons in H99 mutants may send out axonal processes. Therefore, one possible explanation for the defects in the scaffold of axons observed in Dfd^{16} mutants is that *rpr* and thus PCD were not sufficiently induced in these mutants. Presumably, this led to an excess of NBs and neurons within the mandibular and maxillary neuromeres and concomitant to supernumerary axon outgrowth within this region. This hypothesis is in line with previous analyses showing increased numbers of NBs in *Dfd*-loss-of-function mutants and upon clonal *Dfd* or *lab* loss-of-function during postembryonic brain development (Kuert et al. 2012; Kuert et al. 2014; Urbach et al. 2016).

Studies on the homeobox genes *orthodenticle* (*otd*) and *empty spiracles* (*ems*), which specify the SPZ, have revealed that mutants for *ems* showed dramatic defects in brain patterning (Hirth et al. 1995). Brain deletions in the mutant regions were due to a lack of neurons. However, *Dfd* null-mutant embryos do not show brain deletions and as reported previously the number of NBs is rather increased compared to wildtype (Urbach et al.

2016). Nevertheless, *Dfd*^{16} mutants are characterised by defective longitudinal connectives and a reduced or missing mandibular commissure. This is comparable to what is seen in mice lacking *Hoxb1*, which show an abnormal migration of motoneurons resulting in the loss of a main motor nerve in rhombomere r4 of the mouse hindbrain (Studer et al. 1996; Guthrie 2007), where Hoxb1 is selectively expressed (Studer et al. 1994). Interestingly, these motor neurons become differentiated within rhombomere r4, yet are mis-specified and adopt a rhombomere r2/r3-like identity (Studer et al. 1996). Moreover, specific markers of rhombomere r4 identity are not upregulated in these cells. Instead, ectopic expression of rhombomere r2 marker genes occurs, indicative of an altered identity (Studer et al. 1996).

This is in line with the homeotic transformation of specific NBs located within the maxillary neuromere, which usually give rise to uniform lineages comprising of glia cells (Becker et al. 2016). In *Dfd* null-mutant embryos these NBs form progenies equal to those of serially homolog NBs in the labial neuromere, consisting of glial and neurons.

However, this work unravelled changes in the localisation of an important cell-fate determinant, Pros. It is unlikely that the effects occurring upon loss of Dfd lead to a lack in the expression of Mira in the affected cells in a *Dfd*-mutant background, as loss of Mira has been shown to result in the cytoplasmatic distribution of Pros protein (Shen et al. 1997), a phenotype that was never observed in *Dfd*^{16}-mutant embryos. Instead, Pros formed crescents that were randomly localized along the cell membrane of NBs in the mutant background, indicative of an abnormal localisation of the tethering molecule Mira. This observation is in line with the phenotype described for mutants of the *insc*. Embryos homozygous for a null allele of *insc* showed mis-localisation of Pros and Mira along the NB membrane, although both molecules were found to be tightly associated with the cell membrane and overlapped in their expression (Shen et al. 1997; Akiyama-Oda et al. 2000). Insc protein itself is sequestered to the apical cortex of NBs and requires Pins and Baz for its correct localisation (F. Yu et al. 2000;Wodarz et al. 1999; Schober et al. 1999). In mutants of *baz,* Pros was found all around the cell cortex of NBs (Wodarz et al. 1999), resembling *insc* and *Dfd*-mutant phenotypes. Therefore, the mis-localisation of Pros in NBs of *Dfd*^{16}-mutant embryos might be due to the loss of *baz* or *insc* expression in the respective NBs, which needs to be tested further. Interestingly, not only *pros*, but also *baz* and *insc* were uncovered to be potential direct targets of Dfd by ChIPseq analysis (cf. 3.4, Appendix). Defects in the positioning of NB progenies occurring in the *Dfd*-mutant background resemble those observed in mutants for *baz* (Wodarz et al. 1999) and might be explained by an aberrant spindle orientation. In embryos lacking *baz*

function, the mitotic spindles in NBs are mis-oriented and proteins like Mira fail to localise asymmetrically in metaphase, but instead are evenly distributed at the cell cortex (Schober et al. 1999). However, despite these defects during metaphase, Mira has been shown to finally concentrate at the basal cortex of NBs during telophase in *baz*-mutant embryos (Schober et al. 1999), showing that cortical polarity in NBs and thus the segregation of fate determinants can be restored during late mitosis (Ramat et al. 2017). In the context of this study, the cell-fate determinant Pros was localised correctly to NB progenies located in close proximity to the NBs, both in wild-type embryos and Dfd^{16} mutants, indicating that Pros segregation was not affected during asymmetric cell divisions. Nevertheless, the aberrant apical localisation of NB daughters and their progeny strongly suggests defects in apicobasal polarity and therefore spindle orientation, which is likely to affect the neural identity of cells in the maxillary and mandibular neuromeres.

Incorrect specification of neural cells appears to be a possible explanation for the lack or change in the expression of specific sublineage markers in cells mutant for *Dfd*. Usually, each NB expresses a typical and combinatorial set of marker genes. Remarkably, NBs and their progenies are not only characterised by the expression of those identity genes, but also by the neuroectodermal position and time point of their formation (Urbach et al. 2016). In addition, it has been shown that gnathal NBs represent serial homologs of the NBs in the thoracic and abdominal neuromeres although some of these NBs generate modified segment-specific lineages (Rogulja-Ortmann & Technau 2014). This is mainly due to the action of *Hox* genes that shape serially homologous lineages, thereby promoting the diversity of segmental units within the CNS (Rogulja-Ortmann & Technau 2014). Segment-specific lineages are marked by the expression of sublineage markers, like Eve. The absence of Eve expression from cells in the maxillary and mandibular neuromeres in Dfd^{16}-mutant embryos indicates a change in the fate of cells. However, the molecular signature of these mutant cells and hence their identity remains unknown. Cells could either have acquired a novel fate, or switched to fates characteristic of other NB lineages. Interestingly, in mutants that lack *eve* expression, axons of RP2 and aCC motoneurons do not enter the muscle field and remain within the CNS, or exit the CNS, but then fail to project along the correct nerve route (Fujioka et al. 2003). The lack of nerve outgrowth in *eve*-mutant embryos is comparable to what was observed in Dfd^{16}-mutant embryos in this thesis. Nevertheless, Eve expression is limited to only a few NB lineages that give rise to motoneurons (Urbach et al. 2016) and it has not been shown in the scope of this work whether these specific motoneurons are indeed the ones targeting

the MHE. Unfortunately, the neural enhancer of *Dfd* is autoregulatory (Lou et al. 1995) and thus cannot be used to restore expression of *eve* in developing neurons in an otherwise *Dfd*-mutant background. Studying nerve outgrowth in this background would give insights into the significance of Eve in the development of *Dfd*-positive neurons and whether it is sufficient to rescue the formation of nerves in *Dfd*-mutant embryos.

Alterations in neural fate decisions have been shown to induce defects in the formation of the axonal scaffold (Doe et al. 1988; Doe et al. 1991). In Dfd^{16}-mutant embryos, axon tracts and axon outgrowth were grossly defective as illustrated by several immunolabelling experiments. These defects are likely to be a consequence of an incorrect cell specification, as reflected by the altered or lost expression of important fate determinants like Pros or the segmentation gene *eve*. As mentioned before, a lack of PCD and thus an excess of NBs and neurons within the mandibular and maxillary neuromeres might also contribute to the disruption of the axonal scaffold observed in *Dfd*-mutant animals. With the exception of minor modifications, the overall pattern of NBs and their gene expression profile is segmentally repeated. Therefore, defects in the formation of axon pathways in *Antp* and *Abd-B*-mutant embryos correspond to those seen in *Dfd* null mutants and are most likely due to the mis-specification of cells.

Given that the outgrowth of efferent axon projections into the maxillary nerve and in part motor behaviour was rescued when Dfd was reintroduced specifically into motoneurons, it is unlikely that these early occurring defects alone have an impact on maxillary nerve formation and thus feeding-related movements. In line with this assumption, the expression and localisation of important axon guidance factors was affected upon loss of *Dfd*. Besides Robo2 and Robo3, several other putative direct targets of Dfd important for axon guidance and outgrowth, which have been identified by Dfd-ChIPseq analysis, were analysed further for their expression in wild-type versus *Dfd* null-mutant embryos. However, the most striking change in expression was detectable for the two members of the Robo family of axon guidance receptors. Interestingly, Robo2 is implicated in the guidance of motoneurons towards ventral body wall muscles (Santiago et al. 2014). In mutants for *robo2,* axons that normally innervate a set of muscles in the body wall were either absent or stalled before reaching their target muscles (Santiago et al. 2014). It is difficult to attribute any defects seen in *Dfd*-mutant embryos to the de-repression of *robo3* close to the ventral nerve cord. Elevated levels of *robo3* have been shown to cause shifts in the positioning of sensory neuron terminals in the antennal lobe of the *Drosophila* brain (Jhaveri et al. 2004). However, similar shifts in the positioning of axon pathways were not detected in Dfd^{16}-mutant embryos.

In summary, the data provided in this thesis reveal that proper function of Dfd is crucial during early steps in the development of neurons, like cell-fate specification and PCD. Moreover, they also imply that subsequent steps in the establishment of nerve-muscle connections and hence coordinated motor patterns are regulated by Dfd. This late function of Dfd appears to be independent of its early function during neurogenesis.

3.4 Deformed connects Neurons and Muscles

Body wall muscles of *Drosophila* larvae express distinct types of cell-adhesion molecules or secreted factors. These "signals" are interpreted by neural cells in order to form proper synapses on the "correct" muscle targets. Despite the great knowledge of molecules that enable synaptic target recognition between neurons and muscles of the body wall (reviewed by Nose 2012), nothing is known about factors managing the correct matching of synaptic partners in the head of *Drosophila*. Moreover, there is a general lack in understanding the mechanism and regulators upstream of these target recognition cues (Inaki et al. 2010).

Connectin (Con) is usually expressed on a subset of ventral and lateral body wall muscles and on the motor nerves that innervate them (Nose et al. 1992; Raghavan & R. A. White 1997; Nose et al. 1997). The present work revealed the expression of Con in Dfd-negative motoneurons and an internal head muscle, which were devoid of Dfd protein in wild-type embryos. This muscle corresponded to a muscle of unknown origin located on the dorsal side of the muscle cluster, which is most likely associated with the median tooth in first-instar larvae, yet disappears along with the median tooth during the first larval moult. In fact, expression of Con was de-repressed in *Dfd*-mutant cells pointing towards a function of Dfd in negatively regulating Con expression. In line with this finding, expression of a specific enhancer, which has been shown to recapitulate the pattern of Con in the wild-type CNS, was de-repressed in the parasegment (PS)6 of the embryo in mutants for *Ubx* (Gould et al. 1990). Normally, the neuromeres labelled most strongly by this enhancer corresponded to the PS3, 4, 5 and 14, whereas the expression of this regulatory fragment was down regulated in PS6-13. However, in embryos deficient for the whole bithorax-complex, the repression of the enhancer was eliminated in PS6-13. Another study examined the control of a second *Con*-regulatory element, which directed expression in the somatic mesoderm. De-repression of this element was observed in abdominal segments, A1 and A2, in an *Ubx* null-mutant background, showing that Ubx is able to repress this construct (Gould & R. A. White 1992). The authors claimed that Ubx

directly regulates this fragment as it harbours a functional immunopurified binding site (Gould & R. A. White 1992). Here, Con was uncovered as a putative direct target of Dfd by ChIPseq analysis and the expression data of *Con*-mRNA in *Dfd*-mutant embryos further substantiates the ability of Hox transcription factors to repress *Con*.

The finding that Con is de-repressed in cells mutant for *Dfd* raises the intriguing question about whether and/or how Con mis-expression contributes to the characteristic phenotype observed in Dfd^{16}-mutant embryos. It has been reported in the literature that ectopic expression of Con in all muscles did not result in gross developmental defects of the CNS or muscle (Nose et al. 1997). However, upon muscle mis-expression, Con-positive motoneurons projected to a non-target muscle located next to their actual target muscle. Unfortunately, to date no studies have been carried out on the mis-expression of Con in motoneurons. Preliminary experiments using the neural enhancer of *Dfd* to drive expression of Con in the whole SEZ did not provide decisive results, but initially showed that an elevated number of Con-expressing neurons emerged from the Dfd-expression domain and converged into a thickened maxillary nerve in order to innervate the Con-positive muscles described in this work.

These preliminary results are contradictory to those obtained in *Dfd* null-mutant embryos, where efferent maxillary nerve projections are completely missing. Nevertheless, overexpression of Con was not approached in the *Dfd* null-mutant background, due to the autoregulation of the neural enhancer of Dfd, and therefore included the presence of Dfd, which could fulfil its function during neurogenesis. Thus, cells in the SEZ that ectopically expressed Con were most likely specified correctly, but possibly their axonal projections were guided through incorrect pathways out of the CNS and not solely along longitudinal or commissural pathways. Nose and colleagues reported the expression of Con on a subset of longitudinal and commissural axon pathway, which contain interneurons and on at least two specific peripheral glia cells (PG1 and PG3) that are associated with the axonal tracts of motoneurons (Nose et al. 1994; Hilchen et al. 2008). Interestingly, NB1-3 that normally gives rise to PG1 and PG2 does not form in the mandibular neuromere and its existence in the maxillary neuromere is unclear (Urbach et al. 2016). The results presented in this work indicate the existence of those types of PG cells that enable Con-positive motoneurons to exit the CNS. However, it is most likely that in addition to PG1 and PG3 even more glial cells express Con upon mis-expression of Con using the Dfd^{NAE667} enhancer. Do date it has not been shown whether reporter gene expression driven by this enhancer overlaps with a glia-specific marker.

In the previous chapter of this discussion, the role of Dfd in regulating genes required for the guidance of axon was pointed out. It is widely believed that multiple cues act in a combinatorial and simultaneous manner to generate the precise pattern of neuromuscular connectivity (Winberg et al. 1998). This idea is supported by the fact that loss of functional Con and other target recognition molecules only partly disrupt proper targeting, suggesting that their function can be redundant (Nose et al. 1994; Nose et al. 1997; Shishido et al. 1998; Abrell & Jäckle 2001). Therefore, a combination of attractive and repellent cues may serve to allow neurons to be guided onto correct pathways and to undergo specific target recognition. In *Dfd*^{16}-mutant embryos, however, the combinatorial loss or gain in the expression of molecules implicated in the guidance and/or outgrowth of (moto)neurons might be decisive for the overall defects in the axonal scaffold and the inability of neurons to exit the CNS. With regard to the function of glia in this process, the expression of relevant guidance cues certainly was altered in the mutant cells as well, provided that glial cells are adequately specified in a *Dfd* null-mutant embryo. If this interpretation is correct, then it suggests that expression of *Con* in *Dfd*-mutant cells is not sufficient to elicit the same phenotype, namely the ectopic outgrowth of axons, then does the overexpression of Con in the nervous system in an otherwise wild-type background. Another piece of evidence substantiating this assumption is that a rescue of axonal outgrowth was achieved when *Dfd* was reintroduced into neurons. In the future it will be of interest to identify the complete set of molecules that are negatively or positively regulated by Dfd on interacting muscles and neurons.

To summarise, although the findings presented here do not provide any data about specific target recognition molecules expressed in interacting *Dfd*-positive motoneurons and muscles, it demonstrates that factors that are expressed in both cell types to guide the matching of synaptic partners can be negatively regulated by Dfd, at least in neurons.

3.5 Deformed Function is required throughout Embryogenesis and beyond

A longstanding question in the Hox field of research is how *Hox* genes accomplish their segment and tissue-specific functions during development. At least two reasonable explanations exist, the first assuming that early expressed *Hox* genes set in motion a cascade of transcriptional regulators that on their own determine the neural identity of different subtypes of cells. This in turn leads to the activation of subtype-specific developmental programs and to the expression of subtype-specific molecules essential for axon guidance and target innervation. However, a second possibility might be that Hox TFs directly act on early cell-fate specification genes as well as on those crucially required for later aspects of development. Several results reported in this thesis support the latter hypothesis in that Dfd controls the developmental program at different stages of the *Drosophila* life cycle.

Inactivation of Dfd in the established motor unit and after the onset of coordinated movements resulted in motor defects and an inability of first-instar larvae to escape their eggshell. A significant amount of larvae died already before hatching at late stages of embryogenesis, or shortly after as crawling first-instar larva.

In addition, the lifetime of hypomorphic mutants of *Dfd* varied significantly. The majority of animals died at the end of embryogenesis, unable to hatch. Notably, the outgrowth of axons converging into the maxillary nerve appeared to be normal in 74% of these mutants, indicating that cells initially adopt their proper identity. However, the death of Dfd^{13}/*Df(3R)Scr* mutants was observed during all larval as well as pupal stages, suggesting that differences in the level of *Dfd* have an impact on the survival of those animals. In contrast to what has been described before in the literature, the present work unravelled that mutant survivors indeed are able to perform motor patterns associated with the mouthparts and required for the uptake of food. However, these observations are related to young flies, yet the importance of Dfd in ageing flies has not been investigated in the scope of this thesis. Future experiments on ageing hypomorphic *Dfd* mutant flies might be relevant to link the function of Dfd to ageing-related motor disorders in the context of feeding defects.

In line with these results, loss of functional Dfd resulted in severe defects at the synapse, which in turn led to the inability of larvae to perform the appropriate feeding-related motor program. Interestingly, perturbations in the morphology of the NMJ could be attributed to the tissue-specific loss of *Dfd* in neurons, whereas the postsynaptic

knockdown of *Dfd* in muscles did not affect the size and number of presynaptic boutons. Notably, analyses on hypomorphic *Dfd* mutant larvae revealed the same drastic defects in synapse morphology. Hence, the death of animals during larval stages is most likely due to an increasing inefficiency of the motor unit essential for feeding that consequently resulted in starvation.

In summary, it can be clearly stated that Dfd activity is necessary not only during embryonic stages, yet continuously after and even until adulthood. As lethality of animals mutant for *Dfd* occur at different time points of their life's and not at discrete developmental stages, *Dfd* product seems to be continuously required throughout development. This assumption is further substantiated by the permanent activity of the neural enhancer element of Dfd that drives reporter gene expression in the SEZ until adult stages (preliminary observation).

3.6 Deformed is active in Neurons to prevent neuronal Decline

Several lines of evidence point towards a function of Dfd in the control of molecules crucially required during synapse development and for synaptic function. First, a Dfd-ChIPseq analysis carried out previously (Sorge et al. 2012) uncovered a significant amount of putative Dfd targets involved in synapse-related processes. Second, inactivation of Dfd at the end of embryogenesis led to a drastic decline in the survival of affected larvae correlated with their inability to perform proper feeding-associated behaviours. And third, the lack of functional Dfd caused severe defects in the morphology of synapses at the junctions between motoneurons and muscles, indicating neuronal decline.

In the present study, Ank2-XL was shown to act downstream of Dfd. This was revealed by the reduced expression of both, Ank2-XL protein and *ank2*-transcript in larvae mutant for Dfd or upon targeted interference with Dfd. It might seem controversially at first sight, *ank2* and all other putative Dfd target genes were identified by ChIPseq analysis on stage 10-12 embryos. However, here, expression levels were changed in affected third instar larvae. It is well known that synaptic molecules and adhesion proteins have to be supplied constantly to ensure synaptic function and maintenance, from the time point when they are initially expressed. Most of the genes encoding synaptic proteins start to be expressed during embryogenesis, before the onset of the first motor activity. Thus, it seems likely that regulatory regions of these genes are controlled by Dfd already at this early stage of development. The present

study revealed the loss of *ank2*-mRNA expression in cells of the SEZ and upon inactivation of Dfd and hence confirmed the continuous requirement for Dfd to maintain the expression of *ank2*.

Moreover, the levels of MAP1B homolog Futsch, which is known to be closely associated with Ank2-XL (Stephan et al. 2015), were significantly reduced upon inactivation of Dfd. Ank2-XL has been shown to act upstream of MAP1B/Futsch (Stephan et al. 2015) in that the microtubule-crosslinking activity of MAP1B/Futsch caused the formation of aberrant accumulations of microtubules and thus the disruption of normal NMJs in *ank2-XL* mutants. Since expression of *futsch* is not affected in *ank2-XL* mutants, the decrease in the level of MAP1B/Futsch observed upon inactivation of Dfd cannot simply be explained by the loss of *ank2-XL* expression itself, but rather by role of Dfd in the regulation of *futsch* expression. However, *futsch* was not in the list of putative Dfd targets uncovered by Dfd-ChIPseq analysis, indicating that Dfd might regulate factors controlling the expression of *futsch*. Previously, analysis on the *MAP1B* promotor from rat revealed that MAP1B is under transcriptional control of the Fork head-box transcription factor Hepatocyte nuclear factor 3β (HNF3β/Foxa2) (Foucher 2003). The fly homolog of the vertebrate Foxa2 is the nuclear transcription factor Fork head (Fork). In *Drosophila fork head* (*fkh*) has been shown to be regulated by Scr in the embryonic salivary glands (Panzer et al. 1992; Ryoo & Mann 1999). Therefore, it seems plausible that expression of *fkh* in neurons might be regulated by Hox transcription factors, allowing Fork to bind to the regulatory region of *futsch* in order to activate *futsch* expression. Mutations in *futsch* have been shown to disrupt the organisation of synaptic microtubules, reduce the number of boutons and increase the bouton size (Roos et al. 2000), a phenotype that resembles the defects observed in the *Dfd*-mutant backgrounds and upon knock down of *Dfd*.

In *Drosophila* the stabilisation of NMJs is predominantly mediated by the microtubule cytoskeleton. Strikingly, Ank2-XL acts synergistically with MAP1B/Futsch to control the organisation of microtubules and hence neurotransmitter release (Stephan et al. 2015). In the present study *Dfd* mutants were shown to lack both proteins. In addition, the morphology of the NMJ on the MHE was severely affected in various genetic backgrounds, in which Dfd function was abolished. Although this study lacks the visualisation of presynaptic microtubules per se (NMJs on the MHE of affected animals were never stained by anti-tubulin-antibodies), the dramatic phenotypes caused by the loss of functional Dfd argue for a complete disassembly of the presynaptic nerve terminal at these sites. It is debatable if alterations in the level of Ank2-XL and MAP1B/Futsch

alone are sufficient to induce the de-stabilisation and retraction of the NMJ on the MHE. However, the size of synaptic boutons was either significantly increased or reduced in animals devoid of Dfd function, a phenotype consistent with the one described for *ank2-XL*; *futsch* double mutant larvae. While in single mutants for *ank2-XL* the increase in bouton size is assumed to reflect the failed separation of boutons, which is due to the presence of accumulated Futsch/microtubule complexes, double mutants, however, lack such aggregates. Therefore, the changes in bouton dimension described in this work are indicative of a mis-organisation of microtubules. An almost identical, but less dramatic phenotype was observed when *ank2*-transcript levels were reduced by RNAi in the SEZ using *Dfd*^{NAE667}*-Gal4*.

Mis-organisation of microtubules alone might not account for the retraction and elimination of synapses on the NMJ of the MHE in larvae with reduced Dfd function. However, the N-terminus of Ank2-XL contains a spectrin-binding domain that is used at presynaptic terminals to link microtubules and MAP1B/Futsch to the spectrin cytoskeleton, thereby conferring structural stability to the presynaptic terminal (Koch et al. 2008; Stephan et al. 2015). Moreover, MAP1B/Futsch is known to link microtubules to active zone proteins, like Bruchpilot or the calcium channel Cacophony (Lepicard et al. 2014). The retraction of MAP1B/Futsch and Ank2-XL-protein from NMJs of affected larvae certainly promoted the disassembly of the axon terminals. However, compared to mutants in *ank2-L*, single mutants of *ank2-XL* or *futsch* are not characterised by the complete elimination of presynaptic terminals and the subsequent death of animals, which occurs latest at early pupal stages in *ank2-L* mutants (Koch et al. 2008; Pielage et al. 2008). It remains unclear whether *ank2-XL*; *futsch* mutants show similar phenotypes to those described in the literature for *ank2L*-mutants. It will be of interest in the future to investigate the role of Dfd in the regulation of the other giant isoform of Ank2, Ank2-L. In addition, much more putative targets of Dfd involved in synaptic processes were uncovered by ChIPseq analysis, yet have not been examined within this work. The severe NMJ phenotype observed in larvae without Dfd function might be the sum of the loss of several molecules whose expression is dependent on Dfd. Although Syt1 and STNB are amongst those targets supposed to be under the control of Dfd, their protein levels were not affected in the temperature sensitive *Dfd*-mutant background. However, at least expression of *syt1* has been shown recently to be reduced in the SEZ of *Dfd* null-mutant embryos (Bujupi 2016), indicating that other transcriptional regulators might act upstream of Syt1 to control its expression during postembryonic stages of development.

It is well known that disruptions in the microtubule cytoskeleton of axons and synapses, associated with the loss of microtubule binding proteins, are early hallmarks of neurodegenerative diseases (Luo & O'Leary 2005; Goellner & Aberle 2011; Neukomm & Freeman 2014). Remarkably, mutations in the giant isoform of the vertebrate ortholog to Ank2, Ank-G/ANK3, have been linked to neurodegeneration in mice. Knockout of *ank-G* in mice resulted in an abnormal distribution of an important spectrin-binding cell adhesion molecule, a disrupted localisation of ion channels and impairments in the generation of action potentials, showing that Ank-G is fundamentally important for the integrity and stability of neurons and synapses (D. Zhou et al. 1998; Jenkins & Bennett 2001).

Recently, a methylomic profiling analysis using brain samples of Alzheimer's disease patients uncovered a disease-associated variation in the DNA-methylation pattern of ankyrin 1 (ANK1) (Lunnon et al. 2014; De Jager et al. 2014). DNA methylation displays one of the best-studied epigenetic modifications and primarily occurs at CpG-islands. Dependent on its localisation, DNA methylation at promotors disrupts gene transcription by interfering with transcription factors (Klose & Bird 2006). However, methylated regions are prone to be bound by methyl-CpG-binding domain proteins (MBDs), which influence chromatin compaction (Portela & Esteller 2010). Therefore, changes in the DNA methylation status of the *ank1* locus promote gene silencing and thus favour neuronal dysfunction and decline.

It will be of great interest in the future to examine the methylation pattern of the *ank2* locus in *Drosophila* and ideally find an association between *ank2* hypermethylation and synapse-related phenotypes in *Dfd*-mutant animals. In contrast to human patients, *Drosophila* might be advantageous to further investigate the role of epigenetic mechanisms in ageing and age-related neurodegenerative diseases. The brain of *Drosophila* is less complex, the tissue easily accessible and genetically tractable. Despite its role in the formation of the motor unit required for feeding-related behaviours, Dfd might be crucially involved in the maintenance and protection of neurons associated with this unit.

In summary, drastic changes in the structure of motoneuronal nerve terminals in *Drosophila* larvae take place upon removal of functional Dfd. These changes are accompanied by the loss of Ank2-XL and MAP1B/Futsch expression, proteins involved in the organisation of the microtubule cytoskeleton in axons and presynaptic endings. Recent data imply that modifications in the epigenetic landscape of genes like *ank* might

be the cause of neural decline and can be associated to the pathology of neurodegenerative diseases. However, in order to assign Dfd a role in the protection and maintenance of neurons further analyses, including epigenome-wide studies, need to be undertaken.

3.7 The Activity of Deformed is conserved

A question that came up with all these findings from *Drosophila* was whether the establishment of feeding-related motor-units is generally driven by group 4 *Hox* genes and therefore conserved among the animal kingdom. In line with this assumption, the present work identified neurons located within the hindbrain expression domain of *Hox4* genes in medaka (A. Davis & Stellwag 2010), which were activating the neural enhancer element of the fly. This argues for the ability of Hox4 transcription factors, which are specifically expressed in the hindbrain rhombomeres r7/r8 (A. Davis & Stellwag 2010), to bind and activate this regulatory element. Even more convincing, the hypoglossal nerve is known to emerge from this region (Guthrie 2007). In humans this nerve targets the muscles of the tongue (Guthrie 2007).

Another parallelism can be drawn towards feeding behaviour in the basic metazoan *Hydra vulgaris*. The cnidarian *ParaHox* gene *cnox-2* is activated during apical patterning in hydra (Gauchat et al. 2000). It is further required in neural precursors and differentiating neurons during de novo neurogenesis that precedes head formation during head regeneration (Miljkovic-Licina et al. 2007). Intriguingly, *cnox-2* displays a high degree of sequence conservation to *Dfd* in *Drosophila* (Shenk et al. 1993) and *cnox-2* expressing cells are located in the apex of the hypostome and close to the tentacle zone (Miljkovic-Licina et al. 2007). The hypostome represents the mouth of hydra and is associated with feeding activity. During feeding, the mouth at the tip of the hypostome opens and the tentacles deliver the food into the gastric cavity (Wood 1979; Shimizu et al. 2004). The selective elimination of neurons (and secretory gland cells) has been shown to result in the complete loss of digestive movements and those required for the uptake of food (Shimizu et al. 2004), indicating that neurons are essential for feeding behaviour in hydra.

In summary, several lines of evidence point towards a conserved function of *Hox4* genes in the establishment of feeding motor units. First, *Dfd* and its homologs in the fish (*hoxb4*) and the basic metazoan Hydra (*cnox-2*) are expressed in neurons located within specific regions of the head. Second, these neurons have been shown or are assumed to

function in feeding-related movements in all of these species. However, in the future functional studies are needed to validate the role of homology group 4 *Hox* genes in the establishment and regulation of feeding motor patterns throughout the animal kingdom.

4__ Conclusions

The work presented in this thesis highlights the crucial function of the Hox transcription Dfd in establishing and maintaining a larval motor unit required for feeding-related movements in *Drosophila*.

On the one hand, Dfd specifies the identity of motoneurons within the unit, but is additionally required for the development of the muscle innervated by those motoneurons. An anatomically closely related motor unit, which originates from Dfd-expressing cells, yet looses Dfd during development, induce expression of the cell-adhesion molecule Con and thereby allows correct synaptic matching between motoneuron and muscle. Together, these findings imply that the different motor units of the larval head are set up by transcription factors, like Dfd, acting in the neurons as well as the muscles innervated by these neurons. Future work will aim to identify a comprehensive set of Hox-regulated target recognition molecules on interacting synaptic partners.

On the other hand, this study demonstrates a requirement for Dfd beyond its well-established role during development: in the maintenance of the feeding motor unit. Dfd not only specifies cell identity during early development, but sustained activity of Dfd is required in neurons to express key molecules of the synaptic microtubule skeleton. In the absence of this continued transcriptional input, synapses degenerate, feeding- related movements are impaired and larvae starve to death. As defects in the synaptic microtubule architecture are a hallmark of neurodegenerative diseases, reduced input of transcriptional regulators like Dfd represents a putative mechanism leading to the silencing of these important neuronal genes. Since epigenetic mechanisms might have an

impact on ageing and age-related-neurodegenerative disorders, future projects will focus on elucidating the role of these mechanisms in the established model.

5__ Materials

5.1 Equipment and Consumables

Table 5.1: List of Equipment

Device	Model	Supplier
+ 4°C fridge	-	Liebherr
-20°C freezer	Premium	Liebherr
-80°C freezer	Forma900 Series	Thermo Scientific
Balance	EW	Kern & Sohn
Bacterial Shaker	Multitron	Infors HT
Bunsen Burner	-	-
Centrifuge	5424	Eppendorf
Centrifuge	5417R	Eppendorf
CO_2 incubator	-	Binder
CO_2 incubator	-	Binder
Confocal microscope	A1R	Nikon
Confocal microscope	TCS SP8	Leica
Camera	Nikon Digital sight DS-U3	Nikon
Electrophoresis chamber	Perfect Blue Gelsystem Mini M	PeqLab
Electrophoresis Power supply	EPS 301	GE Healthcare Life Sciences
Epifluorescence microscope	Zeiss Axioplan	Zeiss
Gel documentation system	Transilluminator UVIdoc	PeqLab UVITEC Cambridge
Heating block	Thriller	PeqLab
Incubator shaker	Innova® 44	New Brunswick Scientific
Magnetic stirrer with heating	Heidolph MR Hei-Tec	Heidolph instruments
Microscope	Nikon SMZ18 Nikon Intenslight C-HGFI	Nikon

Microscope	AXIO Imager M1 HXP120	Zeiss Kübler codix
Microscope	Discovery.V12	Zeiss
Microwave	Severin900	Severin
Nutating mixer	-	VWR
PCR machine	DNA Engine Dyad	Bio-Rad Laboratories
PH meter	SevenEasy	Mettle Toledo
Pipette boy	Pipetus	Hirschmann Laborgeräte
Pipettes	Pipetman	Gilson
Platform shaker	Unimax 1010	Heidolph instruments
Spectrophometer	NanoDrop® ND-1000	PeqLab
Vortex	VortexGenie2	Scientific industries
Water bath	WBT6	medingen
Water bath	GFL®	GFL
Water purification system	Milli-Q	Millipore
Dissection tools:		
Forceps	-	Fine Science Tools
Micropipette Puller	P-97	Sutter Instruments
Dissection microscope	W-PI 10x/23 CL1500Eco	Zeiss

Table 5.2: List of commercial kits

Kit	Supplier
DIG RNA Labelling Kit (T3)	Roche
DNeasy® Blood & Tissue Kit	Qiagen
In-situ Cell Death Detection Kit, TMR Red	Roche
pENTR™/D-TOPO® Cloning Kit	Thermo Fisher Scientific
Plasmid Midi Kit	Qiagen
Vectastain ABC Kit	Vector Laboratories (Burlington, USA)
Wizard® SV gel and PCR clean-up system	Promega

Table 5.3: List of consumable material and reagents

Material	Supplier
Cellstar®Tubes	Greiner
Filter tips 0.5-10µl	Sarstedt
Filter tips 2-20µl	Sarstedt
Filter tips 200µl	Greiner
Filter tips 100-1000µl	Sarstedt
Heparin ammonium salt	Sigma
Laboratory film/ Parafilm	Bemis
Microscope cover glasses	Carl Roth
Microscope slides	Carl Roth
Pasteur piptettes (disposable)	Carl Roth GmbH
PCR 8er Soft Strips 0.2ml	Biozym Scientific GmbH
Precision Wipes	Kimberly Clark
RiboLock RNase Inhibitor (40 U/µl)	Thermo Fisher Scientific
Rudapor® Surgical tape of white non woven	NOBA GmbH
Serological pipettes	Sarstedt
Sonicated Salmon Sperm DNA	Agilent Technologies
tRNA from brewer's yeast	Roche

Table 5.4: List of Enzymes

Enzyme	Supplier
Gateway® LR Clonase™ II Enzyme Mix	Invitrogen
Proteinase K solution (20mg/ml)	Roche
T3 RNA Polymerase	Roche
T7 RNA Polymerase	Roche
Pfu DNA Polymerase recombinant (2.5 U/µl)	Thermo Fisher Scientific
RiboLock™ RNase Inhibitor	Thermo Fisher Scientific
Restriction Enzymes	Thermo Fisher Scientific

5.2 Antibodies

Table 5.5: List of primary antibodies

Antibody	Host	Dilution	Source
Ankyrin 2-XL	rabbit	1:1000	H. Aberle
Ankyrin 2-L	rabbit	1:1000	H. Aberle
β -Galactosidase	mouse	1:500	Promega
BP102 [anti-CNS axons]	mouse	1:20	DSHB
Connectin [C1.427]	mouse	1:50	DSHB
Deadpan	guineapig	1:1000	R. Urbach
Deformed	guineapig	1:500	B. McGinnis
Deformed [d-129]	rabbit	1:200	Santa Cruz
Digoxigenin-AP Fab fragments	sheep	1:1000	Roche
Digoxiginin-POD Fab fragments	sheep	1:500	Roche
DVGlut	rabbit	1:1000	H. Aberle
Elav[7E8A10]	rat	1:50	DSHB
Elav[9F8A9]	mouse	1:50	DSHB
Engrailed (#sc28640)	rabbit	1:200	Santa Cruz
Fasciclin II [1D4]	mouse	1:10	DSHB
MAP1B/Futsch [22C10]	mouse	1:100	DSHB
GFP [3H9]	rat	1:200	Chromotek
GFP	rabbit	1:300	Invitrogen
HRP-FITC	goat	1:200	Jackson ImmunoResearch
Mef 2	rabbit	1:1000	Bruce Paterson
Myosin [MAC147]	rat	1:1000	Abcam
Prospero	mouse	1:4	DSHB
Robo 2	mouse	1:200	B. Dickson
Stoned B	rabbit	1:500	L. Kelly
Synaptotagmin [3H2 2D7]	mouse	1:30	DSHB

Table 5.6: List of secondary antibodies

Antibody	Host	Dilution	Source
Guineapig-Alexa Flour 647	donkey	1:200	Jackson ImmunoResearch
Guineapig-Cy3	donkey	1:200	Jackson ImmunoResearch
Mouse-Alexa Fluor 647	goat	1:200	Thermo Fisher Scientific
Mouse-Cy3	goat	1:200	Jackson ImmunoResearch
Rabbit-Alexa Fluor 633	goat	1:200	Thermo Fisher Scientific
Rabbit-Alexa Fluor 488	donkey	1:200	Thermo Fisher Scientific
Rat-Alexa 488	goat	1:200	Jackson ImmunoResearch
Rat-Cy3	goat	1:200	Jackson ImmunoResearch

5.3 Oligonucleotides

Table 5.7: List of oligonucleotides for cloning

Oligonucleotide	Sequence
Dfd_NAE_rev	AAG TCA ATG GGA TGG TGG AG
Dfd_NAE_fwd	CAC CCA GCC CTT GAG AGC ATT TTT
DfdNAE_ClaI_fwd	CTT GTC AGC ATC GAT TGA GAG CAT TT
DfdNAE_ClaI_rev	GAA CTG GAC AAA TCG ATG GGA TGG TG

Table 5.8: List of oligonucleotides for in-situ probes

Name	Sequence
ank2XL_fwd	ATG GGC TGT GGT GAT GTC AG
ank2XL_rev_T3	ATT AAC CCT CAC TAA AGG GAT TTA CGG TCT GGG GTT ACG C
Ca-alpha1D_fwd	GCA GCA TTC GCA ACG CTT TC
Ca-alpha1D_rev_T3	ATT AAC CCT CAC TAA AGG GAC CGC TTG TGT GTG TGC GAA C
Con_fwd	GTC TAG TCG CAC TGA TGA TG
Con_fwd_2	GAT GTG GAT GTC CTG ATG AC
Con_rev_T3	ATT AAC CCT CAC TAA AGG GAA GTG TCA CTA TGG CTA ACC G
ems_fwd	CAT GCC GCC CAG TTT ATG CCC AAT
ems_rev_T3	ATT AAC CCT CAC TAA AGG GAC TCT ACT CAA CCT CGA AAC T
exex_fwd	CGA GAC ACC CTG TAT TCT TG
exex_rev_T3	ATT AAC CCT CAC TAA AGG GAC TAA TTC AAT CGC AAT GCG T
gcm2_fwd	CTC GCA GAT CAA GCA TTT GGG TGG
gcm2_rev_T3	ATT AAC CCT CAC TAA AGG GAC ACT ACA CGT ACA GAT GGA A
lbe_fwd	TCC CAC TTG GAC ATC TTC TCG AAC AG
lbe_rev_T3	ATT AAC CCT CAC TAA AGG GAC CGG CTA TGA TTG TTC TGG C
nmr2_fwd	GCC CAC GCC ACC AAG TTC TT
nmr2_rev_T3	ATT AAC CCT CAC TAA AGG GAG AAG AAC TGT ACA GCT TAT

	AC
NLaz_fwd	CGC CAA CTA CAG TCT CAT AG
NLaz_rev_T3	ATT AAC CCT CAC TAA AGG GAA GCA TCT GAA ATA CGA CCT C
pdm2_fwd	CGG CAG TTC CAT CAG TTC AG
pdm2_rev_T3	ATT AAC CCT CAC TAA AGG GAG GAC ATC GTA CAA CAA CAT C
robo1_fwd	TCC ATG CAC CAC AGA AAT GT
robo1_rev_T3	ATT AAC CCT CAC TAA AGG GT AAC AAC TCC CCA CAA GTT CG
robo2_fwd	CTG GTG GAG ATC GGT GAT GAA GTG
robo2_rev_T7	TAA TAC GAC TCA CTA TAG GGC AAA CAT CTC GAT TAC ATA G
robo3_fwd	GCA CCA ATC AGA GCA GGA CT
robo3_rev_T3	ATT AAC CCT CAC TAA AGG GT CCT GAC CCT TGT TGA GCA G
snap25_fwd	CAG TTG CTA ATC AAA GGG CA
snap25_rev_T3	ATT AAC CCT CAC TAA AGG GAA TCC TTG GTA CTG TAT GAA C

5.4 Plasmids

pENTR™/D-TOPO®

The pENTR™/D-TOPO® vector supplied by Thermo Fisher Scientific includes M13 primer sequencing sites and attL recombination sites flanking the PCR product insertion site for insertion into attR containing Gateway® destination vectors. A Kanamycin resistance gene is used for selection in *E. coli*.

pBPGUw

The pBPGUw vector supplied by Addgene (plasmid number 17575) is a Gateway compatible GAL4 vector amenable to high throughput in vitro cloning using LR clonase and specific *in vivo* genomic targeting using PhiC31 integrase.

p339

The p339-transgenesis vector, supplied by the Wittbrodt lab, contains the zebrafish hsp70 minimal promoter and a GFP reporter gene flanked by I-SceI Meganuclease sites.

5.5 Bacterial Strains

One Shot®TOP10 Chemically Competent E. coli

One Shot®TOP10 Chemically Competent *E. coli* are supplied by Thermo Fisher Scientific. Genotype: F- mcrA Δ(mrr-hsdRMS-mcrBC) Φ80lacZΔM15 ΔlacX74 recA1 araD139 Δ(ara-leu)7697 galU galK rpsL (StrR) endA1 nupG.

DH5α™ Competent E. coli

DH5α™ Competent *E. coli* are supplied by Thermo Fisher Scientific. Genotype: F- Φ 80*lac*ZΔM15 Δ(*lac*ZYA-*arg*F) U169 *rec*A1 *end*A1 *hsd*R17(r_k^-, m_k^+) *pho*A *sup*E44 *thi*-1 *gyr*A96 *rel*A1 λ-.

5.6 Fly Stocks

Table 5.9: List of fly stocks

Fly stock (Genotype)	Chromosome	Source
Orgeon-R		Lohmann lab
TM3, P{w[+m*]=Ubx-lacZ.w[+]}TM3, Sb[1]/TM6B, Tb[1]	3	Lohmann lab
TM3, Sb[1]/TM6B, Red[1] Tb[1]	3	BL1792
w[*]; Sb[1]/TM3, P{w[+mC]=ActGFP}JMR2, Ser[1]	1;3	BL4534
w[1118]; P{w[+mC]=UAS-Dfd.B}W4	2	BL7299
y[1] w[*]; P{w[+mC]=UAS-mCD8::GFP.L}LL5, P{UAS-mCD8::GFP.L}2	1;2	BL5137
w[*]; P{y[+t7.7] w[+mC]=20XUAS-IVS-mCD8::GFP}attP2	1;3	BL32194
Dfd[16] red[1] e[1]/TM3, Sb[1] Ser[1]	3	BL2325
Dfd[16] red[1] e[1]/TM3, P{w[+m*]=Ubx-lacZ.w[+]}TM3, Sb[1]	3	this thesis
P{w[+mC]=UAS-Dfd.B}W4;Dfd[16] red[1] e[1]/TM3, P{w[+m*]=Ubx-lacZ.w[+]}TM3, Sb[1]	2;3	this thesis
P{w[+mC]=UAS-mCD8::GFP.L}LL5, P{UAS-mCD8::GFP.L}2;Dfd[16] red[1] e[1]/TM3, P{w[+m*]=Ubx-lacZ.w[+]}TM3, Sb[1]	2;3	this thesis
Df(3R)Scr, red[1] e[1]/TM3, Sb[1], Ser[1]	3	BL1885
Df(3R)Scr, red[1] e[1]/TM3, P{w[+m*]=Ubx-lacZ.w[+]}TM3, Sb[1]	3	this thesis
Dfd[13] red[1] e[1]/TM3, Sb[1]	3	BL2343
Dfd[13] red[1] e[1]/TM3, P{w[+m*]=Ubx-lacZ.w[+]}TM3, Sb[1]	3	this thesis
w*;Dfd[13] red[1] e[1]/TM6B, Tb[1]	3	this thesis
Dfd[3] red[1] e[1]/TM3, Sb[1]	3	BL2332

Dfd[3] red[1] e[1]/ TM6B, Tb[1]	3	this thesis
Dfd[3] red[1] e[1]/TM3, P{w[+mC]=ActGFP}JMR2, Ser[1]	3	this thesis
w[*]; P{y[+t*] w[+mC]=UAS-Flybow.1.1}VIE-260B	1;2	BL35537
DfdNAE667-Gal4;	2	BG9551-1
DfdNAE667-Gal4, P{y[+t*] w[+mC]=UAS-Flybow.1.1}VIE-260B;	2	S. Sorge
DfdNAE667-FLP	2	S. Sorge
UAS-Dfd50110	3	VDRC50110
UAS-Dfd-siRNA	3	BG13928-4
Antp[Ns-rvC1] red[1] e[1]/TM3, P{w[+m*]=Ubx-lacZ.w[+]}TM3, Sb[1]	3	Lohmann lab
mwh[1] jv[1] st[1] red[1] Sb[sbd-2] e[11] ro[1] ca[1] Abd-B[M1] / TM3, P{w[+m*]=Ubx-lacZ.w[+]}TM3, Sb[1]	3	Lohmann lab
Cha-GAL80	3	L. Griffith
y-w-; UAS-rpr, UAS-hid	1;2	JF Evers
w[*]; P{w[+mC]=UAS-TeTxLC.(-)V}B3	1;3	BL28841
w[*]; P{w[+mC]=UAS-TeTxLC.tnt}R3	1;3	BL28997
P{GawB}elavC155 w1118; P{UAS-Dcr-2.D}2	1;2	BL25750
y[1] v[1]; P{y[+t7.7] v[+t1.8]=TRiP.JF03374}attP2	1;3	BL29438
w[1118]; P{w[+mW.hs]=GawB}VGlut[OK371]	1;2	BL26160
P{w[+mW.hs]=GawB}VGlut[OK371];P{y[+t7.7] w[+mC]=20XUAS-IVS-mCD8::GFP}attP2	2;3	this thesis
w-,tubPGal80;P{w[+mW.hs]=GawB}VGlut[OK371];P{y[+t7.7] w[+mC]=20XUAS-IVS-mCD8::GFP}attP2	1;2;3	S. Sorge
w[*]; pros[17]/TM6B, Tb[1]	3	BL5458

5.7 Media and Standard Solutions

10X Phosphate buffered saline (PBS)

75.97 g Sodium chloride (NaCl)

12.46 g Sodium hydrogenphosphate ($NaHPO_4$)

4.14 g Disodium hydrogenphosphate (NaH_2PO_4)

Ingredients were dissolved in 800 ml of deionised water (dH_2O) and the pH adjusted to 7.4 with Sodium hydroxide (NaOH). The volume was adjusted to 1 l and the solution sterilized by autoclaving and stored at room temperature (RT).

1X Phosphate buffered saline (PBS)

10X PBS solution was diluted 1:10 in dH_2O and stored at RT.

$PBST_{W20}$

0.1 % Tween®20 was added to 1X PBS and solution was stored at RT.

$PBST_{X100}$

0.1 % Triton X-100 was added to 1X PBS and solution was stored at RT.

$PBST_{W20, DEPC}$

10X PBS solution was diluted 1:10 in DEPC-H_2O. 0.1 % Tween®20 was added and the solution stored at RT.

DEPC-H_2O

1 ml of Diethylpyrocarbonate (DEPC) was added to 1 l of dH_2O, stirred for 60 minutes on a magnetic stirrer and sterilized by autoclaving.

Embryo fixation solution

3.6 ml 1X PBS

0.4 ml 37 % Formaldehyde

4 ml Heptane

Ingredients were mixed in a clean scintillation vial by vortexing vigorously for 30 seconds.

4 % Paraformaldehyde (PFA)

40 g of paraformaldehyde was diluted in 1 l of 1X PBS by adding 1 ml of 0.1 M NaOH. The solution was placed in a 70 °C water bath until the paraformaldehyde was completely dissolved and cooled down to RT. The pH was adjusted to pH 7.2 with concentrated HCl. Aliquots of 2 ml were stored at -20 °C.

EDTA (0.2 M)

0.058 g ethylenediamenetatraacetic acid (EDTA) were dissolved in a final volume of 1 ml dH_2O, stirred vigorously and adjusted to a pH of 8.0 with NaOH. The solution was sterilized by autoclaving.

LiCl (4 M)

0.167 g lithium chloride (LiCl) were dissolved in MilliQ water. The solution was sterilized by passing it through a sterile filter.

tRNA (20 mg/ml)

20 mg of tRNA crystal powder were dissolved in 1 ml MilliQ water.

Heparin (50 mg/ml)

50 mg of heparine were dissolved in 1 ml MilliQ water. The solution was sterilized by passing it through a sterile filter.

20 X SSC

87.66 g NaCl (3 M)

44.21 g tri-Sodiumcitrate (0.3 M)

The volume was adjusted to 500 ml with dH_2O , the pH set to 7.0 with HCl and the solution sterilized by autoclaving and stored at RT.

Hybridisation solution

50 ml deionized formamide

25 ml 20 X SSC

4 ml Sonicated salmon sperm DNA

500 µl tRNA

50 µl Heparin

20.45 ml DEPC-H_2O

The solution was prepared using filter tips under RNase free conditions. The pH was adjusted to 5.0 with HCl and the solution stored at -20 °C.

Hybridisation solution B

50 ml deionized formamide

25 ml 20 X SSC

25 ml dH_2O

The mixture was stored at -20 °C.

Blocking reagent

Dry milk-powder was dissolved in PBT_{w20} or PBT_{X100} to obtain the final dilution and stored at 4 °C.

Staining buffer

1 ml 1 M Tris(hydroxymethyl)aminomethane (pH 9.5)

500 µl 1 M Magnesium chloride ($MgCl_2$)

200 µl 5 M NaCl

50 µl 20 % Tween®20

8.15 ml dH_2O

Apple agar plates

25 mg Agar-Agar was added to 740 ml of dH_2O, autoclaved, mixed with 250 ml apple juice and 25 mg sugar and poured into petri dishes. The plates were placed at 4 °C.

Glue for time-lapse movies

30-50 cm of brown tape were cut into pieces that were mixed with 25-30 ml n- Heptane in a falcon tube and incubated overnight at RT in a falcon tube. Subsequently, the supernatant was collected and centrifuged for 20 minutes at 8000 rpm until the solution was clear. The glue was stored at RT.

Holocarbon oil mixture

35 ml series HC-700

5 ml series 27

Hoyer's Medium

25 ml dH_2O

15 g gum Arabic

10 ml Glycerine

100 g chloral hydrate

The gum Arabic was mixed with dH_2O and a crystal of chloral hydrate of the size of a pea (to prevent fungal growth). The mixture soaked for 24 hours. Subsequently, 100 g of chloral hydrate were added. The mixture was allowed to dissolve (for several days). Once everything was dissolved glycerine was added.

S.O.C medium

20 g Tryptone

5 g Yeast extract

0.5 g NaCl

0.19 g Potassium chloride (KCl)

0.5 ml sterile $MgCl_2$

1.8 ml sterile Glucose

The mixture was filled up to 1 liter with dH_2O. The pH was set to 7.0 by adding NaOH. Finally the S.O.C medium was autoclaved.

LB-medium

25 g LB powder was dissolved in 1 liter dH_2O and autoclaved for 20 minutes at 121 °C

Antibiotics 1000X stock solutions

Ampicillin	100 mg/ml
Kanamycin	100mg/ml

5.8 Software

Table 5.10: Software

Program	Supplier
NIS-elements	Nikon
LAS X	Leica
Photoshop	Adobe
Excel	Microsoft
Fiji/ImageJ	-
Geneious	Geneious

6__ Methods

6.1 Fly Maintenance

Flies were kept under standard laboratory conditions at 25 °C, unless otherwise noted, as described in (H. Stocker & Gallant 2008).

6.2 Embryo Collection

To collect *Drosophila* embryos for immunohistochemistry and *in-situ* hybridisation, flies were allowed to lay eggs on apple agar plates. Embryos were washed off the plates with water and transferred into a mesh. For dechorionation 50 % bleach solution was applied. The dechorionated embryos were rinsed thoroughly with water and transferred into fixation solution in a scintillation vial. The vials were placed on a platform shaker for 25 minutes. Following fixation, first the aqueous solution and later the heptane phase was removed. In order to split open the vitelline membrane, fresh heptane was added and the same volume of methanol and the vials were vortexed vigorously for 30 seconds. Devitellinized embryos on the bottom of the vials were collected in microcentrifuge tubes, rinsed three times with methanol and stored at -20 °C.

6.3 Drosophila Genetics

6.3.1 The Gal4-UAS binary system

The yeast-derived Gal4-upstream activating sequence (UAS) binary system (Brand & Perrimon 1993) consists of a transactivator (Gal4) that can be expressed in a tissue specific manner using either enhancer-traps or gene-specific promotors, and a protein-coding sequence under the control of UAS. Upon binding of Gal4 to UAS, transcription of downstream responders is initiated (Figure 4.1). Activity of Gal4 can be inhibited by the GAL80 repressor (Lee & Luo 1999). Temporal control of Gal4 expression can be achieved by co-expressing a temperature-sensitive GAL80 repressor ($GAL80^{ts}$) (McGuire et al. 2003), and spatial control by applying intersectional techniques (see 4.3.2 FINGR method). The Gal4-UAS system was used under various points of view in this thesis.

6.3.2 The FINGR method

The Flippase recombinase (FLP)-induced intersectional GAL80/Gal4 repression (FINGR) method (Bohm et al. 2010) is built on the Gal4-UAS system (Brand & Perrimon 1993) with additional components. Broad Gal4 expression can be restricted by using the GAL80-converting tool, tub^{P}>GAL80>, in the 'flip in' approach. The two FRT sites, flanking the GAL80 sequence, mediate *cis*-recombination and excision of the GAL80 upon activation by FLP. Gal4 repression by GAL80 is abolished in cells in which Gal4 and FLP overlap in their expression. For the present work, a specific enhancer-based FLP-line (*Dfd^{NAE667}-Flp*) was generated in the lab and used to enhance restrictiveness of neural expression patterns.

6.3.3 RNA interference

Two independent *Dfd-RNAi*-lines, Vienna line 50110 and a *Dfd-siRNA* line (made by S. Sorge), were crossed to *elav-GAL4;UAS-dcr-2* or *UAS-dcr-2;Mef2-Gal4* flies, respectively. For the knockdown of *Ankyrin2*, a *Ankyrin2* specific dsRNA was expressed under the control of *elav-GAL4;UAS-dcr-2*. In all cases flies were allowed to lay eggs for 60 minutes at 25 °C. Progenies were raised at 29 °C until the third-instar larval stage, followed by dissection and antibody stainings.

6.4 Methods in Molecular Biology

6.4.1 Extraction of genomic DNA from Drosophila flies

Flies of the wild-type strain Oregon-R were anesthetized, collected in microcentrifuge tubes, frozen in liquid nitrogen and grid. For extraction of genomic DNA the DNeasy Blood & Tissue Spin-Column Protocol (Qiagen) was applied.

7.4.2 Transformation of competent bacteria

Competent *E. coli* cells were thawed on ice and an appropriate amount of vector DNA was added. To perform TOPO® cloning reactions 2 µl of the TOPO® cloning reaction was used. The cells were mixed gently by flicking the tube 4-5 times and incubated on ice for 30 minutes. Afterwards the cells were heat-shocked at 42 °C for 30 seconds in a waterbath and immediately transferred to ice for 2 minutes. An appropriate amount of RT S.O.C medium was added and the cells were placed at 37 °C for 60 minutes shaking vigorously at 250 rpm in a heating block. 50-200 µl of the cells were spread onto pre-warmed selection plates with appropriate antibiotics and incubated overnight at 37 °C.

6.4.3 Plasmid DNA preparation

LB medium (5 ml or 100 ml) containing 100µg/ml of the selective antibiotics, ampicillin or kanamycin, was inoculated either with a single colony of transformed bacteria picked from an agar plate (for mini DNA preparation), or from a glycerol stock (for midi DNA preparation), respectively. Bacterial cultures were grown overnight at 37 °C in LB medium and harvested by centrifugation at 14000 rpm for 10 minutes (mini culture) or 8000 rpm for 20 minutes (midi culture) at 4 °C. Plasmid DNA purification was carried out using the QIAGEN® DNA purification Midi/Mini Kit. The precipitated DNA was dissolved in distilled water and the DNA concentration determined using a Nanodrop.

6.4.4 Cloning of Dfd^{NAE667}-Gal4 and Dfd^{NAE661}-GFP

To construct *Dfd^{NAE667}-Gal4*, a 667 bp genomic region containing the known *Dfd* neural autoregulatory enhancer subfragment *HZ0.6* (Lou et al. 1995) was amplified from genomic DNA of *Oregon R* flies using gene-specific primers. PCR products were cloned into the pENTR™/D-TOPO vector and swapped into the pBPGUw destination vector (Addgene #17575) using the Invitrogen LR Clonase Enzyme Mix.

To construct *Dfd*^{NAE661}*-GFP*, a genomic region containing the HZ0.6 subfragment (Lou et al. 1995) was amplified from genomic DNA of *Oregon R* flies using gene-specific primers with Cla I-restriction sites. Following Cla I restriction digest the resulting PCR product was cloned into the p339-transgenesis vector upstream of a zebrafish hsp70 minimal promoter and a GFP reporter gene flanked by I-SceI Meganuclease sites.

6.4.5 Preparation of Digoxigenin (DIG)- and Biotin (BIO)-labelled antisense RNA probes

DNA for several genes of interest was amplified from genomic DNA of the wild-type strain Oregon R using gene specific primers with T3 binding sites. All genes and the respective primers are listed in Table 3-8. The PCR products were purified with the Wizard® SV Gel and PCR Clean-Up system (Promega) and used as a template for *in vitro* transcription (IVT) in the following setup (adapted from the T3-RNA labelling Kit from Roche):

250 ng	purified template DNA
2 µl	10X transcription buffer
2 µl	DIG- or BIOTIN-labelling mixture
2 µl	RNase inhibitor (40 Units)
2 µl	T3-RNA-polymerase

ad 20 µl ddH_2O_{DEPC}.

The labelling reactions were incubated at 37 °C for 2 hours, followed by DNaseI digestion at 37 °C for 15 minutes. Activity of DNase was stopped by adding 2 µl of 0.2 M EDTA (pH 8.0). RNA was precipitated at -80 °C overnight in 10 µl 4 M LiCl, 10 µl tRNA (20 mg/ml), 80 µl ddH_2O_{DEPC} and 300 µl 100 % ethanol (pre-chilled to -15 °C to -25 °C). Following precipitation, the RNA was centrifuged twice, washed in between with 70 % ice-cold ethanol, dried and dissolved in ddH_2O_{DEPC}. Finally, 20 µl of deionized formamide and 60 µl of hybridisation solution were added to the dissolved RNA. The RNA probe was stored at -20 °C until *in-situ* hybridisation.

6.5 Immunohistochemistry

6.5.1 In-situ hybridisation on Drosophila embryos

For *in-situ* hybridisation on *Drosophila* embryos, fixed embryos were rinsed with methanol three times and incubated in a mixture of methanol/xylene (1:5 v/v) for 60 minutes before rinsing them again with methanol. Before post-fixation, embryos were washed in methanol/formaldehyde/$PBST_{w20, DEPC}$ (5:1:4 v/v/v) for 5 minutes and post-fixed in 4 % formaldehyde/$PBST_{w20, DEPC}$ solution for 25 minutes on a nutating mixer at room temperature (RT). Subsequently, embryos were washed with $PBST_{w20, DEPC}$ three times for 20 minutes before Proteinase K digestion. Proteinase K was added at a dilution of 1:10 000 in $PBST_{w20, DEPC}$ for 1 minute at RT. After proteinase K treatment, embryos were rinsed immediately with ice-cold $PBST_{w20, DEPC}$, followed by post-fixation in 4 % formaldehyde/$PBST_{w20, DEPC}$ solution for 25 minutes. Fixation solution was removed and embryos washed with $PBST_{w20, DEPC}$ three times 20 minutes and rinsed in hybridisation solution before pre-hybridisation for 60 minutes at 60 °C. For hybridisation of DIG- and/or BIO-labelled RNA, probes were diluted properly in hybridisation solution and samples incubated overnight at 60 °C in a waterbath. In the following, embryos were washed twice with hybridisation solution B at 60 °C and afterwards with $PBST_{w20}$ four times for 30 minutes. For detection of DIG-labelled RNA, embryos were incubated with antibodies against DIG, which were either conjugated to alkaline phosphatase (AP) for non-fluorescent probe detection, or to horseradish peroxidase (POD) for fluorescent probe detection. AP- or POD-coupled antibodies were diluted in 0.25 % or 0.5 % blocking reagent, respectively, and incubated overnight at 4 °C. For detection of BIO-labelled RNA an antibody against streptavidin conjugated to horseradish peroxidase was diluted in 0.5 % blocking reagent and applied to the samples. For antibody detection in single or double fluorescent *in-situ* hybridisations the TSA™ Plus Cyanine 3 & Fluorescein system was used. In non-fluorescent *in-situ* hybridisations the antibody was removed and embryos washed with $PBST_{w20}$ three times for 20 minutes, followed by rinsing the embryos twice with deionized water, and twice with staining buffer. For signal development embryos were incubated in a staining solution until colour development, subsequently rinsed in deionized water and $PBST_{w20}$, washed with $PBST_{w20}$ once for 20 minutes and finally rinsed with PBS before dehydrated by treatment with a graded ethanol series (30 %, 50 %, 70 %, 85 % and 100% v/v in deionized water). Embryos were dehydrated in 100 % ethanol overnight at 4 °C on a nutating mixer, cleared in histoclear

solution and mounted in Permount mounting medium. Fluorescent *in-situ* hybridisations were mounted in Vectashield mounting medium.

6.5.2 In-situ hybridisation on Drosophila larval dissections

For *in-situ* hybridisation on *Drosophila* third-instar larvae, the head apparatus and associated brain was detached from the carcass. The dissected larvae were collected in a microcentrifuge tube with 0.01 % $PBST_{X100}$ and fixed in 4 % paraformaldehyde (PFA) for 25 minutes. The PFA was removed and the larval dissections washed with 0.1 % $PBST_{w20}$ three times for 5 minutes before dehydrated and rehydrated again in a graded methanol series (80 %, 50 % and 25 % v/v in $PBST_{w20}$). Afterwards, they were rinsed twice and washed in 0.1 % $PBST_{w20, DEPC}$ three times for 20 minutes before Proteinase K digestion. Proteinase K solution (1:1000 in $PBST_{w20, DEPC}$) was pre-heated for 5 minutes at 55 °C in a heating block and added to the samples for 90 seconds. Digestion was performed at 55 °C. After proteinase K treatment, the larval dissections were rinsed immediately with ice-cold $PBST_{w20, DEPC}$, followed by post-fixation in 4 % formaldehyde/$PBST_{w20, DEPC}$ solution for 25 minutes. Fixation solution was removed and embryos washed with $PBST_{w20, DEPC}$ three times 20 minutes and rinsed in hybidisation solution before pre-hybridisation for 60 minutes at 60 °C. For hybridisation of DIG- and/or BIO-labelled RNA, probes were diluted properly in hybridisation solution and samples incubated overnight at 60 °C in a waterbath. Detection of the labelled RNA was done as described in 4.5.1.

6.5.3 Whole-mount antibody stainings on Drosophila embryos

For antibody staining on *Drosophila* embryos, fixed embryos were rehydrated with a graded methanol series (80 %, 50 % and 25 % v/v in $PBST_{w20}$) and subsequently washed three times for 20 minutes in $PBST_{w20}$. Late staged embryos were washed for additional 10 minutes in $PBST_{x100}$ for proper permeabilisation of the cuticle. Nonspecific antibody binding sites were blocked by incubation in 1% blocking reagent/ $PBST_{w20}$ for 60 minutes before antibody treatment. Afterwards the appropriate amount of primary antibody diluted in 1 % blocking reagent was added, incubated overnight at 4 °C and washed off using 0.3 % $PBST_{w20}$. The embryos were washed at least 3 times for 20 minutes with $PBST_{w20}$ before incubated with the appropriate secondary antibody. Secondary antibodies were diluted in $PBST_{w20}$ for incubation at RT (2-3 hours) or in 1 % blocking reagent for overnight incubation. Secondary antibodies were removed and the embryos washed several times in 0.3 % $PBST_{w20}$ for at least 60 minutes, followed by mounting in Vectashield® mounting medium.

6.5.4 Antibody stainings on Drosophila larval dissections

For antibody staining of third-instar *Drosophila* larvae, the head apparatus and associated brain was detached from the carcass. The dissected larvae were collected in a microcentrifuge tube with 0.01 % $PBST_{X100}$ and fixed in 4 % paraformaldehyde (PFA) for 25 minutes. First-instar larvae were dissected inside out without removing the carcasses and washed three times for 20 minutes in 0.1 % $PBST_{X100}$, whereas for third-instar larval dissections 0.3 % $PBST_{X100}$ was used. After blocking in 1 % blocking reagent/ $PBST_{x100}$, an appropriate amount of primary antibody diluted in 1 % blocking reagent/ $PBST_{x100}$ was added, incubated overnight at 4 °C and washed off using $PBST_{x100}$. Larval dissections were washed at least 3 times for 20 minutes with $PBST_{w20}$ before incubated with the appropriate secondary antibody. Secondary antibodies were diluted in $PBST_{x100}$ for incubation at RT (2-3 hours) or in 1 % blocking reagent for overnight incubation. Secondary antibodies were removed and the larval dissections washed several times in $PBST_{x100}$ for at least 60 minutes, followed by fine dissection and mounting in Vectashield® mounting medium.

6.5.5 Tunel labelling

To assay cell death in embryos, the *in-situ* cell death detection kit, TMR red, was used. In brief, embryos were fixed, transferred to methanol and washed once in 30 % ethanol for 10 minutes, twice in PBS for 10 minutes and twice in $PBST_{X100}$ for 20 minutes. Before adding the primary antibody diluted in $PBST_{X100}$, the embryos were blocked in 0.2 % blocking reagent/$PBST_{X100}$. The primary antibodies were incubated overnight at 4 °C and subsequently washed off using $PBST_{X100}$. 250 µl of TUNEL labelling solution was mixed with 25 µl 10 times enzyme solution per staining reaction and applied to the embryos.

6.6 *Drosophila* Cuticle Preparation

To collect *Drosophila* embryos for cuticle preparation, flies were allowed to lay eggs on apple agar plates. Embryos were washed off the plates and transferred into a mesh for dechorionation in 50 % bleach solution. The dechorionated embryos were rinsed thoroughly with water and transferred into a heptane/methanol (1:1 v/v) containing scintillation vial. The vial was shaken vigorously for 30 seconds and the larvae collected into a microcentrifuge tube. Following two washes with ddH_2O supplemented with 0.1 % Tween®20, the larvae were mounted in Hoyer's medium

6.7 Behavioural Assays

6.7.1 Time-lapse movies

To collect *Drosophila* embryos for live imaging, flies were allowed to lay eggs on apple agar plates. Embryos were washed off the plates 18 hours AEL and transferred into a mesh for dechorionation in 50 % bleach solution. The dechorionated embryos were rinsed thoroughly with water, transferred onto a piece of apple agar and aligned in rows at the edges of the apple agar. In the following the embryos were fixed on slides with glue and covered with halocarbon oil. Time-lapse movies from animals before the time point of hatching were recorded using a Zeiss AxioImager M1 upright microscope and a 20 X lens. First-instar larvae were imaged using the Axio Zoom V16 microscope.

6.7.2 Temperature-shift experiments

In a first experimental setup embryos of 60 minutes egg depositions were raised at 18 °C on yeast covered apple juice plates for 28 hours until embryonic stage 17b (Pereanu et al. 2007) and subsequently shifted to 31 °C. Hatching rates were determined 48 hours AEL. Time-lapse movies were taken 5 hours after the temperature shift and shortly before hatching. For dissections and staining of the head apparatus and associated brain, the vitelline membrane was removed manually from first-instar larvae before the time point of hatching. In a second experimental setup embryos of 60 minutes egg depositions were raised at 18 °C for 150 hours until early third-instar larval stage. Subsequently, the larvae were shifted to 31 °C and kept at 31 °C for another 20 hours before antibody staining. To document mouth hook movements, time-lapse movies were made from larvae using the Nikon SMZ18 microscope and Nikon DS-U3 camera. Dissections of the head apparatus and the associated brain combined with antibody stainings were performed 20 hours after the temperature shift.

6.7.3 Tetanus toxin assay in Drosophila embryos

To block synaptic transmission during embryogenesis, we used *Dfd*^{NAE667}*- GAL4;Cha-GAL80* flies crossed to *UAS-TNT-R* or *UAS-IMPTNT*(*V1*) flies. Time-lapse movies were taken to analyse mouth hook movements at late stages of embryogenesis before hatching. Hatching rates were determined 48 hours AEL.

6.7.4 Tetanus toxin assay in Drosophila larvae

Dfd^{NAE667}*-GAL4*;*tub*-GAL80^{ts} flies were crossed to *UAS-TNT-R* or *UAS- IMPTNT*(*V1*) flies, respectively. Embryos of a 2 hour deposition at 25 °C were kept at 18 °C for the next 34 hours before they were shifted to 29 °C. Six hours later, the hatched first-instar larvae were transferred to a piece of agar and placed on a microscope slide.

Dfd^{NAE667}*-Flp*;*UAS-TNT-R* or *Dfd*^{NAE667}*-Flp*;*UAS-IMPTNT*(*V1*) flies were crossed to *OK371-GAL4*,*5xUAS-mCD8-GFP*;*tubP>GAL80>* flies. Embryos of a 2 hour deposition at 25 °C were kept at 25 °C for the next 40 hours until late first-instar larval stages. Larvae were transferred to a piece of agar and placed on a microscope slide. Time-lapse movies were taken from larvae using the Axio Zoom V16 micro- scope and AxioVision Release 4.7.2 software. The angles between the mouth hooks and H-piece were measured using the ''Angle tool'' of the Fiji/ImageJ software.

Adult feeding assay

Flies were starved on apple agar plates o/N. The next day, flies were allowed to feed on apple agar plates covered with red-coloured yeast for 30 minutes. The uptake of yeast into the gut was evaluated under the light microscope.

6.8 Injection of *O. latipes* Embryos

Meganuclease-mediated transgenesis by injection into one-cell stage medaka embryos was performed. The hsp70 core promoter triggers a strong and specific lens expression starting around 3 dpf, a feature used as a technical control for successful genomic integration of the reporter.

6.9 Image Analysis and Statistics

All images were analysed with FIJI/ImageJ and Adobe Photoshop CS6. Statistical analysis was performed using Microsoft Excel. Bar graph data are presented as standard deviation. Unpaired t test, two-tailed, two-sample unequal variance was used to calculate statistical significance. Boxplots were generated with BoxPlotR (http://boxplot.tyerslab.com) in Tukey-style. Central mark represents the median, the edges of the boxes the 25th and 75th percentiles and whiskers indicate 1.5 times interquartile range. Dots indicate outliers. The size of synaptic boutons was determined using horseradish peroxidase (HRP) staining and FIJI.

7__ References

Abrell, S. & Jäckle, H., 2001. Axon guidance of Drosophila SNb motoneurons depends on the cooperative action of muscular Krüppel and neuronal capricious activities. *MOD*, 109(1), pp.3–12.

Akiyama-Oda, Y. et al., 2000. Mechanism of glia-neuron cell-fate switch in the Drosophila thoracic neuroblast 6-4 lineage. *Development*, 127(16), pp.3513–3522.

Albertson, R. & Doe, C.Q., 2003. Dlg, Scrib and Lgl regulate neuroblast cell size and mitotic spindle asymmetry. *Nature Cell Biology*, 5(2), pp.166–170.

Araújo, S.J. & Tear, G., 2003. Axon guidance mechanisms and molecules: lessons from invertebrates. *Nature Reviews Neuroscience*, 4(11), pp.910–922.

Baek, M., Enriquez, J. & Mann, R.S., 2013. Dual role for Hox genes and Hox co-factors in conferring leg motoneuron survival and identity in Drosophila. *Development*, 140(9), pp.2027–2038.

Baines, R.A. et al., 2001. Altered electrical properties in Drosophila neurons developing

without synaptic transmission. *The Journal of neuroscience : the official journal of the Society for Neuroscience*, 21(5), pp.1523–1531.

Barros, C.S., Phelps, C.B. & Brand, A.H., 2003. Drosophila nonmuscle myosin II promotes the asymmetric segregation of cell fate determinants by cortical exclusion rather than active transport. *Developmental Cell*, 5(6), pp.829–840.

Becker, H. et al., 2016. Cell-Autonomous and Non-cell-autonomous Function of Hox Genes Specify Segmental Neuroblast Identity in the Gnathal Region of the Embryonic CNS in Drosophila C. Desplan, ed. *PLOS Genetics*, 12(3), pp.e1005961–31.

Beckervordersandforth, R.M. et al., 2008. Subtypes of glial cells in the Drosophila embryonic ventral nerve cord as related to lineage and gene expression. *Mechanisms of Development*, 125(5-6), pp.542–557.

Bello, B.C., Hirth, F. & Gould, A.P., 2003. A pulse of the Drosophila Hox protein Abdominal-A schedules the end of neural proliferation via neuroblast apoptosis. *Neuron*, 37(2), pp.209–219.

Berger, C. et al., 2004. A critical role for Cyclin E in cell fate determination in the central nervous system of Drosophila melanogaster. *Nature Cell Biology*, 7(1), pp.56–62.

Betschinger, J. & Knoblich, Jürgen A, 2004. Dare to Be Different: Asymmetric Cell Division in Drosophila, C. elegans and Vertebrates. *Current Biology*, 14(16), pp.R674–R685.

Birkholz, O., Rickert, C., et al., 2013. Neuroblast pattern and identity in the Drosophila tail region and role of doublesex in the survival of sex-specific precursors. *Development*, 140(8), pp.1830–1842.

Birkholz, O., et al., 2013. Abdominal-B and caudal inhibit the formation of specific neuroblasts in the Drosophila tail region. *Development*, 140(17), pp.3552–3564.

Bodaleo, F.J. & Gonzalez-Billault, C., 2016. The Presynaptic Microtubule Cytoskeleton in Physiological and Pathological Conditions: Lessons from Drosophila Fragile X Syndrome and Hereditary Spastic Paraplegias. *Frontiers in Molecular Neuroscience*, 9(1837), pp.545–16.

Bohm, R.A. et al., 2010. A genetic mosaic approach for neural circuit mapping in Drosophila. *Proceedings of the National Academy of Sciences of the United States of America*, 107(37), pp.16378–16383.

Bonkowsky, J.L. et al., 1999. Axon routing across the midline controlled by the Drosophila Derailed receptor. *Nature*, 402(6761), pp.540–544.

Bouley, M. et al., 2000. The L1-type cell adhesion molecule neuroglian influences the stability of neural ankyrin in the Drosophila embryo but not its axonal localization.

Journal of Neuroscience, 20(12), pp.4515–4523.

Brand, A.H. & Perrimon, N., 1993. Targeted gene expression as a means of altering cell fates and generating dominant phenotypes. *Development*, 118(2), pp.401–415.

Broadus, J. et al., 1995. New neuroblast markers and the origin of the aCC/pCC neurons in the Drosophila central nervous system. *MOD*, 53(3), pp.393–402.

Broihier, H.T. & Skeath, J.B., 2002. Drosophila homeodomain protein dHb9 directs neuronal fate via crossrepressive and cell-nonautonomous mechanisms. *Neuron*, 35(1), pp.39–50.

Broihier, H.T. et al., 2004. Drosophila homeodomain protein Nkx6 coordinates motoneuron subtype identity and axonogenesis. *Development*, 131(21), pp.5233–5242.

Brose, K. et al., 1999. Slit proteins bind Robo receptors and have an evolutionarily conserved role in repulsive axon guidance. *Cell*, 96(6), pp.795–806.

Brose, N. et al., 1992. Synaptotagmin: a calcium sensor on the synaptic vesicle surface. *Science (New York, N.Y.)*, 256(5059), pp.1021–1025.

Buchman, J.J. & Tsai, L.-H., 2007. Spindle regulation in neural precursors of flies and mammals. *Nature Reviews Neuroscience*, 8(2), pp.89–100.

Bujupi, F., 2016. *Analysis of the HOX gene Deformed: Regulation in the Brain and Importance in*,

Callahan, C.A. & Thomas, J.B., 1994. Tau-beta-galactosidase, an axon-targeted fusion protein. *Proceedings of the National Academy of Sciences*, 91(13), pp.5972–5976.

Catela, C. et al., 2016. Hox Proteins Coordinate Motor Neuron Differentiation and Connectivity Programs through Ret/Gfrα Genes. *CellReports*, 14(8), pp.1901–1915.

Caussinus, E., Kanca, O. & Affolter, M., 2011. Fluorescent fusion protein knockout mediated by anti-GFP nanobody. *Nature Publishing Group*, 19(1), pp.117–121.

Certel, S.J. & Thor, S., 2004. Specification of Drosophila motoneuron identity by the combinatorial action of POU and LIM-HD factors. *Development*, 131(21), pp.5429–5439.

Chia, P.H., Li, P. & Shen, K., 2013. Cell biology in neuroscience: Cellular and molecular mechanisms underlying presynapse formation. *The Journal of Cell Biology*, 203(1), pp.11–22.

Chiba, A. et al., 1995. Fasciclin III as a synaptic target recognition molecule in Drosophila. *Nature*, 374(6518), pp.166–168.

Cobeta, I.M., Salmani, B.Y. & Thor, S., 2017. Anterior-Posterior Gradient in Neural Stem and Daughter Cell Proliferation Governed by Spatial and Temporal Hox Control. *Current biology : CB*, 27(8), pp.1161–1172.

Crisp, S. et al., 2008. The development of motor coordination in Drosophila embryos. *Development*, 135(22), pp.3707–3717.

Crisp, S.J., Evers, J.F. & Bate, M., 2011. Endogenous Patterns of Activity Are Required for the Maturation of a Motor Network. *Journal of Neuroscience*, 31(29), pp.10445–10450.

Dasen, J.S. & Jessell, T.M., 2009. *Chapter 6 - Hox Networks and the Origins of Motor Neuron Diversity* 1st ed., Elsevier Inc.

Davis, A. & Stellwag, E.J., 2010. Spatio-temporal patterns of Hox paralog group 3â€"6 gene expression during Japanese medaka (Oryzias latipes) embryonic development. *Gene Expression Patterns*, 10(6), pp.244–250.

Davis, G.W., Schuster, C.M. & Goodman, C.S., 1997. Genetic analysis of the mechanisms controlling target selection: target-derived Fasciclin II regulates the pattern of synapse formation. *Neuron*, 19(3), pp.561–573.

De Jager, P.L. et al., 2014. Alzheimer's disease: early alterations in brain DNA methylation at ANK1, BIN1, RHBDF2 and other loci. *Nature Publishing Group*, 17(9), pp.1156–1163.

DeBello, W.M., Betz, H. & Augustine, G.J., 1993. Synaptotagmin and neurotransmitter release. *Cell*, 74(6), pp.947–950.

Diederich, R.J., Pattatucci, A.M. & Kaufman, T.C., 1991. Developmental and evolutionary implications of labial, Deformed and engrailed expression in the Drosophila head. *Development*, 113(1), pp.273–281.

Dixit, R., VijayRaghavan, K. & Bate, M., 2008. Hox genes and the regulation of movement in Drosophila. *Developmental Neurobiology*, 68(3), pp.309–316.

Doe, C.Q., 1992. Molecular markers for identified neuroblasts and ganglion mother cells in the Drosophila central nervous system. *Development*, 116(4), pp.855–863.

Doe, C.Q. et al., 1991. The prospero gene specifies cell fates in the Drosophila central nervous system. *Cell*, 65(3), pp.451–464.

Doe, C.Q., Smouse, D. & Goodman, C.S., 1988. Control of neuronal fate by the Drosophila segmentation gene even-skipped. *Nature*, 333(6171), pp.376–378.

Dormand, E.L. & Brand, A.H., 1998. Runt determines cell fates in the Drosophila embryonic CNS. *Development*, 125(9), pp.1659–1667.

Dubreuil, R.R. & Yu, J., 1994. Ankyrin and beta-spectrin accumulate independently of alpha-spectrin in Drosophila. *Proceedings of the National Academy of Sciences*, 91(22), pp.10285–10289.

Egger, B., Chell, J.M. & Brand, A.H., 2008. Insights into neural stem cell biology from flies. *Philosophical Transactions of the Royal Society B: Biological Sciences*, 363(1489), pp.39–56.

Enriquez, J. et al., 2010. Multi-step control of muscle diversity by Hox proteins in the Drosophila embryo. *Development*, 137(3), pp.457–466.

Erben, V. et al., 2008. Asymmetric localization of the adaptor protein Miranda in neuroblasts is achieved by diffusion and sequential interaction of Myosin II and VI. *Journal of Cell Science*, 121(9), pp.1403–1414.

Evans, T.A., 2016. ScienceDirect Embryonic axon guidance: insights from Drosophila and other insects. *Current Opinion in Insect Science*, 18, pp.11–16.

Evans, T.A. et al., 2015. Robo2 acts in trans to inhibit Slit-Robo1 repulsion in pre-crossing commissural axons. *eLife*, 4, p.e08407.

Fambrough, D. & Goodman, C.S., 1996. The Drosophila beaten path gene encodes a novel secreted protein that regulates defasciculation at motor axon choice points. *Cell*, 87(6), pp.1049–1058.

Flood, T.F. et al., 2014. A single pair of interneurons commands the Drosophila feeding motor program. *Nature*, 498(7456), pp.83–87.

Foucher, I., 2003. Joint regulation of the MAP1B promoter by HNF3beta/Foxa2 and Engrailed is the result of a highly conserved mechanism for direct interaction of homeoproteins and Fox transcription factors. *Development*, 130(9), pp.1867–1876.

Fujioka, M. et al., 2003. Even-skipped, acting as a repressor, regulates axonal projections in Drosophila. *Development*, 130(22), pp.5385–5400.

Gauchat, D. et al., 2000. Evolution of Antp-class genes and differential expression of Hydra Hox/paraHox genes in anterior patterning. *Proceedings of the National Academy of Sciences*, 97(9), pp.4493–4498.

Gavrieli, Y., Sherman, Y. & Ben-Sasson, S.A., 1992. Identification of programmed cell death in-situ via specific labeling of nuclear DNA fragmentation. *The Journal of Cell Biology*, 119(3), pp.493–501.

Ghysen, A. & Dambly-Chaudiere, C., 1989. Genesis of the Drosophila peripheral nervous system. *Trends in genetics : TIG*, 5(8), pp.251–255.

Goellner, B. & Aberle, H., 2011. The synaptic cytoskeleton in development and disease A. Ferrús, ed. *Developmental Neurobiology*, 72(1), pp.111–125.

Gordon, M.D. & Scott, K., 2009. Motor Control in a Drosophila Taste Circuit. *Neuron*, 61(3), pp.373–384.

Gould, A.P. & White, R.A., 1992. Connectin, a target of homeotic gene control in Drosophila. *Development*, 116(4), pp.1163–1174.

Gould, A.P. et al., 1990. Targets of homeotic gene control in Drosophila. *Nature*, 348(6299), pp.308–312.

Gummalla, M. et al., 2014. Hox gene regulation in the central nervous system of Drosophila. *Frontiers in Cellular Neuroscience*, 8(e1002720), pp.1689–12.

Guthrie, S., 2007. Patterning and axon guidance of cranial motor neurons. *Nature Reviews Neuroscience*, 8(11), pp.859–871.

Harris, K.P. & Littleton, J.T., 2015. Transmission, Development, and Plasticity of Synapses. *Genetics*, 201(2), pp.345–375.

Harris, R., Sabatelli, L.M. & Seeger, M.A., 1996. Guidance cues at the Drosophila CNS midline: identification and characterization of two Drosophila Netrin/UNC-6 homologs. *Neuron*, 17(2), pp.217–228.

Hessinger, C., Technau, G.M. & Rogulja-Ortmann, A., 2017. The DrosophilaHox gene Ultrabithoraxacts in both muscles and motoneurons to orchestrate formation of specific neuromuscular connections. *Development*, 144(1), pp.139–150.

Hilchen, von, C.M. et al., 2008. Identity, origin, and migration of peripheral glial cells in the Drosophila embryo. *Mechanisms of Development*, 125(3-4), pp.337–352.

Hirth, F. et al., 1995. Developmental defects in brain segmentation caused by mutations of the homeobox genes orthodenticle and empty spiracles in Drosophila. *Neuron*, 15(4), pp.769–778.

Hirth, F., Hartmann, B. & Reichert, H., 1998. Homeotic gene action in embryonic brain development of Drosophila. *Development*, 125(9), pp.1579–1589.

Hoang, B. & Chiba, A., 2001. Single-cell analysis of Drosophila larval neuromuscular synapses. *Developmental Biology*, 229(1), pp.55–70.

Homem, C.C.F. & Knoblich, Juergen A, 2012. Drosophila neuroblasts: a model for stem cell biology. *Development*, 139(23), pp.4297–4310.

Hortsch, M. et al., 2002. The axonal localization of large Drosophila ankyrin2 protein isoforms is essential for neuronal functionality. *Molecular and cellular neurosciences*, 20(1), pp.43–55.

Hu, H., Marton, T.F. & Goodman, C.S., 2001. Plexin B mediates axon guidance in Drosophila by simultaneously inhibiting active Rac and enhancing RhoA signaling.

Neuron, 32(1), pp.39–51.

Hummel, T. et al., 2000. Drosophila Futsch/22C10 is a MAP1B-like protein required for dendritic and axonal development. *Neuron*, 26(2), pp.357–370.

Hückesfeld, S. et al., 2015. Localization of Motor Neurons and Central Pattern Generators for Motor Patterns Underlying Feeding Behavior in Drosophila Larvae. B. D. McCabe, ed. *PloS one*, 10(8), p.e0135011.

Hückesfeld, S., Peters, M. & Pankratz, M.J., 2016. Central relay of bitter taste to the protocerebrum by peptidergic interneurons in the Drosophila brain. *Nature Communications*, 7, pp.12796–9.

Inaki, M. et al., 2010. Drosophila Tey represses transcription of the repulsive cue Toll and generates neuromuscular target specificity. *Development*, 137(13), pp.2139–2146.

Ito, K. et al., 2014. A Systematic Nomenclature for the Insect Brain. *Neuron*, 81(4), pp.755–765.

Ito, K., Urban, J. & Technau, G.M., 1995. Distribution, classification, and development ofDrosophila glial cells in the late embryonic and early larval ventral nerve cord. *Roux's archives of developmental biology : the official organ of the EDBO*, 204(5), pp.284–307.

Jenett, A. et al., 2012. A GAL4-Driver Line Resource for Drosophila Neurobiology. *CellReports*, 2(4), pp.991–1001.

Jenkins, S.M. & Bennett, V., 2001. Ankyrin-G coordinates assembly of the spectrin-based membrane skeleton, voltage-gated sodium channels, and L1 CAMs at Purkinje neuron initial segments. *The Journal of Cell Biology*, 155(5), pp.739–746.

Jhaveri, D. et al., 2004. Positioning sensory terminals in the olfactory lobe of Drosophila by Robo signaling. *Development*, 131(9), pp.1903–1912.

Jiang, Y. & Reichert, H., 2012. Programmed cell death in type II neuroblast lineages is required for central complex development in the Drosophila brain. *Neural Development*, 7(1), p.3.

Kawasaki, F. et al., 2004. Active zone localization of presynaptic calcium channels encoded by the cacophony locus of Drosophila. *The Journal of neuroscience : the official journal of the Society for Neuroscience*, 24(1), pp.282–285.

Keleman, K. et al., 2002. Comm sorts robo to control axon guidance at the Drosophila midline. *Cell*, 110(4), pp.415–427.

Keleman, K., Ribeiro, C. & Dickson, B.J., 2005. Comm function in commissural axon guidance: cell-autonomous sorting of Robo in vivo. *Nature Neuroscience*, 8(2), pp.156–163.

Kelly, L.E. & Phillips, A.M., 2005. Molecular and genetic characterization of the interactions between the Drosophila stoned-B protein and DAP-160 (intersectin). *The Biochemical journal*, 388(Pt 1), pp.195–204.

Kidd, T., Bland, K.S. & Goodman, C.S., 1999. Slit is the midline repellent for the robo receptor in Drosophila. *Cell*, 96(6), pp.785–794.

Kidd, T., Brose, K., et al., 1998. Roundabout controls axon crossing of the CNS midline and defines a novel subfamily of evolutionarily conserved guidance receptors. *Cell*, 92(2), pp.205–215.

Kidd, T., Russell, C., et al., 1998. Dosage-sensitive and complementary functions of roundabout and commissureless control axon crossing of the CNS midline. *Neuron*, 20(1), pp.25–33.

Kim, M.D., Wen, Y. & Jan, Y.-N., 2009. Patterning and organization of motor neuron dendrites in the Drosophila larva. *Developmental Biology*, 336(2), pp.213–221.

Kittel, R.J. et al., 2006. Bruchpilot promotes active zone assembly, Ca2+ channel clustering, and vesicle release. *Science (New York, N.Y.)*, 312(5776), pp.1051–1054.

Klose, R.J. & Bird, A.P., 2006. Genomic DNA methylation: the mark and its mediators. *Trends in Biochemical Sciences*, 31(2), pp.89–97.

Knoblich, Juergen A, 2008. Mechanisms of Asymmetric Stem Cell Division. *Cell*, 132(4), pp.583–597.

Koch, I. et al., 2008. Drosophila ankyrin 2 is required for synaptic stability. *Neuron*, 58(2), pp.210–222.

Kohsaka, H. & Nose, A., 2009. Target recognition at the tips of postsynaptic filopodia: accumulation and function of Capricious. *Development*, 136(7), pp.1127–1135.

Kohsaka, H., Takasu, E. & Nose, A., 2007. In vivo induction of postsynaptic molecular assembly by the cell adhesion molecule Fasciclin2. *The Journal of Cell Biology*, 179(6), pp.1289–1300.

Kolodziej, P.A. et al., 1996. frazzled encodes a Drosophila member of the DCC immunoglobulin subfamily and is required for CNS and motor axon guidance. *Cell*, 87(2), pp.197–204.

Kose, H. et al., 1997. Homophilic synaptic target recognition mediated by immunoglobulin-like cell adhesion molecule Fasciclin III. *Development*, 124(20), pp.4143–4152.

Krueger, N.X. et al., 1996. The transmembrane tyrosine phosphatase DLAR controls motor axon guidance in Drosophila. *Cell*, 84(4), pp.611–622.

Kuert, P.A. et al., 2014. Neuroblast lineage identification and lineage-specific Hox gene action during postembryonic development of the subesophageal ganglion in the Drosophila central brain. *Developmental Biology*, 390(2), pp.102–115.

Kuert, P.A., Bello, B.C. & Reichert, H., 2012. The labial gene is required to terminate proliferation of identified neuroblasts in postembryonic development of the Drosophila brain. *Biology Open*, 1(10), pp.1006–1015.

Kurusu, M. et al., 2008. A Screen of Cell-Surface Molecules Identifies Leucine-Rich Repeat Proteins as Key Mediators of Synaptic Target Selection. *Neuron*, 59(6), pp.972–985.

Landgraf, M. & Thor, S., 2006. Development of Drosophila motoneurons: Specification and morphology. *Seminars in Cell & Developmental Biology*, 17(1), pp.3–11.

Landgraf, M. et al., 2003. Embryonic origins of a motor system: motor dendrites form a myotopic map in Drosophila. *PLoS Biology*, 1(2), p.E41.

Landgraf, M. et al., 1999. even-skipped determines the dorsal growth of motor axons in Drosophila. *Neuron*, 22(1), pp.43–52.

Landgraf, M. et al., 1997. The origin, location, and projections of the embryonic abdominal motorneurons of Drosophila. *Journal of Neuroscience*, 17(24), pp.9642–9655.

Lee, T. & Luo, L., 1999. Mosaic analysis with a repressible cell marker for studies of gene function in neuronal morphogenesis. *Neuron*, 22(3), pp.451–461.

Lepicard, S. et al., 2014. A presynaptic role of microtubule-associated protein 1/Futsch in Drosophila: regulation of active zone number and neurotransmitter release. *The Journal of neuroscience : the official journal of the Society for Neuroscience*, 34(20), pp.6759–6771.

Liu, K.S.Y. et al., 2011. RIM-binding protein, a central part of the active zone, is essential for neurotransmitter release. *Science (New York, N.Y.)*, 334(6062), pp.1565–1569.

Lohmann, I. et al., 2002. The Drosophila Hox gene deformed sculpts head morphology via direct regulation of the apoptosis activator reaper. *Cell*, 110(4), pp.457–466.

Lou, L., Bergson, C. & McGinnis, W., 1995. Deformed expression in the Drosophila central nervous system is controlled by an autoactivated intronic enhancer. *Nucleic Acids Research*, 23(17), pp.3481–3487.

Lunnon, K. et al., 2014. Methylomic profiling implicates cortical deregulation of ANK1 in Alzheimer's disease. *Nature Publishing Group*, 17(9), pp.1164–1170.

Luo, L. & O'Leary, D.D.M., 2005. Axon retraction and degeneration in development and disease. *Annual review of neuroscience*, 28(1), pp.127–156.

Mahr, A. & Aberle, H., 2006. The expression pattern of the Drosophila vesicular glutamate transporter: A marker protein for motoneurons and glutamatergic centers in the brain. *Gene Expression Patterns*, 6(3), pp.299–309.

Massaro, C.M., Pielage, J. & Davis, G.W., 2009. Molecular mechanisms that enhance synapse stability despite persistent disruption of the spectrin/ankyrin/microtubule cytoskeleton. *The Journal of Cell Biology*, 187(1), pp.101–117.

McGuire, S.E. et al., 2003. Spatiotemporal rescue of memory dysfunction in Drosophila. *Science (New York, N.Y.)*, 302(5651), pp.1765–1768.

Menon, K.P., Carrillo, R.A. & Zinn, K., 2013. Development and plasticity of the Drosophilalarval neuromuscular junction. *Wiley Interdisciplinary Reviews: Developmental Biology*, 2(5), pp.647–670.

Merrill, V.K., Turner, F.R. & Kaufman, T.C., 1987. A genetic and developmental analysis of mutations in the Deformed locus in Drosophila melanogaster. *Developmental Biology*, 122(2), pp.379–395.

Miljkovic-Licina, M. et al., 2007. Head regeneration in wild-type hydra requires de novo neurogenesis. *Development*, 134(6), pp.1191–1201.

Mitchell, K.J. et al., 1996. Genetic analysis of Netrin genes in Drosophila: Netrins guide CNS commissural axons and peripheral motor axons. *Neuron*, 17(2), pp.203–215.

Nassif, C., Noveen, A. & Hartenstein, V., 1998. Embryonic development of the Drosophila brain. I. Pattern of pioneer tracts. *The Journal of comparative neurology*, 402(1), pp.10–31.

Neher, E. & Sakaba, T., 2008. Multiple roles of calcium ions in the regulation of neurotransmitter release. *Neuron*, 59(6), pp.861–872.

Neukomm, L.J. & Freeman, M.R., 2014. Diverse cellular and molecular modes of axon degeneration. *Trends in Cell Biology*, 24(9), pp.515–523.

Nose, A., 2012. Generation of neuromuscular specificity in Drosophila: novel mechanisms revealed by new technologies. pp.1–11.

Nose, A., Mahajan, V.B. & Goodman, C.S., 1992. Connectin: a homophilic cell adhesion molecule expressed on a subset of muscles and the motoneurons that innervate them in Drosophila. *Cell*, 70(4), pp.553–567.

Nose, A., Takeichi, M. & Goodman, C.S., 1994. Ectopic expression of connectin reveals a repulsive function during growth cone guidance and synapse formation. *Neuron*, 13(3), pp.525–539.

Nose, A., Umeda, T. & Takeichi, M., 1997. Neuromuscular target recognition by a homophilic interaction of connectin cell adhesion molecules in Drosophila.

Development, 124(8), pp.1433–1441.

Owald, D. et al., 2010. A Syd-1 homologue regulates pre- and postsynaptic maturation in Drosophila. *The Journal of Cell Biology*, 188(4), pp.565–579.

Panzer, S., Weigel, D. & Beckendorf, S.K., 1992. Organogenesis in Drosophila melanogaster: embryonic salivary gland determination is controlled by homeotic and dorsoventral patterning genes. *Development*, 114(1), pp.49–57.

Pereanu, W. et al., 2007. The emergence of patterned movement during late embryogenesis ofDrosophila. *Developmental Neurobiology*, 67(12), pp.1669–1685.

Philippidou, P. et al., 2012. Sustained Hox5 gene activity is required for respiratory motor neuron development. *Nature Neuroscience*, 15(12), pp.1636–1644.

Phillips, A.M., Ramaswami, M. & Kelly, L.E., 2009. Stoned. *Traffic*, 11(1), pp.16–24.

Pielage, J. et al., 2008. A presynaptic giant ankyrin stabilizes the NMJ through regulation of presynaptic microtubules and transsynaptic cell adhesion. *Neuron*, 58(2), pp.195–209.

Pielage, J., Fetter, R.D. & Davis, G.W., 2006. A postsynaptic spectrin scaffold defines active zone size, spacing, and efficacy at the Drosophila neuromuscular junction. *The Journal of Cell Biology*, 175(3), pp.491–503.

Pielage, J., Fetter, R.D. & Davis, G.W., 2005. Presynaptic spectrin is essential for synapse stabilization. *Current biology : CB*, 15(10), pp.918–928.

Portela, A. & Esteller, M., 2010. Epigenetic modifications and human disease. *Nature Biotechnology*, 28(10), pp.1057–1068.

Prokop, A., 1999. Integrating bits and pieces: synapse structure and formation in Drosophila embryos. *Cell and tissue research*, 297(2), pp.169–186.

Prokop, A. & Technau, G.M., 1994. Early tagma-specific commitment of Drosophila CNS progenitor NB1-1. *Development*, 120(9), pp.2567–2578.

Pulver, S.R. et al., 2009. Temporal Dynamics of Neuronal Activation by Channelrhodopsin-2 and TRPA1 Determine Behavioral Output in Drosophila Larvae. *Journal of Neurophysiology*, 101(6), pp.3075–3088.

Raghavan, S. & White, R.A., 1997. Connectin mediates adhesion in Drosophila. *Neuron*, 18(6), pp.873–880.

Rajagopalan, S., Nicolas, E., et al., 2000. Crossing the midline: roles and regulation of Robo receptors. *Neuron*, 28(3), pp.767–777.

Rajagopalan, S., Vivancos, V., et al., 2000. Selecting a longitudinal pathway: Robo

receptors specify the lateral position of axons in the Drosophila CNS. *Cell*, 103(7), pp.1033–1045.

Ramat, A., Hannaford, M. & Januschke, J., 2017. Maintenance of Miranda Localization in Drosophila Neuroblasts Involves Interaction with the Cognate mRNA. *Current biology : CB*, 27(14), pp.2101–2111.e5.

Regulski, M. et al., 1987. Developmental and molecular analysis of Deformed; a homeotic gene controlling Drosophila head development. *The EMBO Journal*, 6(3), pp.767–777.

Rickert, C. et al., 2011. Morphological Characterization of the Entire Interneuron Population Reveals Principles of Neuromere Organization in the Ventral Nerve Cord of Drosophila. *Journal of Neuroscience*, 31(44), pp.15870–15883.

Rieckhof, G.E. et al., 2003. Presynaptic N-type calcium channels regulate synaptic growth. *The Journal of biological chemistry*, 278(42), pp.41099–41108.

Rogulja-Ortmann, A. & Technau, G.M., 2014. Multiple roles for Hoxgenes in segment-specific shaping of CNS lineages. *Fly*, 2(6), pp.316–319.

Rogulja-Ortmann, A., Renner, S. & Technau, G.M., 2008. Antagonistic roles for Ultrabithorax and Antennapedia in regulating segment-specific apoptosis of differentiated motoneurons in the Drosophila embryonic central nervous system. *Development*, 135(20), pp.3435–3445.

Roos, J. et al., 2000. Drosophila Futsch regulates synaptic microtubule organization and is necessary for synaptic growth. *Neuron*, 26(2), pp.371–382.

Ryoo, H.D. & Mann, R.S., 1999. The control of trunk Hox specificity and activity by Extradenticle. *Genes & Development*, 13(13), pp.1704–1716.

Sanes, J.R. & Lichtman, J.W., 1999. Development of the vertebrate neuromuscular junction. *Annual review of neuroscience*, 22(1), pp.389–442.

Santiago, C., Labrador, J.-P. & Bashaw, G.J., 2014. The Homeodomain Transcription Factor Hb9 Controls Axon Guidance in Drosophila through the Regulation of Robo Receptors. *CellReports*, 7(1), pp.153–165.

Schmid, A., Chiba, A. & Doe, C.Q., 1999. Clonal analysis of Drosophila embryonic neuroblasts: neural cell types, axon projections and muscle targets. *Development*, 126(21), pp.4653–4689.

Schober, M., Schaefer, M. & Knoblich, J.A., 1999. Bazooka recruits Inscuteable to orient asymmetric cell divisions in Drosophila neuroblasts. *Nature*, 402(6761), pp.548–551.

Schoofs, A. et al., 2010. The brain can eat: Establishing the existence of a central pattern generator for feeding in third instar larvae of Drosophila virilis and Drosophila

melanogaster. *Journal of Insect Physiology*, 56(7), pp.695–705.

Schuster, C.M. et al., 1996. Genetic dissection of structural and functional components of synaptic plasticity. I. Fasciclin II controls synaptic stabilization and growth. *Neuron*, 17(4), pp.641–654.

Shen, C.P., Jan, L.Y. & Jan, Y.N., 1997. Miranda is required for the asymmetric localization of Prospero during mitosis in Drosophila. *Cell*, 90(3), pp.449–458.

Shenk, M.A., Bode, H.R. & Steele, R.E., 1993. Expression of Cnox-2, a HOM/HOX homeobox gene in hydra, is correlated with axial pattern formation. *Development*, 117(2), pp.657–667.

Shimizu, H., Koizumi, O. & Fujisawa, T., 2004. Three digestive movements in Hydra regulated by the diffuse nerve net in the body column. *Journal of Comparative Physiology A*, 190(8), pp.1–8.

Shishido, E., Takeichi, M. & Nose, A., 1998. Drosophila synapse formation: regulation by transmembrane protein with Leu-rich repeats, CAPRICIOUS. *Science (New York, N.Y.)*, 280(5372), pp.2118–2121.

Siegrist, S.E. & Doe, C.Q., 2006. Extrinsic cues orient the cell division axis in Drosophila embryonic neuroblasts. *Development*, 133(3), pp.529–536.

Siekhaus, D.E. & Fuller, R.S., 1999. A role for amontillado, the Drosophila homolog of the neuropeptide precursor processing protease PC2, in triggering hatching behavior. *The Journal of neuroscience : the official journal of the Society for Neuroscience*, 19(16), pp.6942–6954.

Simpson, J.H., Bland, K.S., et al., 2000. Short-range and long-range guidance by Slit and its Robo receptors: a combinatorial code of Robo receptors controls lateral position. *Cell*, 103(7), pp.1019–1032.

Simpson, J.H., Kidd, T., et al., 2000. Short-range and long-range guidance by slit and its Robo receptors. Robo and Robo2 play distinct roles in midline guidance. *Neuron*, 28(3), pp.753–766.

Skeath, J.B. & Thor, S., 2003. Genetic control of Drosophila nerve cord development. *Current opinion in neurobiology*, 13(1), pp.8–15.

Slattery, M. et al., 2011. Cofactor Binding Evokes Latent Differences in DNA Binding Specificity between Hox Proteins. *Cell*, 147(6), pp.1270–1282.

Sorge, S. et al., 2012. The cis-regulatory code of Hox function in Drosophila. *The EMBO Journal*, 31(15), pp.3323–3333.

Spana, E.P. & Doe, C.Q., 1995. The prospero transcription factor is asymmetrically localized to the cell cortex during neuroblast mitosis in Drosophila. *Development*,

121(10), pp.3187–3195.

Stephan, R. et al., 2015. Hierarchical Microtubule Organization Controls Axon Caliber and Transport and Determines Synaptic Structure and Stability. *Developmental Cell*, pp.1–18.

Stocker, H. & Gallant, P., 2008. Getting started: An overview on raising and handling *Drosophila*. *Methods in molecular biology (Clifton, N.J.)*, 420(Chapter 2), pp.27–44.

Stocker, R.F., 1994. The organization of the chemosensory system in Drosophila melanogaster: a review. *Cell and tissue research*, 275(1), pp.3–26.

Stork, T., Bernardos, R. & Freeman, M.R., 2011. Analysis of Glial Cell Development and Function in Drosophila. *Cold Spring Harbor Protocols*, 2012(1), pp.pdb.top067587–pdb.top067587.

Studer, M. et al., 1996. Altered segmental identity and abnormal migration of motor neurons in mice lacking Hoxb-1. *Nature*, 384(6610), pp.630–634.

Studer, M. et al., 1994. Role of a conserved retinoic acid response element in rhombomere restriction of Hoxb-1. *Science (New York, N.Y.)*, 265(5179), pp.1728–1732.

Suster, M.L. et al., 2004. Refining GAL4-driven transgene expression inDrosophila with a GAL80 enhancer-trap. *genesis*, 39(4), pp.240–245.

Sweeney, S.T. et al., 1995. Targeted expression of tetanus toxin light chain in Drosophila specifically eliminates synaptic transmission and causes behavioral defects. *Neuron*, 14(2), pp.341–351.

Technau, G.M., Berger, C. & Urbach, R., 2006. Generation of cell diversity and segmental pattern in the embryonic central nervous system of Drosophila. *Developmental Dynamics*, 235(4), pp.861–869.

Thor, S. et al., 1999. A LIM-homeodomain combinatorial code for motor-neuron pathway selection. *Nature*, 397(6714), pp.76–80.

Trimble, W.S., Cowan, D.M. & Scheller, R.H., 1988. VAMP-1: a synaptic vesicle-associated integral membrane protein. *Proceedings of the National Academy of Sciences*, 85(12), pp.4538–4542.

Udolph, G. et al., 1993. A common precursor for glia and neurons in the embryonic CNS of Drosophila gives rise to segment-specific lineage variants. *Development*, 118(3), pp.765–775.

Urbach, R., 2003. Molecular markers for identified neuroblasts in the developing brain of Drosophila. *Development*, 130(16), pp.3621–3637.

Urbach, R. & Technau, G.M., 2003. Segment polarity and DV patterning gene expression reveals segmental organization of the Drosophila brain. *Development*, 130(16), pp.3607–3620.

Urbach, R., Jussen, D. & Technau, G.M., 2016. Gene expression profiles uncover individual identities of gnathal neuroblasts and serial homologies in the embryonic CNS of Drosophila. *Development*, 143(8), pp.1290–1301.

Urbach, R., Schnabel, R. & Technau, G.M., 2003. The pattern of neuroblast formation, mitotic domains and proneural gene expression during early brain development in Drosophila. *Development*, 130(16), pp.3589–3606.

Weber, T. et al., 1998. SNAREpins: minimal machinery for membrane fusion. *Cell*, 92(6), pp.759–772.

White, K. et al., 1994. Genetic control of programmed cell death in Drosophila. *Science (New York, N.Y.)*, 264(5159), pp.677–683.

Winberg, M.L., Mitchell, K.J. & Goodman, C.S., 1998. Genetic analysis of the mechanisms controlling target selection: complementary and combinatorial functions of netrins, semaphorins, and IgCAMs. *Cell*, 93(4), pp.581–591.

Wodarz, A. et al., 1999. Bazooka provides an apical cue for Inscuteable localization in Drosophila neuroblasts. *Nature*, 402(6761), pp.544–547.

Wood, R.L., 1979. The fine structure of the hypostome and mouth of hydra. I. Scanning electron microscopy. *Cell and tissue research*, 199(2), pp.307–317.

Xing, B. et al., 2005. Developmental consequences of neuromuscular junctions with reduced presynaptic calcium channel function. *Synapse (New York, N.Y.)*, 57(3), pp.132–147.

Yoshikawa, S. et al., 2003. Wnt-mediated axon guidance via the Drosophila Derailed receptor. *Nature*, 422(6932), pp.583–588.

Yu, F. et al., 2000. Analysis of partner of inscuteable, a Novel Player of Drosophila Asymmetric Divisions, Reveals Two Distinct Steps in Inscuteable Apical Localization. *Cell*, 100(4), pp.399–409.

Yu, H.H. et al., 1998. The transmembrane Semaphorin Sema I is required in Drosophila for embryonic motor and CNS axon guidance. *Neuron*, 20(2), pp.207–220.

Zhang, W., Ge, W. & Wang, Z., 2007. A toolbox for light control of Drosophila behaviors through Channelrhodopsin 2-mediated photoactivation of targeted neurons. *European Journal of Neuroscience*, 26(9), pp.2405–2416.

Zhou, D. et al., 1998. AnkyrinG is required for clustering of voltage-gated Na channels at axon initial segments and for normal action potential firing. *The Journal of Cell*

Biology, 143(5), pp.1295–1304.

Zhou, L. et al., 1995. Programmed cell death in the Drosophila central nervous system midline. *Current biology : CB*, 5(7), pp.784–790.

8__ Appendix

List of GO-terms associated with group 1 genes.

GO-term
asymmetric neuroblast division
establishment or maintenance of neuroblast polarity
ganglion mother cell fate determination
negative regulation of neuroblast proliferation
negative regulation of neurogenesis
neuroblast development
neuroblast fate determination
neuroblast fate specification
neuron development
neuron differentiation
neuron fate commitment
neuron fate specification
regulation of neurogenesis
regulation of neuron differentiation

List of GO-terms associated with group 2 genes.

GO-term
axon choice point recognition
axon extension
axon extension involved in axon guidance
axon extension involved in development
axon guidance
axon midline choice point recognition
axon target recognition
axonal defasciculation

axonal fasciculation
defasciculation of motor neuron axon
motor axon guidance
muscle attachment
neuron projection morphogenesis
regulation of axon extension
regulation of axon extension involved in axon guidance
synaptic target attraction
synaptic target recognition

List of GO-terms associated with group 3 genes.

GO-term
calcium ion-dependent exocytosis of neurotransmitter
integral to synaptic vesicle membrane
maintenance of presynaptic active zone structure
negative regulation of synaptic transmission
neuromuscular junction
neuromuscular junction development
neuromuscular synaptic transmission
neuron-neuron synaptic transmission
neurotransmitter secretion
positive regulation of synaptic growth at neuromuscular junction
regulation of neurotransmitter secretion
regulation of synapse structure and activity
regulation of synaptic activity
regulation of synaptic growth at neuromuscular junction
synapse assembly
synapse maturation
synapse organisation
synaptic target attraction
synaptic transmission
synaptic transmission, glutamatergic
synaptic vesicle
synaptic vesicle coating
synaptic vesicle docking involved in exocytosis
synaptic vesicle endocytosis
synaptic vesicle exocytosis
synaptic vesicle fusion to presynaptic membrane
synaptic vesicle priming
synaptic vesicle transport
transmission of nerve impulse

List of GO-terms associated with muscle development and shared by genes expressed in muscles and CNS

GO-term
larval somatic muscle development
mesoderm development
mesoderm morphogenesis
mesodermal cell fate commitment
mesodermal cell fate determination
mesodermal cell fate specification
muscle attachment
muscle organ development
muscle tissue development
myoblast fusion
myoblast proliferation
somatic muscle developmen

List of group 1 genes

Gene Symbol
ac
ana
aPKC
ase
baz
dac
Dbx
Dr
ems
en
ey
gcm2
grh
gsb-n
HGTX
insc
inv
Kr
l(1)sc
lbe
mid
mira
mts

N
nkd
nub
pdm2
pros
run
stau
wg
wor

List of group 2 genes

Gene Symbol
ab
Alk
aos
ap
beat-Ia
beat-Ib
beat-Ic
beat-IIa
betaTub60D
CadN
CadN2
caps
CG33960
chb
CkIIalpha
comm
Con
Dab
dac
daw
Dbx
dnt
drl
Dscam
Dscam2
dsx
en
ena
exex
Fas3

Fps85D
fra
fru
Gef64C
gukh
haf
Hsc70-4
jeb
jing
ko
Kr
kuz
Lar
Lim3
Liprin-gamma
lola
mid
msn
N
NetA
NijA
otk
plexA
Psc
Ptp61F
Ptp99A
retn
Rich
robo
robo2
robo3
run
sad
sbb
Sdc
Sema-1a
Sema-5c
Sh
side
sim
sm
sna

spz5
stan
tey
tok
Trim9
trio
trn
tup
tutl
uzip
vvl
Wnk
Wnt2
zfh1

List of group 3 genes

Gene Symbol
Ace
Ank2
aPKC
apt
Atg1
Atpalpha
axo
baz
bchs
btsz
cac
cals
Caps
CG14691
CG1909
comm
Con
cpo
cv-c
Dab
dnc
dtr
Dys
Exn
Frq1

fz2
gb
Gem3
GluRIIC
Hsc70-4
Imp
lpp
kay
Khc-73
lap
Lar
Liprin-beta
mGluRA
Miro
neuroligin
Nlg1
nmo
Nos
Pka-C1
pum
Rab3
rab3-GEF
Rab5
Rdl
Rich
Rim
rut
Sap47
Scamp
scramb1
scrib
Sema-1a
sff
sfl
Sh
Shab
sif
Snap25
spas
spin
stan
stnA

stnB
Syn
Syn2
Syt1
Syt4
Syt7
Sytalpha
Sytbeta
Syx1A
Syx7
tkv
Tl
ttv
unc-104
unc-13
unc-13-4A
VGlut
Vmat

List of genes expressed in muscles and CNS

Gene Symbol
ab
Alk
ap
ase
caps
Con
Dr
drl
Dys
Fas3
fru
haf
insc
ko
Kr
kuz
lbe
N
NetA
retn
run

sna
tkv
Tl
wg
Wnt2
zfh1

List of genes tested for differential CNS-expression in embryos

Gene Symbol	Expression in *Dfd*^{16}-mutants (vs wildtype)	Group	Method and References
ank2	n.e.	3	is
ca-alpha1D	n.e.	3	is
cac	n.e.	3	is {Bujupi:2016ub}
caps	gain	2	is (Bujupi 2016)
Con	gain	2	is
ems	n.e.	1	is
en	gain	1,2	IF
exex	n.e.	2	is
Fas3	abnormal	2	IF
gcm2	n.e.	1	is
HGTX	n.e.	2	is (Bujupi 2016)
lbe	n.e.	1,3	is
lim3	n.e.	2	is {Bujupi:2016ub}
mid	n.e.	1,2	is
mira	n.e.	1	is (Bujupi 2016)
netA	n.e.	2	IF
NLaz	loss	2	is
nub	n.e.	1	is (Bujupi 2016)
pdm2	n.e.	1	is
pros	abnormal	1	IF
robo	n.e.	2	is
robo2	gain	2	is, IF
robo3	gain	2	is
scrib	n.e.	3	is {Bujupi:2016ub}
snap25	n.e.	3	is
Syt1	loss	3	is (Bujupi 2016)
VGlut	n.e.	3	is {Bujupi:2016ub}/IF
vvl	gain	2	is
zfh1	n.e.	2,3	is/IF

n.e./not evaluable, is/*in-situ* hybridisation, IF/immunfluorescene